Disruption of *Fusobacterium nucleatum* biofilm using innovative anti-microbial compounds to prevent and treat periodontal disease

Julia Kaburaki
a1769397

Supervisors
A/Prof. Peter Zilm, BSc (Hons.), PhD
Dr. Stephen Kidd, BSc (Hons.), PhD

A thesis submitted to the Adelaide Dental School within the Faculty of Health and Medical Sciences at the University of Adelaide in fulfillment of the requirements for the degree of

Master of Philosophy (Dentistry)

Word Count: 25,258

TABLE OF CONTENT

DECLARATION

I, Julia Kaburaki certify that this work contains no material which has been accepted for the award of any other degree or diploma in my name, in any university or other tertiary intuition and, to the best of my knowledge and belief, contains no material previously published or written by another person, expect where due reference has been made in the text. In addition, I certify that no part of this work will, in the future, by used in a submission in my name, for any other degree, diploma in any university or other tertiary institution without prior approval of the University of Adelaide and where applicable, any partner intuition responsible for the joint award for this degree.

I give permission for the digital version of my thesis to be made available on the web, via the University's digital research repository the Library Search and also through web search engines, unless permission has been granted by the University to restrict access for a period of time.

I acknowledge the support I have received for my research through the provision of an Australian Government Research Training Program Scholarship.

Declared by: _ Julia Kaburaki

Date: 06/12/2023

Witnessed by: _____ A/Prof. Peter Zilm

Date: 06/12/2023

ACKNOWLEDGEMENTS

I would like to start off by offering my sincere thanks to both my supervisors Associate Professor Peter Zilm and Dr Stephen Kidd. I greatly appreciate the constant guidance and support you both have given me throughout the last 4 years.

To Peter, thank you for your never-ending support and trusting me with this amazing project which I was able to pour all my interest in microbiology into. I still remember the first lecture you took for first year dentistry back in 2019 which inspired me to join your lab. You consistently allowed this project to be my own work but steered me to the right direction whenever I needed it. We did have a little bit of a rough start trying to figure out the protocols along with COVID-19 situation, but I'm proud that we made it through. Thank you for always understanding my situation of juggling both dentistry as well as this Masters project. Without you I would not have made it through these past 4 years.

To Stephen, thank you very much for your invaluable guidance and unwavering support throughout the entire journey of this research. Your expertise, dedication, and insightful feedback have been instrumental in shaping the direction and quality of this thesis.

To the other lab members Victor, Yanping, Kevin, Andrew, Richard and Migle, I always look forward to bump into one of you in the lab. Special thank you to Andrew who was the first person to show me how to use the xCELLigence platform back in 2019 and has greatly helped me with tips and tricks along the way. My time in the lab has been thoroughly enjoyable with you all around. You all are amazing scientists and never fail to inspire me.

Next, I would like to thank all the people at the University of Adelaide especially staff in Helen Mayo South building who made this project possible. Special thanks to the staff at Adelaide Microscopy, especially Jane Sibbons. I greatly appreciate your help and patience over many weeks trying to help me image my bugs on the confocal. Also, a big thank you to Chris Leigh and Ken Neubauer who helped with SEM imaging of my biofilm. I would also like to extend my gratitude to Dr Tom Sullivan who has greatly helped me with the statistical analysis. Without each of you, my thesis will not be complete.

To my friends namely Vanessa and Lulu, thank you for being there when I need extra moral support and thank you for always relocating to the North Terrace Campus to study just so I can be close to the lab when I need to run experiments but also study at the same time. I appreciate that you understand that this project means a lot to me. Also, to my friends back in Melbourne who has supported me through my research journey since Honours back in Melbourne, Kim and Annie, you guys have supported me since day one and I couldn't have gotten through this without your continuous support and friendship.

Last but not least, thank you to my parents, my furry friends, Hachi and Charli and my partner Warren for providing me with unfailing support and continuous encouragement and supporting my love for research.

Finally, I would like to acknowledge the financial support from the University of Adelaide for awarding me the Oliver Rutherford Turner Supplementary Scholarship in 2021. This scholarship has been a pivotal source of assistance, enabling me to pursue my studies and research with unwavering dedication and focus. This accomplishment would not have been possible by myself. Once again, thank you to everyone who was part of this journey.

LIST OF ABBREVIATIONS

$AgNO_3$	Silver nitrate
AgNP	Silver Nanoparticles
AI-2	Autoinducer-2
ARG	Antibiotic resistance genes
Au_2Cl_6	Gold chloride
AuNP	Gold Nanoparticles
B-PEI	Branched PEI
B. subtilis	*Bacillus subtilis*
BPEI-AgNP	BPEI-Silver nanoparticles
BPEI-AuNP	BPEI-Gold nanoparticles
CFU	Cell Forming Unit
CI	Cell Index
CLSM	Confocal Laser Scanning Microscopy
CV	Crystal violet
D-Ala	D-alanine
D-Glu	D-Glutamic acid
D-Leu	D-leucine
D-Met	D-Methionine
D-Trp	D-Tryptophan
D-Tyr	D-Tyrosine
DAA	D-amino acids
EPS	Extrapolymeric substance
F. nucleatum	Fusobacterium nucleatum
FA	Formaldehyde
FNF	*F. nucleatum* subsp. *fusiforme*
FNN	*F. nucleatum* subsp. *nucleatum*
FNP	*F. nucleatum* subsp. *polymorphum*
FNV	*F. nucleatum* subsp. *vincentii*
Gal-GalNac	D-galactose-β(1–3)-N-acetyl-D-galactosamine
GCF	Gingival Crevicular fluid
HMDS	Hexamethyldisilane

IgG	Human immunoglobulin G
IMPEDE	Inflammation-Mediated Polymicrobial-Emergence and Dysbiotic-Exacerbation
LAA	L- amino acids
MALDI-TOFMS	Matrix-assisted Laser Desorption Ionization-time of flight Mass Spectrometry
MBC	Minimum Bactericidal Concentration
MIC	Minimum Inhibitory Concentration
MORN2	Membrane Occupation and Recognition Nexus
$NaBH_4$	Sodium borohydride
NCDAA	Non-canonical D-amino acid
NK cells	Natural Killer Cells
ORF	Open Reading Frames
OsO_4	Osmium tetroxide
P. gingivalis	Porphyromonas gingivalis
PBS	Phosphate Buffered Saline
PG	Peptidoglycan
PLL	Poly-L-Lysine
QSI	Quorum Sensing inhibitor
RTCA	Real-time Cell Analysis
SD	Standard Deviation
T. denticola	Treponema denticola
TAA	Autotransporter Adhesin
TLR4	Toll-like Receptor 4

ABSTRACT

Background: Periodontal disease, colloquially known as 'gum disease', contributes heavily to the global burden of chronic diseases known to affect between 35% and 50% of the world population. It is defined as a progressive loss of the supporting tissues of the teeth including the gingiva, alveolar bone and periodontal ligaments leading to tooth mobility or tooth loss and ultimately loss of function. It is a complex pathophysiology: characterised by a host inflammatory response against microorganisms in the sub-gingiva and their by-products.

One of the key microorganisms that is responsible for the sequential maturation of subgingival plaque is *Fusobacterium nucleatum (F. nucleatum)*. *F. nucleatum* plays a significant role as a bridging organism between the early colonisers including Gram-positive *streptococci* sp. and the late colonizers. It is the late colonizers that are disease causing and tissue destructing periodontopathogens including *Porphyromonas gingivalis, Tannerella forsythia* and *Treponema denticola.* Furthermore, *F. nucleatum* has been attracting wide attention due to, not only its pivotal role in disease progression, but also its role in other systemic disease such as adverse pregnancy outcomes, arthritis and colorectal cancer. Different subspecies of *F. nucleatum* have been located around the human body and have been contributing to different diseases processes. This is thought to stem from *F. nucleatum* subspecies having great genetic diversity. Therefore, this project looked at characterising the biofilm forming ability of four different subspecies, *F. nucleatum* subsp. *nucleatum* (FNN), *polymorphum* (FNP), *fusiforme* (FNF) and *animalis* (FNA).

Current treatment of periodontitis includes mechanical debridement by a specialist and in severe periodontitis, antibiotics may be indicated. However, antimicrobial resistance is a serious problem due to over prescription of antibiotics and bacteria in biofilms exhibiting up to 1000- fold increase in antibiotic resistance compared to planktonic bacteria. Therefore, it is crucial to investigate other methods to control oral biofilms, such as the use of novel antimicrobial agents to reduce periodontal disease progression. In recent years, novel antimicrobial and antibiofilm compounds have emerged to combat this issue. These include D-amino acids (DAAs), silver nanoparticles (AgNPs) and gold (AuNPs) nanoparticles.

DAAs have been shown to have biofilm inhibiting and biofilm dispersion effects. A mixture of D-Leucine D-Methionine D-Tyrosine D-Tryptophan has been shown to reduce biofilm formation and initiate biofilm breakdown. Nanoparticles including silver (AgNPs) and gold (AuNPs) have also been of growing interest due to their antimicrobial activity showing both bactericidal and bacteriostatic effects on Gram-positive and Gram-negative bacteria including multi-drug resistant strains present in the oral environment.

Successfully growing and characterising *F. nucleatum* biofilms is the first step in investigating the effectiveness of novel antimicrobial/antibiofilm agents. Our further understanding will contribute to the development of clinical treatments against *F. nucleatum* mediated pathologies including periodontitis.

Aims: The aim of this project is to grow and characterise biofilms produced by *F. nucleatum* subsp. *nucleatum* (FNN), *polymorphum* (FNP), *fusiforme* (FNF) and *animalis* (FNA) to investigate if there are sub-species specific differences in biofilm formation. The second aim is to characterise and investigate the efficacy of novel antimicrobial/antibiofilm agents including DAAs and AgNPs and AuNPs.

Methods: Single-species *Fusobacterium nucleatum (F. nucleatum)* were grown under anaerobic conditions and characterised through growth curves, crystal violet staining, viable cell counts, xCELLigence® platform, SEM and confocal imaging and Imaris software analysis. When the protocol was established, biofilms were treated with novel antibiofilm agents including D-amino acids (DAAs), and antibacterial agents: silver (AgNPs) and gold nanoparticles (AuNPs) to investigate their biofilm inhibiting abilities and biofilm dispersing abilities.

Results: There were sub-species specific differences in *F. nucleatum* growth where FNP and FNA showed increase in sensitivity to oxygen. FNF and FNN consistently showed better growth with minimal sensitivity to oxygen. SEM imaging showed differences in cellular morphology amongst the four subspecies. Furthermore, protocol optimisation to improve *F. nucleatum* biofilm growth was successful for crystal violet staining and confocal imaging. Unfortunately, *F. nucleatum* biofilm growth was unable to be successfully detected by the xCELLigence® platform.

DAAs reduced the growth of FNP, FNF and FNN with minimal differences between the control and DAA treated growth curves for FNA. FNF and FNN treated with DAAs showed similar results when added at the start of the experiment where over the first 6 hours produced a 2-fold increase in doubling time (log phase) and stationary phase was reached earlier near 4 hours in the DAA treated groups. DAA treated FNP, FNF and FNN groups showed a reduced capacity to grow, reflected in a reduction of the maximum OD_{600nm} reached. On the contrary, minimal differences were observed between the control and DAA treated growth curves for FNA, which was consistently observed throughout the experiment repeated in triplicate.

SEM imaging further showed changes in biofilm architecture after DAA treatment where FNP and FNF showed absence of EPS compared to the control groups and FNA produced elongated cells. All four subspecies including FNN showed to have almost vesicular looking irregularities on the surface of the bacteria after DAA treatment.

Qualitative results from confocal imaging further confirmed a decrease in bacterial cell numbers after DAA treatment for all 4 subspecies. Interestingly, contradictory to results seen through assessing growth in the spectrophotometer, DAA treated FNP showed minimal changes in biofilm volume, whereas FNF and FNN biofilms showed almost 4-fold decrease in mean volume and FNA showed almost 3-fold decrease in mean volume after quantitative analysis using Imaris Software. Furthermore, while decrease in bacterial cell numbers was observed, no significant difference in viability between DAA treated and control groups were observed through viable cell counts and Imaris analysis of viability (%). Similar results were observed for DAA treatment on established *F. nucleatum* biofilm where a decrease in biofilm volume due to biofilm dispersal, but no significant difference in viability was observed. Results from these experiments indicate that DAAs are a promising biofilm breaker with minimal effects of viability of *F. nucleatum* cells after treatment.

AgNPs and AuNPs showed a concentration dependant effect where the concentration of nanoparticles was inversely proportional to viability. Confocal imaging showed that all four subspecies of *F. nucleatum* had a reduction in bacterial cell number after being treated with 60μg/ml AgNPs. Due to the Imaris analysis tool's inability to differentiate between *F. nucleatum* and AgNPs, quantification analysis of the biofilms was unable to be performed.

Conclusion: This project successfully produced a protocol to successfully grow all four subspecies of *F. nucleatum* in a spectrophotometer. DAAs showed promising results as a biofilm breaker with minimal effects of viability of *F. nucleatum* cells after treatment. On the other hand, AgNPs and AuNPs both exhibited potential bactericidal effects. Therefore, future studies may conduct investigations on effects of combinations of these novel antimicrobials and antibiofilm compounds on *F. nucleatum* biofilm. Clinically, incorporating these novel antimicrobials and antibiofilm compounds may have application in periodontitis treatment. This may overcome the issue of increased antibiotic resistance in the community and become a useful adjunct to mechanical removal of subgingival biofilm by the specialist, reducing the number of appointments and cost needed by the patient for periodontitis treatment in the future.

CHAPTER 1: INTRODUCTION

1.1 Periodontal disease

1.1.1 Prevalence of periodontal disease and cost to the health system

Periodontal disease, also termed as 'gum disease' is known to affect between 35% and 50% of the world population according to the World Health Organisation (Petersen and Ogawa, 2012). It is one of the most important oral disease contributing to the global burden of chronic diseases along with dental caries (Murray et al., 2012; Petersen and Ogawa, 2012). It is characterised by a host inflammatory response against microorganisms in the dental plaque and their by-products within the gingiva (gum tissues) (Genco, 1992).

There is a spectrum of gum diseases with the least severe being gingivitis which is characterised by the reversible local inflammation of the gingival tissue along the gingival margin caused by bacteria (Page, 1986). However, if not treated, the condition can progress to periodontitis. The overall prevalence of severe periodontitis is estimated to be 11.2% which is equivalent to around 743 million people being affected globally (Kassebaum et al., 2014). Periodontitis is characterised by chronic inflammation where bacteria and bacterial products in the subgingival region induces a host inflammatory response within the periodontal tissues resulting in a progressive loss of the supporting tissues of the teeth including the gingiva, alveolar bone and periodontal ligaments leading to tooth mobility or tooth loss and ultimately loss of function (Armitage, 1999; Loesche, 1996). Destruction of the periodontium can either be caused by local factors from bacteria in the dental biofilm or may reflect an inadequate host immune response. Unlike gingivitis, this tissue destructive process is irreversible. Due to its polymicrobial nature and complex interaction between the bacteria and inflammatory response of the host's body, its temporal relationship contributing to the pathogenesis of periodontitis has been long debated. The most recently suggested theory termed Inflammation-Mediated Polymicrobial-Emergence and Dysbiotic-Exacerbation (IMPEDE) suggests pathogenesis of periodontitis is thought to be driven by inflammation which then modulates the polymicrobial biofilm in certain individuals who are suspectable to this disease (Van Dyke et al., 2020).

1.2 Oral biofilms

1.2.1 Oral biofilms

Bacterial biofilms in the mouth, more commonly known as plaque, are complex polymicrobial communities present on all oral surfaces including both the hard and soft tissues and are known to have a significant impact on the health and disease progression of the periodontium. Most of these species in the oral environment are considered as being commensal while some are considered pathogenic.

There are two different types of biofilms that can exist on a tooth surface depending on its location. They differ in bacterial composition and have unique spatial organisations that changes as the biofilm grows and matures. Supragingival biofilm is dental plaque that exists on exposed enamel surfaces on the tooth that are not covered by the gingiva. There are various factors including the concentrations of Ca^{2+}, PO_4^{3-} and OH^- in saliva, dietary intake, biofilm composition and host immune response (Marsh, 2003) that may transition the supragingival biofilm into a cariogenic biofilm. The latter being characterised by increased lactate production causing a decrease in localised pH leading to development and progression of caries (Becker et al., 2002; Marsh, 1994).

Another biofilm that exists in the mouth is the subgingival biofilm that forms on the tooth below the gingival margin. When the subgingival biofilm transitions to a pathogenic biofilm, due to inadequate oral hygiene, this can lead to periodontal diseases also known has periodontitis (Socransky et al., 2002). Over 700 species of bacteria have been detected in the subgingival plaque of both healthy subjects as well as subjects with periodontal disease. Over half of the species are unable to be cultivated so detection relies on the use of 16S rRNA sequencing (Paster et al., 2006). Current theory on the causes of periodontal disease puts great emphasis on the subgingival biofilm. An imbalance in the proportion of bacteria present can drive autogenic changes that lead to disease progression. The link between disease and changes in the subgingival microbiota are described by the ecological plaque hypothesis, (Marsh, 1994, 2003). This recognises that no single bacteria causes periodontal disease but rather the changes in relative numbers of subgingival bacteria and increase in proportion of pathogenic bacteria ultimately leads to disease progression such as a shift from reversible gingivitis to irreversible periodontitis (Darveau et al., 1997; Kolenbrander et al., 2006; Marsh, 2003).

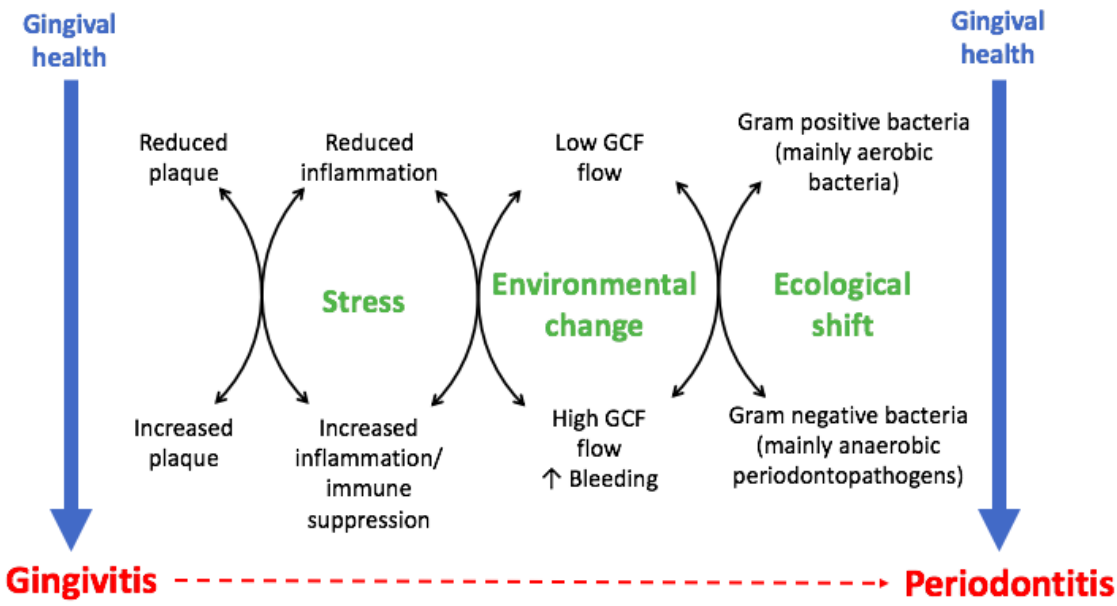

Figure 1: Schematic representation of 'ecological plaque hypothesis' relating to periodontal disease

In the subgingival biofilm, accumulation of bacteria can evoke a host inflammatory host response which causes a microbial shift in favour of Gram-negative anaerobic bacteria which leads to the progression of periodontal diseases such as gingivitis and periodontitis.

(Adapted from Marsh et al., 2011)

Human oral bacteria within dental biofilm forms and matures in an ordered sequence through a process called coaggregation which results in a structurally and functionally organised microbial community. This process is defined as a specific cell-cell recognition that occurs between genetically distinct cell types through coaggregation mediators on their surface called adhesins and receptors (Kolenbrander et al., 2006). Coaggregation of different bacterial species is crucial for growth and development of the dental biofilms and it is thought that close cell-cell distance is key to driving biofilm formation in a spatiotemporal manner (Kolenbrander et al., 2010).

A healthy oral cavity has a highly diverse but distinctive bacterial microbiota which is site and subject specific (Aas et al., 2005) and consists mainly of aerobic early colonizers which are primarily Gram-positive *streptococci* sp. and *Actinomyces* sp. (Diaz et al., 2006; Dige et al., 2009; Li et al., 2004; Nyvad and Kilian, 1987). These early colonizers possess surface components such as fimbriae and receptor polysaccharides (Clark et al., 1989; Palmer et al.,

2003; Yoshida et al., 2006) which allows them to adhere directly to the salivary pellicle on the tooth surface, preventing them from being removed when food or saliva is swallowed.

1.2.2 Supragingival biofilm

Oral bacteria in the supragingival biofilm are exposed to the harsh open environment where they must constantly tolerate changes in the surrounding conditions, withstand fluid shear forces created by saliva as well as occlusion forces. Therefore, bacteria need mechanisms to cooperate within the biofilm to enhance resistance to environmental stress and increase their survival (Bowden and Hamilton, 1998; Haffajee and Socransky, 2005). Bacteria growing as a biofilm function as a cooperative consortium and secrete sticky extra-polymeric substances (EPS) also known as the extracellular matrix (Davey and O'Toole G, 2000; Marsh, 2005). EPS consisting of proteins, polysaccharides and nucleic acid helps maintain the biofilm structure, protect the bacterial community from the external environment as well as assist in adherence to surfaces and to act as a communication medium (Huang et al., 2011). Fluid filled channels traverse within the EPS, creating a primitive circulatory system that delivers nutrients such as oxygen but also removes metabolic wastes. This creates a highly regulated environment which increases bacterial survival in the oral environment (de Beer et al., 1994; Hall-Stoodley et al., 2004).

1.2.3 Bacterial complexes in the subgingival biofilm

Bacterial succession within the subgingival during transition to periodontal disease is characterised by a decrease in aerobic early colonizers and an increase in anaerobic Gram-negative periodontal pathogens, also known as the late colonizers (Loe et al., 1965). This has been confirmed through culture studies using blood agar plates and Gram staining (Moore and Moore, 1994) as well as using whole genomic DNA probes and checkerboard DNA-DNA hybridisation both using samples isolated from human subjects (Ximenez-Fyvie et al., 2000). As the biofilm thickens, supply of nutrients become limited along with shortage of oxygen which promotes the survival of the mostly anaerobic species (Socransky et al., 2004).

While exposure to shear forces within the oral environment can be one of the major stressors for the survival of the bacteria in the supragingival biofilm, this is less of a concern for bacteria in the subgingival biofilm due to protection by the gingiva. Furthermore, while exogenous nutrients are the main source of energy for the supragingival biofilm, subgingival

bacteria derive energy from the increased production of gingival crevicular fluid (GCF), which is part of the host inflammatory response against bacteria. GCF contains a range of host proteins and glycoproteins that can be used as the alternative energy source (ter Steeg et al., 1987).

Using DNA-DNA hybridization methods, subgingival bacteria have been grouped into 5 major complexes based on how closely they are physically associated with one another as well as their pathogenic potential (Socransky et al., 1998). One of the complexes called the 'red-complex' consists of *Porphyromonas gingivalis (P. gingivalis), Tannerella forsythia* and *Treponema denticola (T. denticola).* Elevated numbers of these periodontopathogens are frequently associated with periodontitis (Mira et al., 2019; Socransky et al., 1998). Further research has shown that *P. gingivalis* is a 'key-stone pathogen' in the remodelling of the subgingival biofilm from a healthy to a harmful microbiota and is last to colonise the biofilm (Slots, 1999). This can eventually progress to the destruction of host tissues as observed in *in vivo* models (Hajishengallis et al., 2011). Of the three that make up the red complex, *P. gingivalis* and *T. denticola* are usually found together (Kigure et al., 1995) and they show strong synergism as increased biofilm biovolume and thickness is observed when cultured together (Zhu et al., 2013). Furthermore, gingipains (cysteine proteases) are the major virulence factors produced by *P. gingivalis* which have a catalytic domain and a non-catalytic adhesin domain that may facilitate attachment with other bacteria and the host (Potempa et al., 2003). While *P. gingivalis* is considered to be the main periodontal disease-causing pathogen, its interactions with other bacteria such as *T. denticola* has an important role in biofilm maturation.

Another group of bacteria collectively known as the 'orange complex' colonizers create environmental changes that are conducive to the growth of the red complex periodontopathogens. The orange complex consists of *Fusobacterium nucleatum (F. nucleatum), Prevotella intermedia, Peptostreptococus micros* and *Eubacterium*. Interestingly, members of the 'red complex' are only found when there was simultaneous presence of the 'orange complex' and most importantly, *F. nucleatum* (Socransky et al., 1998). The microbial succession seen in subgingival plaque is highly dependent on specific interactions between certain bacterial species and is not considered a random occurrence (Dige et al., 2007; Kolenbrander et al., 2002; Mark Welch et al., 2016; Wecke et al., 2000). The complex interactions that bacteria exhibit within the biofilm highlights the importance of working with

multispecies bacteria rather than only using single species (axenic) as it more accurately simulates ecosystem diversity that exists within the oral environment.

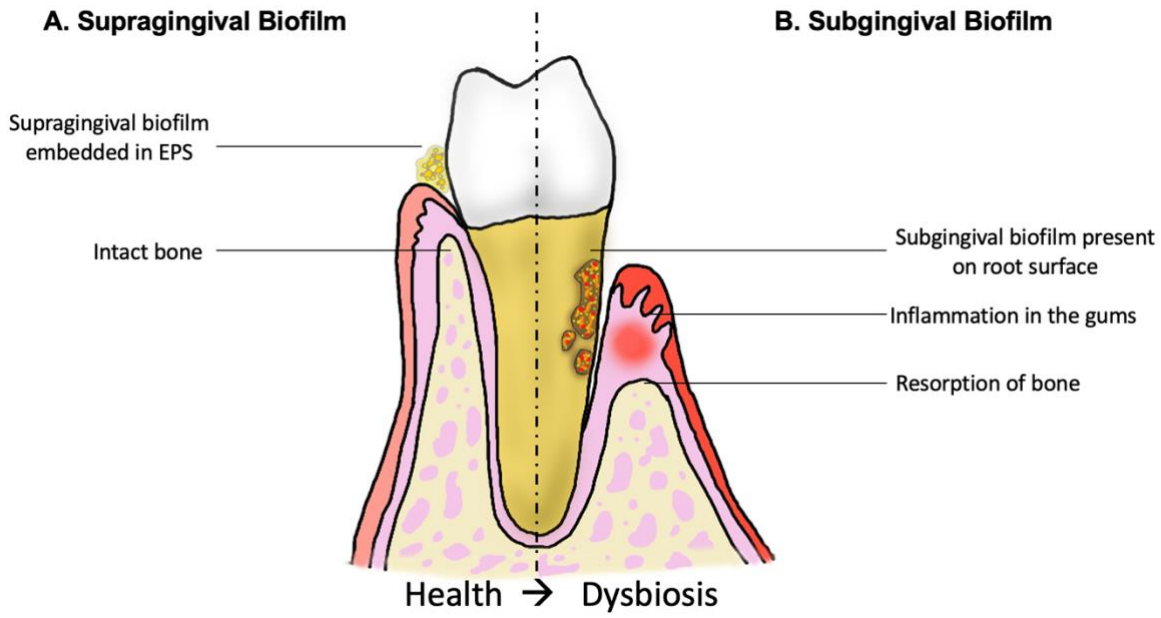

Figure 2: **Schematic diagram of supragingival and subgingival biofilm on the tooth** **(A)** Supragingival biofilm exists above the gingiva and is commonly populated by facultative anaerobes which leads to inflammation of the gingiva (gingivitis) but no destruction of the periodontium is observed **(B)** Subgingival biofilm exist below the gum line within periodontal pockets. Periodontal disease is driven by a small number of pathogenic anaerobic bacteria which leads to destruction of periodontal tissues including the gingiva, alveolar bone, and periodontal ligament.

1.2.4 Altering host immune response

Periodontal disease is characterised by an inappropriate regulation of the host defence mechanism in susceptible individuals with genetic predisposition (Van Dyke et al., 2020). Periodontopathogens including *P. gingivalis* and *T. denticola* from the red complex have shown to have the ability to modulate the host immune and inflammatory response (Graves, 2008; Huang et al., 2001; Zhang et al., 2007). Endogenous "danger" molecules of which the members from the 'red complex' have been shown to release have immunomodulating abilities, which possibly contribute to the progression of periodontal disease (Jun et al., 2017). Furthermore, *P. gingivalis* has been shown to down-regulate inflammasomes which is important in the activation of the innate immune system. Dampening of the host immune response may favour the survival of the bacteria in the subgingival biofilm (Belibasakis et al.,

2013). By altering the host immune response, the periodontopathogens can increase the likelihood of survival and disease progression.

1.2.5 Advantages of biofilm growth

As the biofilm continues to mature, EPS plays an important role in bacterial survival. Not only is it important for protection, experimental evidences have suggested that EPS can act as a medium for horizontal gene transfer of antibiotic resistance genes (ARG) between microorganisms in the oral biofilm (Hannan et al., 2010; Roberts et al., 1999; Wang et al., 2002). This contributes to the emergence of antibiotic resistant oral bacteria, seen more commonly in patients with periodontitis (Kim et al., 2011). Additionally, the matrix itself can act as a physical barrier for the antibiotics to penetrate and have an effect (Van Acker et al., 2014; Xiao et al., 2012). Antibiotic resistance is problematic as it may reduce efficacy of antibiotic therapy on patients with periodontal disease (Sukumar et al., 2020; Teoh et al., 2018).

Besides physical interactions of oral bacteria within a biofilm, they can further interact through molecular mechanisms involved in bacterial communication (quorum sensing) within the same species as well as across different species. This process involves bacteria producing and detecting signalling molecules which detect bacterial numbers (quorum), thereby coordinating their gene expression and behaviour in a cell-density dependent manner to optimise virulence factors (Fuqua et al., 1994; Marsh, 2004). These virulence factors include adherence factors which are involved in biofilm formation, invasion factors contributing to progression of periodontal disease and activation of host immune response through release of endotoxins. This ability to communicate within and between species is an important mechanism to ensure survival of the bacteria in the harsh oral environment.

1.3 Biofilm control

1.3.1 Managing the oral biofilm

As seen in periodontitis, the maturation of the bacterial biofilm triggers the host inflammatory response which contributes to destroying surrounding tissues. Current treatment regime for periodontitis can include prescription of antibiotics in conjunction to mechanical disruption of the biofilm through debridement (Haffajee et al., 2003; Kwon et al., 2021; Winkel et al., 2001). However, antimicrobial resistance is a very big problem due to over prescription of

antibiotics. Dentistry accounts for 3-11% of all antibiotic prescription (Teoh et al., 2018) and within those prescriptions, 66% are not clinically indicated (Amy and Thayalan, 2020). Therefore, it is crucial to investigate other methods to control oral biofilm, such as through the use of novel antimicrobial agents to decelerate periodontal disease progression.

There are two broad ways to control the oral biofilm. The first being through prevention of initial biofilm formation. The second is through disrupting already established biofilm. The latter can further be divided into two mechanisms. First through the physical destruction of the bacterial cell wall and the second is through interrupting the quorum sensing mechanisms. In recent years, novel compounds that can potentially inhibit biofilm maturation or growth have become an area of interest to avoid the over use of antibiotics and increase in numbers of antibiotic resistant bacteria (Kim et al., 2011). Some novel anti-microbial compounds include the use of metal nanoparticles, quorum sensing inhibitors as well as D-amino acids.

1.3.2 Silver and gold nanoparticles

In recent years, silver nanoparticles (AgNPs) has been of growing interest due to their antimicrobial activity showing both bactericidal and bacteriostatic effects on Gram-positive and Gram-negative bacteria as well as multi drug resistant strains present in the oral environment (Bahador et al., 2015; Hernandez-Sierra et al., 2008; Jia et al., 2016; Shahverdi et al., 2007). Additionally, their biocompatibility has been confirmed (Nunez-Anita et al., 2014). AgNPs interact with and disrupt bacterial cell membranes causing increased membrane permeability and subsequently lysis (Li et al., 2013). It is thought that uptake of AgNPs in Gram-negative bacteria is through porins on the outer-membrane (Radzig et al., 2013). Furthermore, their nanoscale dimensions and increased surface-to-volume ratio allows them to penetrate effectively stopping further biofilm growth (Seil and Webster, 2012). Cationic AgNPs attracted to the negative charge on the microbial cell surface shows effective anti-biofilm effects on dental cariogenic biofilm consisting of *S. mutans, Streptococcus sanguinis (S. sanguinis), Streptococcus sobrinus*, and *Actinomyces naeslundii* and shows to be a promising dental antimicrobial, potentially just as effective as chlorhexidine and silver fluoride (He et al., 2023). Although, very few studies have tested the effect of AgNPs on periodontal pathogens, it has been shown that periodontal anaerobic bacteria were less susceptible to AgNPs than aerobic oral bacteria (Lu et al., 2013). Furthermore, less studied than AgNPs, gold nanoparticles (AuNPs) have also shown to have both bactericidal and

bacteriostatic effects on oral bacteria at a higher concentration compared to AgNPs (Hernandez-Sierra et al., 2008), including *F. nucleatum* biofilm demonstrated through *in vitro* and *in vivo* experiments (Zhang et al., 2022a).Therefore, AgNPs and AuNPs have considerable potential as an alternative to antibiotic therapy that can be used to treat individuals with periodontitis.

1.3.3 D-Amino Acids

The general structure of amino acids consists of four functional groups connected to the central α-carbon. The functional groups are an amine group ($-NH_2$), a carboxyl group (-COOH), a hydrogen group (-H) and a side chain (-R) which varies depending on the particular natural amino acid. This structure makes the α-carbon a stereogenic centre, creating two stereoisomers for each amino acid excluding glycine which has a hydrogen group (-H) as the side chain. Therefore, each amino acid has two forms it can exist in: the D-form and the L-form.

L-amino acids (LAAs) are essential to living organisms and is used as ribosomal synthesis of protein. This makes it the predominant and natural form of amino acids. Conversely, D-amino acids (DAAs) have minor function in biological processes but D-alanine (D-Ala) and D-glutamic acid (D-Glu) are routinely found as a constituent in the peptidoglycan (PG) cell wall in bacteria (Vollmer et al., 2008). Furthermore, other than the DAAs are incorporated ino PG, bacteria in mature biofilm release DAAs during stationary phase, known as non-canonical D-amino acids (NCDAAs). They are released under stressful conditions to aid in modification and adaptation of the bacterial cell wall in accordance to surrounding environmental challenges as part of their protective mechanism (Cava et al., 2011; Lam et al., 2009). Breaking down of biofilm and dispersing of bacteria from the site of stress allows for new biofilm to form elsewhere in the body increasing chances of survival (Donlan and Costerton, 2002).

DAAs has also been demonstrated to have antibiofilm and biofilm breakdown effects. DAA mixture of D-Leucine (D-Leu), D-Methionine (D-Met), D-Tyrosine (D-Tyr), D-Tryptophan (D-Trp) at nanomolar concentrations shows prevention of *Bacillus subtilis (B. subtilis)* biofilm formation and initiates breakdown (Kolodkin-Gal et al., 2010), with D-Tyr being the most potent amino acid (Champney and Jensen, 1969). Through these experiments, it is

thought that the DAAs that are experimentally added can incorporate themselves into the peptide side chain of the PG cell wall in place of the naturally occurring D-Ala. This ultimately leads to the release of the TasA fibres from the cell wall and causes dispersion of the biofilm (Kolodkin-Gal et al., 2010). TasA fibres is a functional amyloid which plays an important role in providing structural integrity in a biofilm (Romero et al., 2010). Further investigations using *B. subtilis* concludes that DAAs may also have proteotoxicity effects contributing to the inhibition of biofilm formation (Leiman et al., 2013).

DAAs also prevents biofilm formation of other oral bacteria such as *Staphylococcus aureus, Pseudomonas aeruginosa* (Brandenburg et al., 2013; Kolodkin-Gal et al., 2010). More recent studies shows that a DAA cocktail is a successful *Enterococcus faecalis* biofilm dispersing agent (Zilm et al., 2017) and similar effects are seen in biofilm formed in dental unit waterlines (Ampornaramveth et al., 2018). This has led to DAAs to be identified as a novel antimicrobial agent.

These antibiofilm and antimicrobial effects makes DAAs an attractive possible alternative to antibiotics for the treatment of periodontitis.

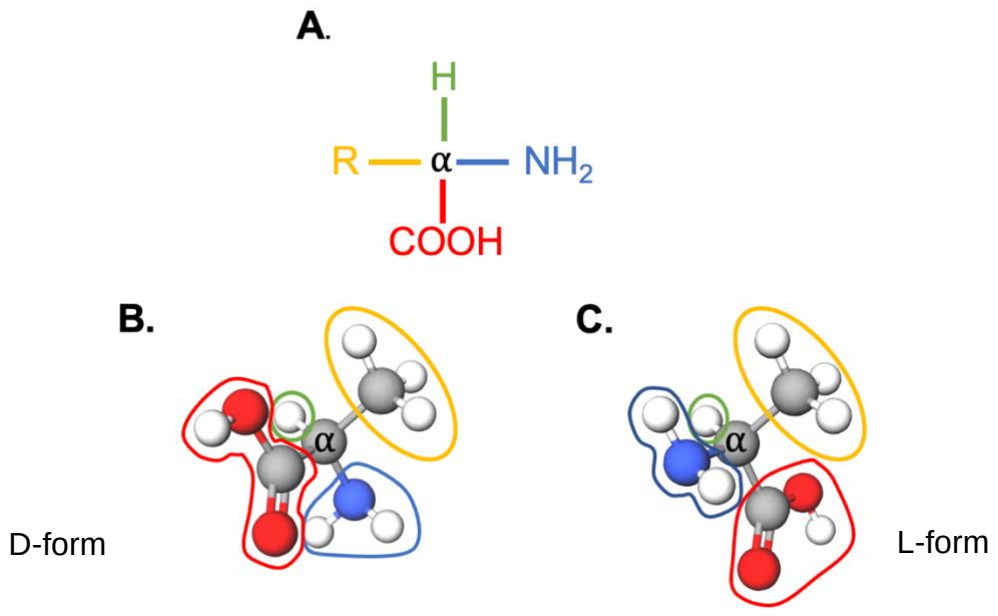

Figure 3: Diagram of structure of amino acids and example of Alanine stereoisomer
(A) General structure of amino acids **(B)** D-Alanine– side chain CH_3 **(C)** L-Alanine – side chain CH_3 Amine group ($-NH_2$) is coded blue, carboxyl group (-COOH) is coded red, side chain is coded yellow and hydrogen group is coded green. Central α-carbon is labelled with α. Molecules were designed with MolView software.

1.3.4 Evolution of laboratory techniques to study dental biofilms

For decades, much of our understanding of dental biofilms have been through the use of *in vitro* models. Over the years, number of *in vitro* models have been developed to help better understand not only biofilm biology, but also to study the response of the biofilm after exposure to external stimuli such as the addition of antibacterial agents and changes in pH of the surrounding environment (Subramanian et al., 2020). There are two approaches that have been developed to study biofilms. First, is the open system, also known as the flow cell system which provides a continuous supply of nutrients (Shu et al., 2000). The advantage of this method is that it more closely resembles *in vivo* conditions. However, multiple factors cannot be screened at once and the process can be laborious. Second is the closed culture systems, which allow the growth of oral biofilms on different surfaces including pegs (Kistler et al., 2015) and plastic multi-welled plates (Guggenheim et al., 2001).Closed systems typically grow biofilms over several hours and have the limitation of a finite supply of nutrients which does not accurately resemble *in vivo* conditions. The main advantage of this method is its high reproducibility, high yield and its ability to screen for multiple factors at once, making it a method frequently used to study biofilms at a macro level. In both open and closed system, the standard approach of analysing biofilms is through end-point analysis (Lemos et al., 2010; Yu et al., 2017a). This has the main limitation of only providing a single data point and is accompanied by the destruction of the biofilm. In addition, end point analysis provides limited data about the dynamics of the biofilm formation over time. Therefore, conventional end-point analysis only allows assessment at defined times, making real-time cell analysis over a certain period of time impossible.

While these methods are still well accepted and practiced to study biofilms, other techniques have been developed to overcome these limitations. Microfluidics is a system that has been developed to have the ability to monitor cells continuously in a non-invasive manner while providing a stable microenvironment (Hung et al., 2005; Lam et al., 2016a). This method has been widely applied in oral biofilm studies due to its ability to mimic various oral environmental conditions such as changes in pH (Gashti et al., 2016), shear stress (Shumi et al., 2013), oxygen levels (Lam et al., 2016a) as well as testing of antimicrobial agents (Nance et al., 2013). Furthermore, another significant advantage of using microfluid systems is its ability to integrate microfabricated sensors including optical microsystems (Samarian et al.,

2014) and impedimetric microsystems (Bruchmann et al., 2015) to have a more comprehensive understanding of the dynamics of biofilm structures and functions, allowing for real-time, non-invasive and non-destructive label free method to monitor biofilm composition.

1.3.5 xCELLigence®

One of the commercially available microfluidic cell analysers that integrates impendence-based technology is xCELLigence®. The system has revolutionised biofilm research in the recent years (Mira et al., 2019) and unlike standard end-point cell assays, it is designed to allow continuous real-time cell analysis (RTCA) to monitor biofilm growth dynamics in a non-invasive and label free manner as well as producing accurate and reproducible results. Specialised E-plates have gold microelectrodes embedded within the bottom of surface of the microtiter wells. As the biofilm grows, the presence of adherent cells impedes the current flow. The magnitude of the impendence depends on the number and size of the cells, therefore being able to monitor both biofilm growth and breakdown in real time. As the biofilm develops, the impedance, measured as cell index also increases proportionally. Real-time analysis of growth of both single- and multi-species oral biofilms have been successfully demonstrated using this system (Mira et al., 2019). To date, *Streptococcus mutans* (Mira et al., 2019; Muras et al., 2018), *S. sanguinis, Candida albicans* (Abrantes and Africa, 2020) and *lactobacilli* spp. (Martinez et al., 2020) are few of the oral microorganisms that have successfully shown to grow as biofilms using the xCELLigence® platform. These studies also demonstrate that the oral bacteria are not affected by the gold microelectrodes or the electrical potential present during biofilm growth. xCELLigence® has been proposed as a valid *in vitro* model to study oral biofilms due to its capability to monitor growth and development of biofilms in real-time. It also allows for the screening of newly developed antimicrobial agents that may destroy or disrupt biofilms, making it a promising new technology that may replace conventional cell culture of single- and multi-species oral biofilms.

Previous oral biofilm studies have been predominately focused on characterising the supragingival biofilm which is most commonly populated by facultative anaerobes (Espinoza et al., 2018; Haffajee et al., 2008; Keijser et al., 2008). On the contrary, the in vivo investigation of obligatory anaerobes such as *F. nucleatum* and *P. gingivalis* residing in

subgingival biofilm has been proven to be difficult due to two main reasons. The first being the accessibility of the subgingival biofilm. To obtain and investigate the human subgingival microbiota, a dentist must first scale subgingivally. This process is invasive and uncomfortable compared to harvesting the supragingival biofilm which can easily be scraped off the tooth surface non-invasively. The second reason is that monitoring of the growth and development of subgingival biofilm can be more difficult due to its necessity of having a tightly controlled environment, especially oxygen requirements. Obligatory anaerobes such as *P. gingivalis* require a capnophilic environment in order to survive (Diaz and Rogers, 2004). Therefore, to characterise the subgingival biofilm *in vitro*, great care must be taken to tightly regulate the surrounding environment. For these reasons, studies on subgingival biofilms are currently limited.

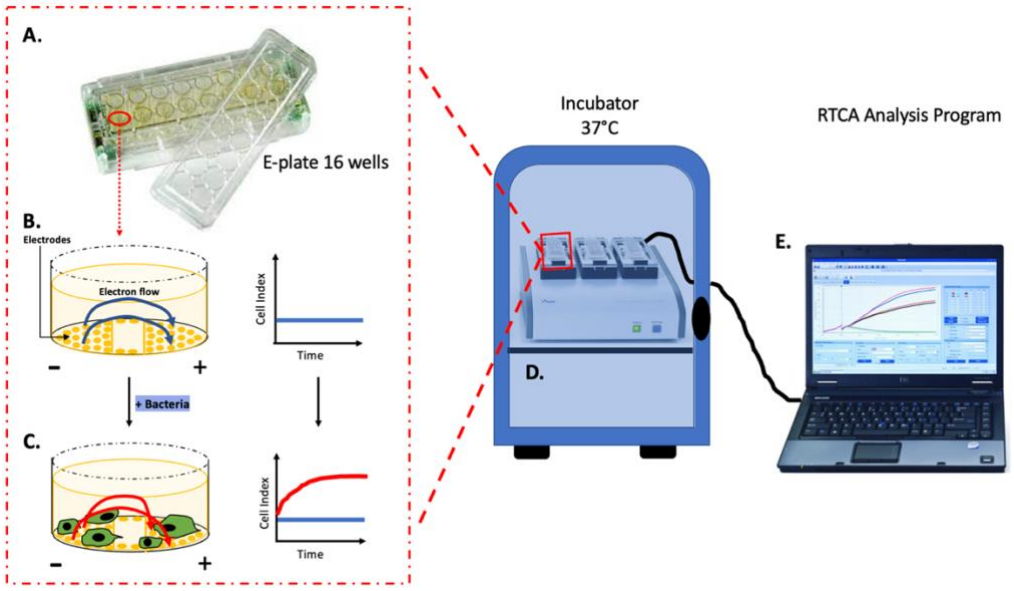

Figure 4: Diagram of xCELLigence® platform set up

(A) Single well of a xCELLigence® E-plate 16 outlined (red) **(B)** Side view of a single well of the E-plate with gold electrodes embedded within the wells (not drawn to scale). Unimpeded electron flow from the negative to positive terminal in the presence of medium only (control sample) is reflected on the graph as low background reading **(C)** Once bacteria are added to the wells (experimental sample) and biofilm is formed, this impedes the electron flow from the negative to positive terminal. This is plotted as arbitrary units called Cell Index (CI). Cell adherence and breakdown can be monitored at real-time. xCELLigence® 16 wells E-plate is engaged into the **(D)** RTCA Multiplate Station, which is kept in the incubator which is further connected to the **(E)** RTCA Control Unit which is a laboratory computer with pre-installed RTCA software. This program allows for experimental protocol set-up, real-time data acquisition, numeric and graphic data display.

1.4 Fusobacterium nucleatum

1.4.1 The Genus

The bacterial genus *Fusobacterium* spp. traditionally includes a variety of Gram-negative bacteria that are fusiform shaped and ferment amino acids and glucose to produce butyric acid as a major end product (Jousimies-Somer, 1997). Now, *Fusobacterium* spp. includes 13 species that are primarily anaerobic, non-motile, non-spore-forming Gram-negative rods that are opportunistic pathogens (Citron, 2002). *Fusobacterium* spp. can broadly be separated into passively invading and actively invading *Fusobacterium* species (Huggan and Murdoch, 2008). Passively invading *Fusobacterium* species need additional factors such as coinfection to invade the host cell due to a lack of virulence-associated factors, this includes *F. necrophorum* and *F. gonidiaformans* (George et al., 1981; Tadepalli et al., 2009). In contrast, actively invading *Fusobacterium* species can independently invade host cells and include *F. nucleatum* and *Fusobacterium periodonticum* (*F. periodonticum)* both isolated from patients with periodontitis (Socransky et al., 2000). Compared to the passive invader genome, active invaders are larger in size and their genome contains twice as many genes which encode for membrane-associated proteins. Interestingly, MORN2 (Membrane Occupation and Recognition Nexus) domain of which its function is still not understood is the most frequent domain in active invader genomes and occurs near other genes encoding for adhesins, virulence-related proteins and membrane proteins, possibly suggesting its role in adhesion and invasion. From these findings, large comparative genome analysis suggests that the *Fusobacterium* genus likely underwent an adaptive radiation resulting in three linages (Manson McGuire et al., 2014).

In recent years, genomic analysis has enabled accurate sequencing, investigating differences and similarities between the *Fusobacterium* spp. (Manson McGuire et al., 2014; Todd et al., 2018). Amongst the *Fusobacterium* spp., *F. nucleatum* which has most frequently been isolated in humans, has steadily gained attention not only due to its presence in the oral cavity causing progression of periodontitis but also its role in extraoral infections (Han, 2015; Moore et al., 1982). This Gram-negative, obligate anaerobe is thought to have evolved as a lineage with *F. periodonticum* through adaptive radiation evident through having similar host cell adherence and invasion (Manson McGuire et al., 2014).

1.4.2 Genetic diversity amongst *F. nucleatum* subspecies

There are four subspecies of *F. nucleatum* which has been identified, subsp. *nucleatum, polymorphum, fusiforme/vincentii* and *animalis* (Gharbia and Shah, 1989; Kim et al., 2010; Kook et al., 2013; Nie et al., 2015). *F. nucleatum* subsp. *fusiforme* and *vincentii* has been classified as a single species due to its genetic similarity (Conrads et al., 2002; Gharbia et al., 1990; Kim et al., 2010; Strauss et al., 2008). Determined through 16S-23S rRNA, the four confirmed type strains are *F. nucleatum* subsp. *nucleatum* (FNN) ATCC 25586, *F. nucleatum* subsp. *animalis* (FNA) ATCC 51191, *F. nucleatum* subsp. *polymorphum* (FNP) ATCC 10953 and *F. nucleatum* subsp. *fusiforme* (FNF) ATCC 55190 (NCTC 11326).

1.4.2.1 *F. nucleatum* subsp. *nucleatum* genomic analysis

Genomic sequencing of these type strains of *F. nucleatum* has emphasised their heterogeneity. Most commonly found in the oral cavity in patients with periodontitis (Gharbia et al., 1990), the genomic sequence of FNN (Kapatral et al., 2002) shows that despite it being recognised as a Gram-negative bacterium, it has 27% GC content making it more closely related to Gram-positive bacteria. However, its inner and outer cells wall structures have characteristics that makes it Gram-negative (Mira et al., 2004). Out of 2,067 ORFs (Open Reading Frames), 67% (1,394 OFRs) have putative functions and consequently 32% (673 OFRs) have unknown functions. While *F. nucleatum* subsp. are known to prefer using amino acids such as glutamate, histidine, serine and lysine as their energy source (Bolstad et al., 1996; Rogers et al., 1998), further analysis of FNN shows that it only has biosynthetic pathways for only 3 amino acids: aspartate, asparagine and glutamate (Kapatral et al., 2002). Nutrients from the gingival crevicular fluid undergo fermentation to produce butyrate (Rogers et al., 1998) which may cause gingival inflammation through arresting fibroblast growth, thus preventing wound healing and promoting penetration of the epithelium (Bartold et al., 1991). Therefore, the remaining amino acids have to be obtained through degradation of small peptides. Furthermore, oral bacteria are able to secrete proteases that break down protein into amino acids which can be used for energy. Amongst the 1,394 ORFs, 6% in the genome is known to be dedicated for transporters for sugar, peptides, metal ions and cofactors. In addition, ORFs of heat shock proteins and microbial resistance proteins were also identified. Interestingly, lack in choline-binding proteins may confine the organisms to the oral cavity and not the nasopharynx despite being connected (Kapatral et al., 2002). Complete genomic sequencing of FNN has created a base line for other

Fusobacterium spp. and *F. nucleatum* subsp. genomic sequencing to be compared upon to analyse any similarities and dissimilarities.

1.4.2.2 *F. nucleatum* subsp. *vincentii* genomic analysis

The following year, partial genomic sequencing of FNV was published in comparison with the previously sequenced FNN (Kapatral et al., 2003). Sequencing of FNV, which also has been isolated from the oral cavity (Dzink et al., 1990), out of the 2,277 ORFs of which 69% (1576 ORFs) are genes with known functions, 26% (570 ORFs) are hypothetical proteins and 5% (118 ORFs) are unique to FNN (Kapatral et al., 2003). Due to both FNN and FNV having a similar periodontal niche, it is expected that they share similar metabolic capabilities such as possessing ORFs for butyrate fermentation, similar to those of FNN (Kapatral et al., 2002). The same genes that contribute to antimicrobial resistance in FNN are also present in FNV. Although there is over 85% systeny between FNN and FNV, there are still 441 ORFs that are unique to FNV. This includes the presence of a ferrous iron transporter operon which is not seen in FNN. Ferrous iron transporters are commonly seen in anaerobes for soluble ferric iron transport under anaerobic conditions. Other unique genes encode for anaerobic sulphite reductase allowing conversion of sulphide from sulphite that may play a role in accepting electrons during oxidative phosphorylation (Kapatral et al., 2003).

1.4.2.3 *F. nucleatum* subsp. *fusiform* genomic analysis

Most recently, draft sequencing of FNF shows that 73.8% (1,344 ORFs) were known proteins (Park et al., 2012). While FNN has shown to synthetise three amino acids (Kapatral et al., 2002), FNF has shown a different amino acid biosynthesis of at least four amino acids: aspartate, asparagine, glutamate and glutamine. Analysis has revealed 4% of the genes are transport related and it possesses genes for virulence factors and oxidative stress. However, further genomic sequencing will be needed before further comparisons with the previous subspecies.

1.4.2.4 *F. nucleatum* subsp. *polymorphum* genomic analysis

The sequencing of FNP (Karpathy et al., 2007) revealed that FNP has the greatest number of genes compared to FNN and FNV, yet only 62% (1,514 ORFs) of the genes are shared, consequently, 38% of the genes are completely unique to FNP. Although genomically more similar to FNN (213 ORFs), this is not conclusive as the FNP genome is only partially

sequenced. Furthermore, 25% (627 ORFs) have no ortholog in either FNN or FNV. Out of the 287 hypothetical proteins, 38 ORFs were unique to FNP and was involved in transport of amino acid, oligopeptide and metal ions. Most interestingly, the presence of LuxS gene is responsible for encoding for AI-2 synthase (Schauder et al., 2001), important for AI-2 synthesis suggests FNP has the ability to communicate with other bacteria through quorum sensing, which is not seen in the previous two *F. nucleatum* strains (Karpathy et al., 2007). This confirmation that FNP synthesises AI-2 involved in bacterial communication makes it potentially a target for biofilm disruption.

1.4.2.5 High throughput genomic sequencing

More recently, DNA sequencing technologies have shown rapid evolution through the use of short-read technologies such as Illumina and longer-read technologies such as MinION (Wick et al., 2017a, b). Currently FNN and other *Fusobacterium* spp. have been sequenced using this platform (Todd et al., 2018). This combination has made genomic sequencing more time and cost efficient as well as increased accessibility through readily available online platforms (Sanders et al., 2018). Genomic sequencing has allowed a better understanding of the genetic, metabolic and pathogenic features within *Fusobacterium* spp, and *F. nucleatum* subsp. allowing further microarray and proteomics experiments to be conducted.

The difference in genomic composition of the four different subspecies of *F. nucleatum* is reflected by their virulence. *F.nucleatum* subsp. *fusiforme*/*vincentii* is often isolated from healthy site in normal oral cavity flora whereas *F. nucleatum* subsp. *nucleatum* is associated with periodontal disease (Gharbia et al., 1990). The subspecies associated with extraoral translocation leading to adverse pregnancy outcomes is *F. nucleatum* subsp. *polymorphum* and *animalis* (Han and Wang, 2013), the latter also known to be associated with inflammatory bowel disease (Strauss et al., 2011) and colorectal cancer (Ye et al., 2017).

A genomic study analysing the 16S rRNA, rpoB, zinc protease and 22 other housekeeping genes of each *F. nucleatum* subspecies found only 59% of the orthologs being shared amongst the different subspecies making them genetically divergent enough to be considered a separate species (Kook et al., 2017; Manson McGuire et al., 2014). This was confirmed through different methods such as DNA-DNA hybridisation (Kook et al., 2017) and matrix-assisted laser desorption ionization-time of flight mass spectrometry (MADI-TOF MS) (Nie

et al., 2015). A more recent study has shown that different *F. nucleatum* subsp. shows various growing capabilities in the biofilm which consequently affects interactions with surrounding species and the biofilm architecture. Late colonizers have been shown to grow better in the presence of *F. nucleatum* subsp. *nucleatum* in a subgingival biofilm model (Thurnheer et al., 2019). This emphasises the importance of recognising which *F. nucleatum* subsp. to work with when doing experiments.

1.4.3 The role of *F. nucleatum* in dental biofilm

F. nucleatum is found in abundance in the oral cavity of both healthy and diseased individuals (Han, 2015). It is the only bacteria that is known to coaggregate with both early and late colonizers (Kapatral et al., 2002; Kolenbrander and London, 1993) making it a unique bacterium which plays a critical role in biofilm formation and periodontal disease progression. Many other bacteria only coaggregate with a few specific partners (Kolenbrander et al., 2006). Its fusiform shape allows it to interact with many other microorganisms including bacteria such as *S. sanguinis*, an early colonizer and when co-cultured they organise themselves into a highly ordered corncob like structures (Lancy et al., 1983), thus playing a crucial role in structural organisation of the dental biofilm.

F. nucleatum has surface adhesins that binds to both early/initial colonizers as well as late colonizers (Kolenbrander et al., 1989), playing a crucial role for coaggregation and the advance in biofilm formation. RadD is an adhesin which coaggregates with early colonizers through binding to SpaP adhesin of *Streptococcus mutans* (Guo et al., 2017). *F. nucleatum* mutants that lacked RadD adhesins showed significantly decreased coaggregation with the early colonizer, *S. sanguinis* (Kaplan et al., 2009). Interestingly, it is not limited to binding only to bacteria, it also has the ability to bind to other microorganisms such as the fungus *Candida albicans* present in the oral environment (Grimaudo and Nesbitt, 1997). This coaggregation is again mediated through RadD (Wu et al., 2015). Furthermore, FomA is a major outer membrane protein that is thought to play an important role in coaggregating *F. nucleatum* with late colonizers such as *P. gingivalis* by functioning as a non-specific hydrophilic channels in the lipid bilayer membranes called porins (Kleivdal et al., 1995). *F. nucleatum* is also able to attach to oral mucosal cells through another adhesin called FadA (Babu et al., 1995; Han et al., 2005). Interestingly, its adherence properties differ amongst the subspecies (Xie et al., 1991) which leads to the speculation that there are strain dependent

differences in biofilm formation and development further supporting the idea of genetic diversity amongst the *F. nucleatum* subspecies.

1.4.4 The role of *F. nucleatum* in periodontal disease

If an individual has inadequate oral hygiene, the growth and maturation of a pathogenic dental biofilm causing an inflammatory response subgingivally may eventually lead to periodontitis (Lertpimonchai et al., 2017). *F. nucleatum* achieves this through its ability to coaggregate with disease causing anaerobic late colonizers including *P. gingivalis* (Rickard et al., 2003) through various adhesins including RadD, Fap2 and FomA (Coppenhagen-Glazer et al., 2015; Liu et al., 2010; Park et al., 2016). These two bacteria have a positive symbiotic relationship where *F. nucleatum* helps create a capnophilic environment enabling maximal *P. gingivalis* growth (Bradshaw et al., 1998; Diaz et al., 2002), therefore enhancing biofilm formation when co-cultured together (Saito et al., 2008b). Furthermore, co-culture of *F. nucleatum* and *P. gingivalis* shows increased in invasion of gingival epithelial cells (Saito et al., 2008a; Saito et al., 2012), which is also reflected in the observations made in the mouse model where the co-infected mouse developed larger lesions than when infected with a single strain (Feuille et al., 1996). This evidence implicates that these two oral bacteria cooperatively work together to evade destruction by the host immune system during periodontitis. *F. nucleatum* is known to be a physical 'bridge' between early and late colonizers, thus playing a crucial role in the growth of the biofilm (Bradshaw et al., 1998; Kolenbrander, 2000). When *F. nucleatum* is not present in the biofilm, there is a significant decrease in numbers of late pathogenic colonizers (Ding and Tan, 2016). This makes it a possible target for inhibiting biofilm maturation that may lead to progression of periodontitis which can eventually lead to tooth exfoliation as a result of the destruction of the periodontal supporting tissues (Polak et al., 2009).

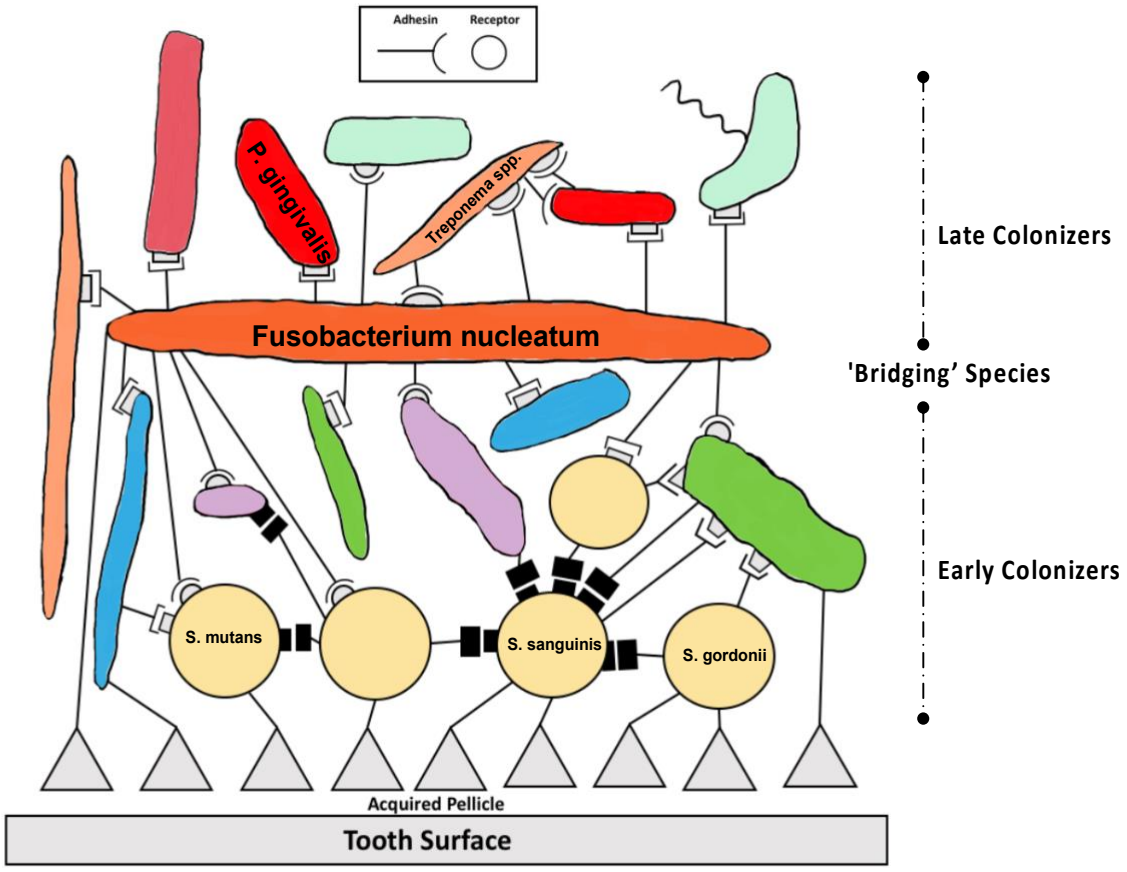

Figure 5: Schematic diagram of dental biofilms architecture

F. nucleatum (orange) coaggregates with various microorganism in the oral environment. It is able to coaggregate with early colonizers such as *S. sanguinis* (yellow) as was as periodontopathogens such as *P. gingivalis* (red). Therefore, *F. nucleatum* has been labelled as the physical 'bridge' that plays a pivotal role in the spatiotemporal succession and development of the oral biofilm that may ultimately contribute to the progression of periodontitis. (Diagram adapted from Kolenbrander et al., 2002)

1.4.5 *F. nucleatum* aids survival *of P. gingivalis*, a late colonizer

F. nucleatum within the dental biofilm complex will be exposed to constant changes within the surrounding oral environment. Therefore, it needs mechanisms to increase its chances of survival. Although *F. nucleatum* is an obligate anaerobe, it also possesses Gram-positive like characteristics (Kapatral et al., 2003). Being the important physical bridge between early and late colonizers, *F. nucleatum* may also play a crucial role in aiding survival of periodontopathogens that are more vulnerable to changes in the surrounding environment.

Bacteria in the oral environment may experience changes in oxygen and carbon dioxide levels, especially those residing in the subgingival biofilm deep in the periodontal pockets that may be exposed to residual amounts of oxygen (Marquis, 1995). Although being an obligate anaerobe, *F. nucleatum* is capable of growing in culture containing 20% oxygen which is much higher than normal oxygen content in air, possibly mediated through NADH oxidase activity (Diaz et al., 2000b). This cannot be said about *P. gingivalis* where it is unable to survive in culture with more than 6% oxygen. Additionally, *P. gingivalis* was able to survive in increasingly oxygenated environment when co-cultured with *F. nucleatum*, suggesting the role of *F. nucleatum* in protecting *P. gingivalis* during exposure to toxic levels of oxygen. Interestingly, *F. nucleatum* cells grew to 5 times their normal length in culture with 20% oxygen compared to anerobic conditions (Diaz et al., 2002). Although *F. nucleatum* itself is not thought to be pathogenic, it seems to play in direct role in the progression of periodontal diseases through supporting and protecting *P. gingivalis* and possibly other periodontal pathogens by creating a capnophilic environment.

Additionally, the pH of the oral environment is subject to constant changes not only through host diet but also through changes in bacterial metabolic activities, the latter the more important in subgingival biofilm. Studies show that *P. gingivalis* is acid sensitive (McDermid et al., 1988; Takahashi and Schachtele, 1990) while *F. nucleatum* strains were more acid tolerant and grew with or without glucose. Its metabolic flexibility to changes in surrounding pH in the oral environment could explain its wide distribution in periodontal sites (Takahashi et al., 1997). Furthermore, *F. nucleatum* has the highest acid-neutralising activities producing hydroxyl ions as a result of amino acid fermentation producing nitrogenous compounds which elevate the localised pH. This has the potential of creating a more suitable environment for acid-sensitive *P. gingivalis* which prefers to grow at a neutral pH (McDermid et al., 1988) seen in the subgingival biofilm (Eggert et al., 1991). Unlike *F. nucleatum*, *P. gingivalis* exclusively uses peptides as their source of energy (Stegink et al., 1987). Conversely, *P. gingivalis* initiates metabolic changes in *F. nucleatum* via gene expression modulation which can further accelerate biofilm formation (Yamaguchi-Kuroda et al., 2023).

These are several examples of how *F. nucleatum* is important in the development of mature biofilm and has a supportive role of late colonising periodontopathogens that are more sensitive to the changes in the environment. Therefore, *F. nucleatum* may be a potential target for biofilm disruption, thus leading to decrease periodontopathogen load.

1.4.6 Immunological pathways triggered by *F. nucleatum* and late colonizers in periodontitis

Periodontitis is caused by a complex interaction between periodontopathogens and the host immune response causing an inflammatory response, ultimately leading to destruction of the periodontium. *F. nucleatum* may play a role in periodontal disease progression by directly shaping the host immune response and increase infectivity of other periodontal pathogens. Studies have shown that *F. nucleatum* can significantly increase the production of proinflammatory cytokines including IL-8 and TNF-α and increased phagocytic elimination of neutrophils (Kurgan et al., 2017) as well as initiating apoptotic cell death of neutrophils as a protective effect by dampening the host innate immunity (Jewett et al., 2000). *F. nucleatum* and *P. gingivalis* both possess virulence factors and they work synergistically to ensure survival by modulating the host immune-inflammatory response. Inflammasomes are an important part of the host immune response to infections and/or cellular stress which activate caspases which produce proinflammatory cytokines to induce a type of cell death called pyroptosis (Almeida-da-Silva et al., 2016; Broz and Dixit, 2016). NLRP3, a well characterised inflammasome and secretion of IL-1β are critical in the host defence against infection, *P. gingivalis* (Yamaguchi et al., 2017) is known to supress *F. nucleatum*-mediated inflammasome activation (Bui et al., 2016) through reduced endocytosis (Taxman et al., 2012) which is a protective mechanism against the host immune response which ensures survival and progression of periodontitis. More recently, *F. nucleatum* has demonstrated polymicrobial synergy with *S. gordonii* and *P. gingivalis* promoting invasion of dendritic cells and consequently negatively affecting the host immune response (El-Awady et al., 2019)

F. nucleatum may also influence the host's adaptive immunity due to the chronic nature of the disease. It is suggested to play an immune-modulating role, synergistically interacting with *P. gingivalis* (Feuille et al., 1996) which affects the T-cell immune response (Choi et al., 2001). Both bacteria are also known to be associated with osteoclastic reabsorption leading to alveolar bone loss (Polak et al., 2009) possible through $CD4^+$ T cells and the proinflammatory cytokines they secrete which is an important effector of bone loss during periodontitis (Baker et al., 1999). This experimental evidence demonstrates that periodontitis is a complex disease involving the microbial community and the host immune system. *F.*

nucleatum and *P. gingivalis* can synergistically cooperate to subvert both innate and adaptative host immunity, thereby promoting bacterial invasion, survival, and progression of periodontitis.

1.5 *F. nucleatum* beyond the oral cavity

1.5.1 Systemic effects of *F. nucleatum*

Considerable evidence has shown that the effects of periodontitis can go beyond the oral cavity resulting in systemic effects originating from bacteria and bacterial products as well as inflammatory mediators from the inflamed periodontium. However, its role in other pathologies remain unclear. While it can have a symbiotic relationship in the oral environment it is known to display invasive characteristics causing opportunistic infections systemically through invasion of epithelial cells (Han et al., 2000; Saito et al., 2008a; Saito et al., 2012; Strauss et al., 2011), T cells (Kaplan et al., 2010) and macrophages (Weiss et al., 2000) through adhesins such as FadA and RadD (Ikegami et al., 2009; Kaplan et al., 2010; Xu et al., 2007). Bacterial adherence is an essential virulence factor in infections and pathogenesis.

F. nucleatum is a multifaceted bacterium that is thought to play a role in systematic diseases including gastrointestinal tract disorders (appendicitis (Swidsinski et al., 2011), inflammatory bowel disease (Strauss et al., 2011)) cardiovascular disease (Ford et al., 2006; Truant et al., 1983) and rheumatoid arthritis (Temoin et al., 2012) causing morbidity and mortality in the population (Arimatsu et al., 2014; Han and Wang, 2013). Currently there are ongoing debates on whether *F. nucleatum* is a causative or indirect agent of these infections and their route of infection still remains to be clarified (Tjalsma et al., 2012).

1.5.2 Adverse pregnancy outcomes

Interestingly, there is some evidence for *F. nucleatum* to be involved in adverse pregnancy outcomes (Han, 2011) including chorioamnionitis (Altshuler and Hyde, 1988), early onset neonatal sepsis (Wang et al., 2013) and still birth (Han et al., 2010). Pre-clinical studies have shown that intravenous administration of *F. nucleatum* in mouse models have shown to localise in the placenta which leads to still birth, suggesting that the route of infection could be hematogenous (Han et al., 2004). It has also be shown that *F. nucleatum* translocates and

invades murine placenta through binding and crossing of the endothelium then progressing onto colonising the amniotic fluid and the fetus through activation of Toll-like receptor 4, resulting in prematurity and other adverse pregnancy outcomes (Han et al., 2004; Liu et al., 2007). FadA adhesins have been implicated to play an important role in placental invasion and colonisation (Ikegami et al., 2009; Xu et al., 2007) possibly through loosened cell-cell junctions (Han and Wang, 2013).

1.5.3 Association with colorectal cancer (CRC)

More recently, there are increasing evidence that *F. nucleatum* is an oncobacterium as it is found in overabundance in human colorectal carcinoma specimens compared to healthy specimens confirming its invasive nature in the gut (Komiya et al., 2019; Zepeda-Rivera et al., 2024). According to the 'driver-passenger' model, it has been speculated that *F. nucleatum* may be a bacterial passenger rather than a driver of intestinal dysbiosis resulting in CRC and driven by the gut microbial community (Koliarakis et al., 2019; Tjalsma et al., 2012). However, its involvement in pathogenesis and tumorigenesis is still unknown (Castellarin et al., 2012). More strikingly, patients with poorer prognosis had higher abundance of *F. nucleatum* (Kostic et al., 2012; Mima et al., 2016) which could be explained by its ability to promote resistance to chemotherapy through autophagy (Yu et al., 2017b). Furthermore, *F. nucleatum* is known to promote the progression of CRC in both *in vitro* and *in vivo* systems (Kostic et al., 2013; Rubinstein et al., 2019). However, it is still uncertain if *F. nucleatum* is a marker for prognosis and management of patients with colorectal cancer (Kunzmann et al., 2019).

F. nucleatum is known to actively invade colon epithelial cells (Han, 2015; Kostic et al., 2013) through its surface adhesins. The FadA adhesin is thought to be responsible for preterm labour and has also been shown to up-regulate Annexin A1 expression thorough E-cadherin and β-catenin activation in the Wnt signalling pathway promoting growth of cancerous cells (Rubinstein et al., 2019; Rubinstein et al., 2013). Wnt pathways are important in cell development which is commonly affected during cancer (White et al., 2012). Another adhesin that may be responsible, in part, for promoting *F. nucleatum* invasion is Fap2, which directly interacts with natural killer cells to inhibit immune cell activity therefore dampening the host immune response (Gur et al., 2015). Furthermore, Fap2 is also thought to mediate adeno-carcinoma specific binding to the host factor D-galactose-β(1–3)-N-acetyl-D-

galactosamine (Gal-GalNac) which is known to be over expressed in colorectal cancer cells, leading to localisation of *F. nucleatum* in the area (Abed et al., 2016). More recent studies show that *F. nucleatum* may spread through a hematogenous route of infection and enhances the host's tumour environment by altering gene expression which promotes the hosts inflammatory response (Cochrane et al., 2020). These findings support the idea that *F. nucleatum* is not only localised and enriched in the CRC cells but may have a role in tumour development and growth.

1.6 *F. nucleatum* virulence

Bacterial pathogens exhibit virulent phenotypes through expression of surface exposed and secreted proteins that interact with other bacteria as well as host cell receptors (Casadevall and Pirofski, 1999; Ham et al., 2011). *F. nucleatum* spp. have steadily gained attention through implication in multiple clinical pathologies not only within the oral cavity but also systemically. However, due to its complex interactions with other microbes, the mechanisms of pathologies are still not well understood.

Experimental evidences show that *F. nucleatum* is unique in that they lack all varieties of protein secretion machinery expect for type 5 secreted autotransporters, and yet they are highly invasive, opportunistic pathogens that can invade different cells around the body (Liu et al., 2019; Umana et al., 2019).

1.6.1 Adhesive and invasive properties of *F. nucleatum*

Attachment precedes invasion; hence it is these surface adhesins that play a pivotal role in the disease initiation and progression. *F. nucleatum* possesses numerous outer membrane proteins called adhesins which are important in the maturation of plaque through bridging between the early colonisers and the late colonizers. RadD and CmpA are type 5a autotransporters which are known to be important for coaggregation to early colonizers (Guo et al., 2017; Kaplan et al., 2009; Lima et al., 2017). As the biofilm matures, *F. nucleatum* can further coaggregate with late colonizers such as *P. gingivalis* through FomA (Kleivdal et al., 1995) and Fap2 (Coppenhagen-Glazer et al., 2015). This demonstrates the importance of adhesins as a virulence factor of *F. nucleatum* which can contribute disease initiation and progression of periodontitis.

Other than attaching to other bacteria, *F. nucleatum* can bind to various mammalian cell types including epithelial cells (Babu et al., 1995; Han et al., 2000), endothelial cells (Han et al., 2004; Zhang et al., 2022b), PMNs, erythrocytes, fibroblasts, HeLa cells (Ozaki et al., 1990) as well as human immunoglobulin G (IgG) (Kleivdal et al., 1999). The ability to bind to various cell types permits an oral bacterium like *F. nucleatum* to colonise and disseminate away from the oral cavity and contribute to other diseases beyond the oral cavity.

More recent whole genome sequencing has brought more insight to potential virulence factors contributing to the invasion of host cells (Manson McGuire et al., 2014; Umana et al., 2019), but FadA is by far one of the best-characterised adhesins on *F. nucleatum* (Han et al., 2005). FadA is a novel adhesin unique to oral Fusobacteria and has been associated with preterm births, still births as well as promoting CRC (Han et al., 2004; Rubinstein et al., 2013). FadA deletion mutants in mice show defective host cell attachment *in vitro* (Ikegami et al., 2009).

Furthermore, FadA is not only an adhesin but also an invasin, having ability to invade various cells including normal host cells (Han et al., 2000), host immune cells (Kleivdal et al., 1999; Xu et al., 2007), tumour cells (Rubinstein et al., 2013) and placental cells (Ikegami et al., 2009). FadA has been observed to bind to cadherins on colorectal cancer cells (Rubinstein et al., 2013) and loosen the cell-cell junction molecules. Through this mechanism it is thought that *F. nucleatum* is able invade numerous tissues and body sites. In addition, FadA can also alter endothelial integrity by binding to cadherins on endothelial cells which can allow it to cross the blood barrier leading to systemic dissemination (Fardini et al., 2011). It is evident that *F. nucleatum* has various adhesins and invasins that are crucial for disease initiation and progression.

1.6.2 Interaction and evasion of host immune system

F. nucleatum can directly engage with the host immune system and induce an array of responses. FomA, which plays a role in plaque formation, is not only an adhesin (Kleivdal et al., 1995) but is also a known virulence factor which can facilitate the evasion of the host immune system by binding to human immunoglobulin G (IgG) (Kleivdal et al., 1999). Interestingly, *E. coli*-based vaccination against surface FomA of *F. nucleatum* has shown that after 3 days of inoculation of *F. nucleatum* and *P. gingivalis*, FomA immunised mice showed

supressed gingival swelling compared to the control mice. Gingival swelling was quantified through calculation of gingival volume through of digital caliper (Liu et al., 2010). Therefore, concluding that FomA on *F. nucleatum* plays an important role in progression of periodontitis through immunomodulatory effects.

Furthermore, *F. nucleatum* can activate lymphocyte apoptosis through Fap2 and RadD (Kaplan et al., 2010), stimulate inflammatory cytokine release including interleukin-8 and 6 (Han et al., 2000; Park et al., 2014) as well as influencing natural killer (NK) cells which can ultimately affect the outcome of periodontitis (Chaushu et al., 2012). In mouse studies, *F. nucleatum* shows activation of Toll-like receptor-4 (TLR4) mediated inflammatory responses in the placenta which can lead to preterm births and still births (Han et al., 2004; Liu et al., 2007). It can also promote colorectal cancer through induction of inflammatory and tumorigenic response via FadA (Rubinstein et al., 2013). Therefore, *F. nucleatum* has been termed as an opportunistic pathogen due to its ability to interact with host immune system to increase its chances of survival within the host.

1.6.3 Other virulence Factors

1.6.3.1 MORN2

Other potential virulence factors include MORN2 family domain which is another type 5 autotransporter of which its exact functions are still unknown but it is speculated to enhance adhesin and possibly invasion due to its location near other known adhesins and virulence proteins including FadA and RadD (Umana et al., 2019). It is highly specific to the *Fusobacterium* genome (Manson McGuire et al., 2014). Furthermore, the previous belief that passive invaders need additional factors such as coinfection to invade the host cell has been challenged. Whole genomic sequencing has revealed that passive invader *F. necrophorum* has the ability to bind to colonocytes even with the lack of the whole MORN2-domain (Umana et al., 2019)

1.6.3.2 CbpF and other unidentified adhesins

Recently, CbpF, a Trimeric Autotransporter Adhesin (TAA) protein family consisting of important virulence factors has been identified on *F. nucleatum* and is shown to bind to human cells (Brewer et al., 2019). In other Gram-negative bacteria, the TAA protein family is known to be important for invasion of cells (El Tahir and Skurnik, 2001; Raghunathan et al.,

2011). Although further research must be done, it is proposed that TAAs could potentially be another virulence factor that contributes to the invasive nature of *F. nucleatum* (Umana et al., 2019)

There are still genes within the *F. nucleatum* genome with unknown functions, therefore, further bioinformatic research must be done to identify the different virulence factors to further understand the virulence potential of *F. nucleatum* and the underlying mechanisms that makes it an opportunistic pathogen leading to systemic effects around the body. This will allow for future development of vaccines, screenings, and treatments to be designed against *F. nucleatum* mediated pathologies.

1.7 Future directions and overall aim of the study

1.7.1 Future directions

Although over the recent years, the role of *F. nucleatum* in extra-oral disease such as in adverse pregnancy outcomes and colorectal cancer has been highlighted, understanding its role in the pathogenesis of periodontitis is just as pivotal due to the steady increase in the number of people with periodontitis with approximately 743 million people being affected globally (Kassebaum et al., 2014).

F. nucleatum has been a focal point of oral biofilm research as it plays a crucial role in the growth of the oral biofilm due to its role in the subgingival biofilm development. It acts as a physical 'bridge', coaggregating between both early and late colonizers as well as other microorganisms. This causes a microbial shift from a healthy to a disease-causing biofilm when there is inadequate oral hygiene (Bradshaw et al., 1998; Kolenbrander, 2000). Furthermore, *F. nucleatum* has synergistic relationships with the periodontopathogen *P. gingivalis* to assist its survival in the subgingival biofilm (Diaz et al., 2002; McDermid et al., 1988) as well as playing an active part in the progression of periodontitis through modulating the host immune response (Feuille et al., 1996). This makes it a promising potential target for biofilm disruption and prevention of the progression of periodontitis which can ultimately have a negative effect on the quality of life of an individual through its role in both intra and extra oral diseases.

By *F. nucleatum* playing an important role in creating an organised biofilm in a spatiotemporal manner within the matrix produced by the bacteria, they have evolved to

obtain the ability to undergo horizontal gene transfer, transferring resistance genes that leads to antimicrobial resistance. Thereby, reducing the efficacy of antibiotic therapy on patients with periodontal disease (Hannan et al., 2010; Roberts et al., 1999; Wang et al., 2002).

Thus, investigation of novel antimicrobial agents has steadily gained attention over recent years, including silver and gold nanoparticles. Nanoparticles is thought be a considerable potential as an alternative to antibiotic therapy through interaction and disruption of the bacterial cell membrane causing increased membrane permeability which subsequently leads to bacterial lysis (Li et al., 2013).

Furthermore, development of accurate and readily available genomic sequencing of the type strains of *F. nucleatum* has not only indicated that the genome between the subspecies are vastly different enough to be considered different species, but also has enabled identification of various surface bound proteins thought to play an important role in virulence (Kook et al., 2017; Manson McGuire et al., 2014; Wick et al., 2017a). However, there are still many domains with unknown functions. Therefore, further investigations of these adhesins are needed in order to identify the functions of the surface proteins, providing better understanding of the virulence potential of *F. nucleatum* and its role in disease, both intra and extra orally as an opportunistic pathogen.

Standard approach to investigating oral biofilm has utilised end point analysis to assess biofilm dynamics (Lemos et al., 2010; Yu et al., 2017a). However, this involves destruction of the biofilm, therefore providing only a single data point with no information about the dynamics of the biofilm formation. However, more recent techniques overcome this limitation by integrating microfluidics and impendence technique, allowing for real-time, non-invasive and non-destructive label free method to monitor biofilm composition. The commercially available platform, xCELLigence® has revolutionised biofilm research by making Real-Time Cell Analysis (RTCA) of oral bacterial biofilms possible (Mira et al., 2019). Therefore, using this platform allows real-time monitoring of biofilm dynamic as well as analysis of the effects of novel antimicrobial agents.

1.7.2 Aims of the investigation

Thus, the first aim of this project is to grow and characterise the mono-species biofilm using *F. nucleatum* subsp. *nucleatum, polymorphum, fusiforme* and *animalis* to investigate if there are sub-species differences in biofilm formation. To achieve this, a protocol for growing anaerobic biofilm in a plate reader will need to be developed. For all aims, heart infusion broth (HIB) supplemented with Heamin and Vit K1 was utilised to culture the different subspecies of *F. nucleatum* including subsp. *nucleatum* ATCC 25586, subsp. *polymorphum* ATCC 10953, subsp. *fusiforme* ATCC 55190 (NCTC 11326) and subsp. *animalis* ATCC 51191.

The second aim will be to grow *F. nucleatum* subsp. *nucleatum, polymorphum, fusiforme* and *animalis* in the xCELLigence® platform under anaerobic conditions for real-time analysis of biofilm dynamics. To date, there is limited data of growing anaerobic single species oral bacteria in the xCELLigence® platform. This will then allow for further investigations such as the addition of antimicrobial agents that could potentially affect biofilm formation and maturation.

Once the protocol for growing *F. nucleatum* biofilm was established, the third aim was to characterise and investigate the efficacy of alternative and novel antimicrobial agents including D-amino acids (DAA) (Ampornaramveth et al., 2018; Zilm et al., 2017) and silver and gold nanoparticles (Kim et al., 2011; Zhang et al., 2022a). This holds importance as current treatment of periodontitis includes the use of antibiotics (Kwon et al., 2021), however, due to increase in numbers of antibiotic resistant oral bacteria this can hinder treatment of periodontitis. For all novel antimicrobial agents, different concentrations were tested to find the Minimum Inhibitory Concentration (MIC) and Minimum Bactericidal Concentration (MBC).

Successfully growing and characterising *F. nucleatum* biofilm was important to investigate the effectiveness of novel antimicrobial/antibiofilm agents that could potentially reduce biofilm formation and growth. This is clinically relevant, as further understanding contributes to the development of treatments against *F. nucleatum* mediated pathologies including periodontitis.

CHAPTER 2: MATERIAL AND METHODS

2.1 Growth Parameters

2.1.1 Bacterial strains and growth conditions

The bacterial strains used in this study were *F. nucleatum* subsp. *nucleatum* ATCC 25586, *fusiforme,* NCTC 11326, *polymorphum* ATCC 10953, *animalis* ATCC 51191. The bacteria were stored at -80°C and cultured on anaerobic blood agar plates (Thermo Scientific). Plates were incubated at 37°C in an anaerobic jar with Oxioid™AnaeroGen™ (Thermo Scientific) to create an anaerobic environment. Anaerobic conditions were confirmed using anaerobic indicator strips (Thermo Scientific). After 24 hours incubation, a single bacterial colony was transferred into 10ml of sterile heart infusion broth (HIB; Oxoid), enriched with yeast extract (5.0g/L Oxoid), L-Cysteine (0.5g/L; Aldrich), Haemin (5mg/L; Sigma) and Vitamin K1 (2mg/L; Sigma), and maintained at 37°C under anaerobic conditions. After 24 hours, bacterial suspensions were transferred into modified HIB medium and incubated under anaerobic conditions until mid-exponential growth phase (4-6 hours) for all 4 subspecies (supplementary Figure 1). Culture purity was periodically assessed using Gram staining (Bartholomew and Mittwer, 1952) and mass spectrometry (MALD-TOF) and Biotyper software (Bruker).

2.1.2 Biofilm formation in 96-well microtiter plates under anaerobic conditions in a spectrophotometer

Once mid-exponential phase was reached, bacterial suspensions were adjusted to an optical density (OD_{600nm}) of 0.3 using a NanoDrop 2000 spectrophotometer (Thermo Scientific™). 200µl of cell suspension was then added into each well of 96-well microtiter plate in triplicate with the following methods to achieve anaerobic conditions within the plate reader (Figure 6).

The microtiter plate was placed into a Synergy HTX multi-mode reader (Biotek) which was pre-heated to 37°C. Readings were taken every 15 minutes after 5 seconds of linear shaking at 600nm over 24 hours using Gen 5 software.

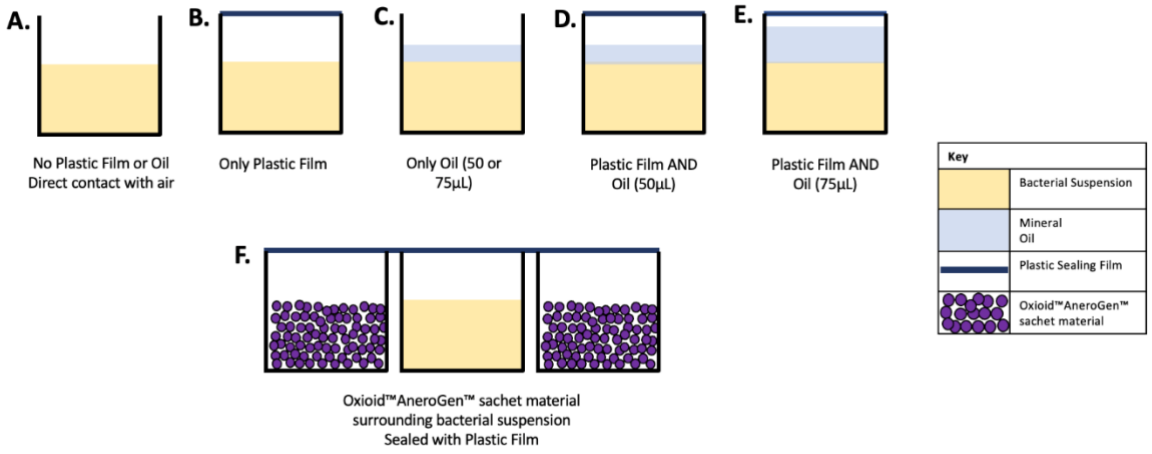

Figure 6: Schematic diagram of a cross-section of 96-well microtiter plate wells with different methods to create anaerobic environment most suitable for *F. nucleatum* biofilm to grow

(A) Bacterial suspension only. **(B)** Bacterial suspension with AxySeal Plastic Sealing Film (Axygen®) covering the wells. **(C)** Bacterial suspension with either 50µl or 75 µl of sterile mineral oil placed on top of the culture. **(D)** Bacterial suspension with 50µl of sterile mineral oil and plastic film covering the wells. **(E)** Bacterial suspension with 75µl of sterile mineral oil and plastic film covering the wells. **(F)** Bacterial suspension with Oxioid™AneroGen™ sachet material added to outermost edges of the microtiter plate sealed with AxySeal Plastic Sealing Film film covering the wells

2.1.3 Experimental protocol for Biofilm formation in a 96-well microtiter plate to test novel antimicrobial treatments

The effects of novel antimicrobial treatments were assessed in two aspects: its effect on biofilm formation and established biofilm breakdown (Figure 7). To assess the inhibition of biofilm formation using novel antimicrobial compounds, each compound was added at the start of the experiment (Figure 7.A). A broth culture was grown in modified HIB and once mid-exponential phase was reached; bacterial suspensions were adjusted to an optical density (OD_{600nm}) of 0.3 with a NanoDrop 2000 spectrophotometer (Thermo Scientific™). Then 20µl of cell suspension and 180µl of novel antimicrobial compounds diluted in modified HIB to different concentrations were added into each well of 96-well microtiter plate. Plates were incubated at 37°C in an anaerobic jar with Oxioid™AnaeroGen™(Thermo Scientific) to create an anaerobic environment. Anaerobic conditions were confirmed using anaerobic indicator strips (Thermo Scientific). Further experiments including viable cell counts, imaging (Confocal/SEM) and crystal violet staining of the biofilm were conducted afterwards to assess effectiveness of each treatment.

To assess the established biofilm breakdown of the novel antimicrobial treatments (Figure 7.B), *F. nucleatum* biofilm was first grown for 24 hours in an anaerobic jar with Oxioid™AnaeroGen™(Thermo Scientific) sachet in an 37°C incubator. The particular treatment was then added to wells and plates which were incubated at 37°C for a further 24 hours in an anaerobic jar to assess biofilm breakdown. Anaerobic conditions were confirmed using anaerobic indicator strips (Thermo Scientific). Further experiments including viable cell counts, imaging (Confocal/SEM) and crystal violet staining of the biofilm were conducted afterwards to assess effectiveness of each treatment.

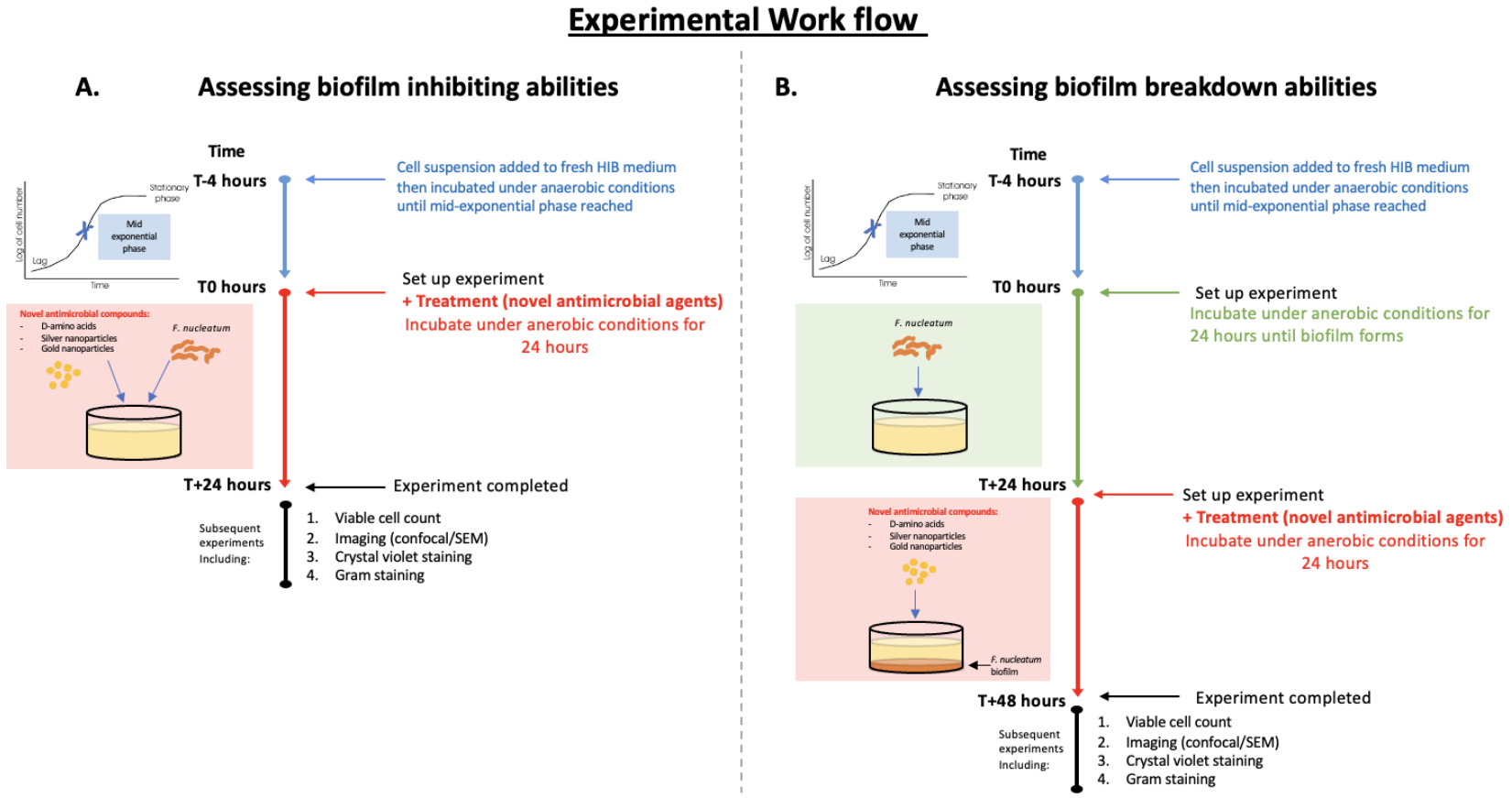

Figure 7: Flow diagram of experiments to assess biofilm inhibiting and biofilm breaking abilities by novel antimicrobial agents

(A) biofilm inhibiting abilities where novel antimicrobial agents were added at the start of the experiment and **(B)** biofilm breakdown abilities where novel antimicrobial treatments agents were added to an already established biofilm

2.2 Preparation of novel antimicrobial compounds

2.2.1 D-amino acid and L-amino acid preparation

Mixture of four D-amino acids, consisting of D-Methionine (Sigma-Aldrich; D-met), D-Leucine (Sigma-Aldrich; D-Leu), D-Tryptophan (Sigma-Aldrich; D-Trp), D-Tyrosine (Sigma-Aldrich; D-Tyr) was dissolved in to HIB (Oxoid) and supplemented with yeast extract (5.0g/L Oxoid), L-Cysteine (0.5g/L; Aldrich), Haemin (5mg/L; Sigma) and Vitamin K1 (2mg/L; Sigma). Concentrations of DAA previously described by Zilm et al (2017) was used at 25mM for D-Leu, D-Met, D-Trp and 0.25mM for D-Tyr.

The procedure was repeated using using L-Methionine (Sigma-Aldrich; L-Met), L-Leucine (Sigma-Aldrich; L-Leu), L-Tryptophan (Sigma-Aldrich; L-Trp) and L-Tyrosine (Sigma-Aldrich; L-Tyr) at the same concentration as the D-amino acid mixture.

2.2.2 Silver nanoparticle preparation

Polycationic silver nanoparticles preparation was conducted by Yanping He as part of her PhD project (He et al., 2023). Synthesis was initiated by adding 1mL of aqueous silver nitrate ($AgNO_3$; Sigma-Aldrich) solution and 1mL of prepared Branched PEI (BPEI) solution in 6mL of deionized water while stirring in an ice bath for 15 minutes. Subsequently, 35µl of freshly prepared 45nM of sodium borohydride ($NaBH_4$; Sigma-Aldrich) solution was added into the mixture in a dropwise manner under continuous stirring at 1100rpm for 2 days. After synthesis was completed, BPEI-Silver nanoparticles (BPEI-AgNP) suspension was centrifuged at 10,000g for 3 minutes, supernatant was removed and kept in the fridge until further use (He et al., 2023).

2.2.3 Gold nanoparticle preparation

Similar protocol to synthesising gold nanoparticles was conducted by Yanping He as part of her PhD project. Synthesis was initiated by adding 1mL of aqueous gold chloride (Au_2Cl_6; Sigma-Aldrich) solution and 30µL of prepared Branched PEI (BPEI) solution in 6mL of deionized water under stirring in an ice bath for 15 minutes. Subsequently, 30µl of freshly prepared 45nM of sodium borohydride ($NaBH_4$; Sigma-Aldrich) solution was added into the mixture in a dropwise manner under continuous stirring at 1100rpm for 2 days. After synthesis was completed, BPEI-Gold nanoparticles (BPEI-AuNP) suspension was

centrifuged at 10,000g for 3 minutes, supernatant was then removed and kept at 4ºC until further use.

2.3 Viable cell count

Bacterial growth after the conclusion of the experiments was assessed through viable cell counts. Bacterial suspensions were serially diluted (1:10) and 10µl of each dilution was dispensed as a drop on to anaerobic blood agar plates (Thermo Scientific) and incubated at 37°C in an anaerobic jar with Oxioid™AnaeroGen™(Thermo Scientific) for 48 hours. Each experiment was conducted in duplicate or triplicate. Colonies were then counted and the number of cells in the initial sample was determined and expressed as Colony Forming Units (CFU)/ml. Only plates containing colony numbers between 10-100 were counted.

2.4 Assessing *F. nucleatum* biofilm volume through crystal violet staining

2.4.1 Biofilm quantification by crystal violet staining

Crystal violet (CV) staining protocol was slightly modified from the method described by Muchova et al (2022). To quantify *F. nucleatum* biofilm, after experimental completion, biofilms were washed carefully with 100µl PBS, avoiding excessive biofilm dispersion. Plates were then air-dried at 37°C before stained with CV solution (200µl, 0.1% w/v) for 1 hour at room temperature. Biofilms were then gently washed once with 200µl PBS and air dried for 3 hours in the incubator. To de-stain the biofilm, ethanol (100%, 200µl) was added then left at room temperature for 1 hour. Finally, each sample was diluted with sterile Milli-Q water (1:10) in a 96-well microtiter plate before absorbance was measured at 600nm using Synergy HTX multi-mode reader (Biotek). Each experiment was conducted using a row of 96-well microtiter plate (12 replicates).

2.4.2 Surface coating before crystal violet staining

To investigate if *F. nucleatum* biofilm adherence could be increased before crystal violet staining, a row of wells in the 96-well microtiter plate were coated with either Poly-L-Lysine (PLL) or sterile saliva. 30µl of PLL (0.1% w/v) solution was added to evenly coat the bottom of the wells and left for 5 minutes at room temperature. Solution was then removed by aspiration and washed once with sterile PBS as per the manufacture's recommendation. Plates were then left in the laminar flow hood to dry before use.

Saliva coating was performed by evenly coating the bottom of the wells with 30µl of filtered human saliva which was left to air dry in a fume hood for one hour. Any remaining saliva was removed, and the plate was dried for further one hour in the fume hood before experimental samples were added.

2.4.3 Biofilm fixing before crystal violet staining

After experimental completion, to decrease the dispersion of biofilms and decrease variability between replicates, some samples were fixed with 4% Formaldehyde for 10 minutes at room temperature before continuing with the crystal violet staining protocol mentioned above.

2.5 Imaging

2.5.1 Confocal Imaging

To assess biofilm volume and viability of the bacteria within the biofilm, *F. nucleatum* single species were cultured with and without treatments in µ-Slide 8 Well ibidiTreat plates (Ibidi) in preparation for confocal imaging.

Once mid-exponential phase was reached, bacterial suspensions were adjusted to an optical density (OD_{600nm}) of 0.3 with a NanoDrop 2000 spectrophotometer (Thermo Scientific™). Some samples were further diluted 1:10 or 1:100 into modified HIB medium with or without novel antimicrobial compounds suspended in modified HIB media to give a total volume of 200µl in each well. Experiments were conducted in duplicate.

After completion of experiment, selected samples were fixed with 4% paraformaldehyde (Chem-supply) for 10 minutes. Then each well was stained following manufacturer's instruction using the LIVE/DEAD™ Baclight™ Bacterial Viability Kit (Invitrogen™). One PBS wash was used to minimise dispersion and disruption of biofilms. Samples were then imaged immediately using Confocal Laser Scanning Microscopy (CLSM) using the Olympus FV3000 at 40x and 60x magnifications (Adelaide Microscopy, The University of Adelaide).

Confocal microscopy images were analysed using Imaris 3D/4D 260 image visualization and analysis software was used to calculate biofilm volume and bacterial cell viability.

2.5.2 SEM imaging

SEM imaging was conducted to examine axenic-subspecies *F. nucleatum* biofilm architecture. Biofilm was grown on 12mm diameter round cover glasses (Thermo Scientific) in 24 well cell culture plates (Costar®) overnight in an anaerobic jar. After the completion of the experiment, biofilms were then fixed for at least one hour in EM fixative solution (4% Paraformaldehyde/ 1.25% Glutaraldehyde in PBS with 4% sucrose, at pH 7.2). Washing buffer (PBS with 4% sucrose) was used to rinse the fixation solution for 5 minutes.

Following fixation, biofilms were left in osmium tetroxide (OsO_4) in water for 1 hour. Biofilms were then dehydrated with two changes of increasing ethanol concentrations (70%-100%) for 15 minutes.

Drying agent made up of hexamethyldisilane (HMDS; Electron Microscopy Sciences) 1:1 with 100% ethanol was applied for 10 minutes before 2 changes of 100% HMDS was applied for 10 minutes each time. Remaining HMDS was removed, and coverslips were left to dry for at least 2 hours before they were mounted onto SEM specimen stubs (ProSciTech), coated with 3mm platinum, and visualised using scanning electron microscope (FEI ESEM Quanta 450). Images were taken at 5,000x and 40,000x magnifications (Adelaide Microscopy, The University of Adelaide).

2.6 xCELLigence® RTCA System

2.6.1 Real-time biofilm analysis of *F. nucleatum* biofilms

The xCELLigence® E-plates are equipped with gold electrodes at the bottom of each well (Figure 8.A). Electrical impedance between the electrodes is proportional to biofilm formation and expressed as an arbitrary unit called Cell Index (CI) by the RTCA Analysis Program (Figure 8.E).

All four *F. nucleatum* subspecies were grown individually in the xCELLigence® E-plate 16 PET (ACEA, Biosciences Inc.) to monitor biofilm dynamics. Experimental samples were prepared by transferring bacterial suspensions into modified HIB medium and incubating at

37ºC under anaerobic conditions until mid-exponential growth phase (4-6 hours) for all 4 subspecies. Bacterial suspensions were then adjusted to an optical density (OD_{600nm}) of 0.3 with a NanoDrop 2000 spectrophotometer (Thermo Scientific™). 200µl of cell suspension was then added into each well. The E-plates were incubated at 37°C for 24 hours and each experiment was conducted in duplicate (Figure 8.D). The xCELLigence® E-plate 16 VIEW (ACEA, Biosciences Inc.) was also used for confocal microscopy evaluation of biofilms.

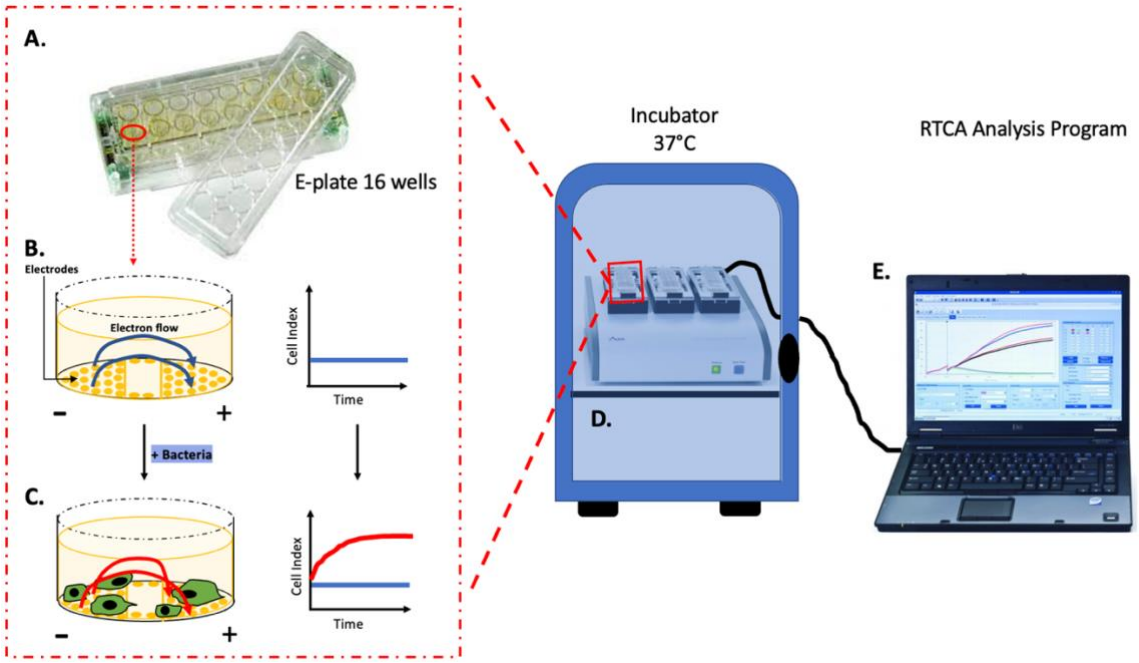

Figure 8: Using xCELLigence® RTCA system to monitor *F. nucleatum* biofilm formation
(A) Image of xCELLigence® E-plate with 16 wells (single well outlined in red) **(B)** Magnified view of a single well of the xCELLigence® E-plate without any biofilm formation. No change in electrical impedance is reflected as no changes in CI. The number and size of electrodes are not drawn to scale and are for illustrative purposes. **(C)** When biofilm forms the electrical impedance is increased, this is reflected as increase in CI. **(D)** The E-plate is placed into a cradle within the RTCA station and is incubated at 37°C for 24 hours. **(E)** This data is then recorded via the RTCA Analysis Program installed into the computer which is then used for further analysis once experiment is completed.

2.6.2 Creating anaerobic environment within xCELLigence® E-plates

To create an anaerobic environment required for the *F. nucleatum* biofilm to develop, after bacterial suspensions were added into the xCELLigence® E-plate, AnaeroGen™(Thermo

Scientific) anaerobic sachet material was dispensed into the central evaporation wells (Figure 9.A and B) and the lid was sealed with dental impression material (Honigum-Mono- DMG). Anaerobic conditions were confirmed using anaerobic indicator strip in an evaporation well (Thermo Scientific).

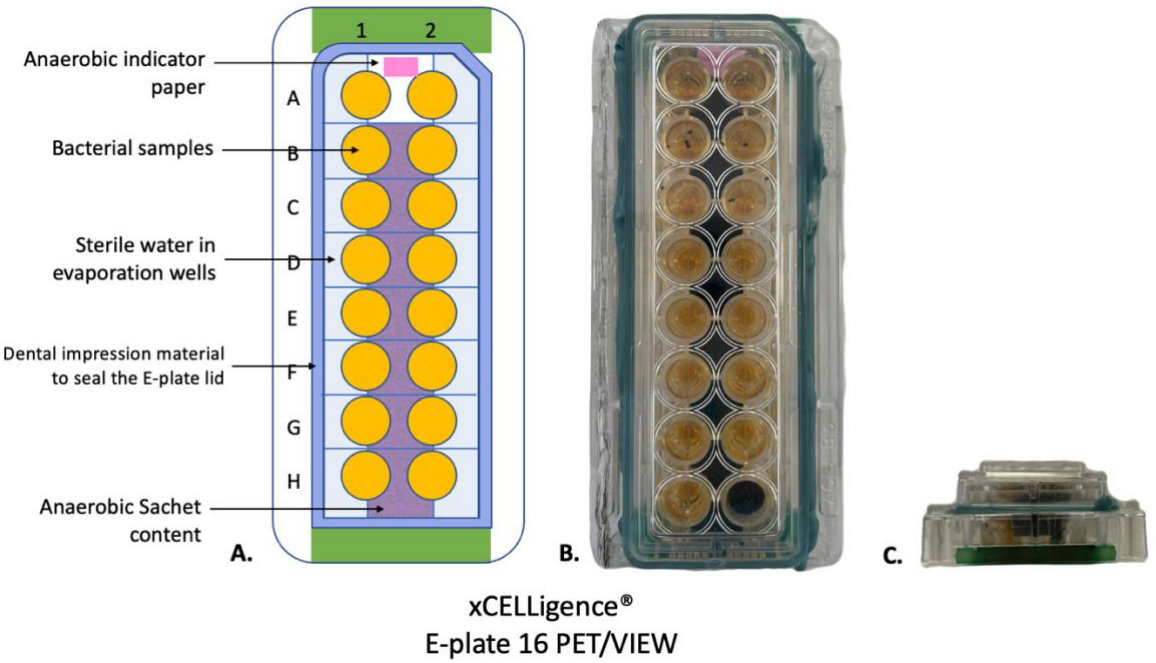

Figure 9: Schematic diagram of xCELLigence® E-plate 16

(A) Illustration of experimental set up in a xCELLigence® E-plate with 16 wells, modified to create an anerobic environment within the E-plate for *F. nucleatum* biofilm form. **(B)** Photo of modified xCELLigence® E-plate experimental setup to create an anaerobic environment. **(C)** Side view of xCELLigence® E-plate

2.6.3 Human saliva collection

Author's own stimulated human whole saliva samples were collected into sterile 30ml tubes while chewing on sugar free gums for 5 minutes. Samples were diluted with sterile PBS to decrease viscosity and filtered using a 0.22µm MS® sterile syringe filter (Membrane solutions). Sterilised human saliva was stored at -20°C until required.

2.6.4 Saliva coating xCELLigence® E-plates

The xCELLigence® E-plate wells were coated with 100µl of filtered saliva which was left to air dry in a fume hood for one hour. Any remaining saliva was removed, and the plate was dried for further one hour in the fume hood before experimental samples were added.

2.6.5 Preparing xCELLigence® E-plates for confocal imaging

The xCELLigence® E-plate 16 VIEW was used for confocal imaging due to the different arrangements of the gold electrodes embedded at the bottom of the wells which allows larger imaging windows (Figure 10.B; Green arrow) compared to the PET E-plates (Figure 10.A; Yellow arrow). In addition, the VIEW E-plates also have glass bottom wells suitable for imaging.

After the completion of the experiment, the xCELLigence® E-plate 16 VIEW was prepared for confocal imaging by using the Bunsen burner to heat a scalpel blade which was used to score the periphery of the E-plates (Figure 11.A; Red dotted line). Caution was taken while using pliers to remove the plastic to ensure samples where not disrupted during the process (Figure 11.B). E-plates were customised to ensure there was no gap in between the bottom of the wells and the confocal microscopy lens, which could affect overall image quality (Figure 12). Once all 4 sides of the E-plate were removed, the modified xCELLigence® E-plate 16 VIEW was prepared for confocal imaging (Figure 11.C).

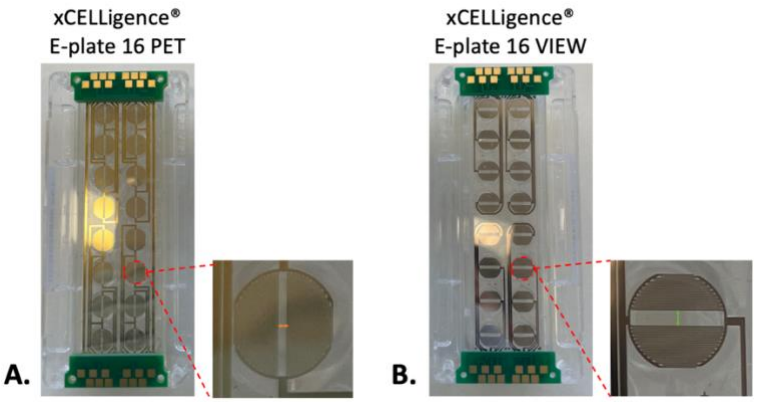

Figure 10: Comparison of xCELLigence® E-plate 16 well PET and VIEW

(A) Image of underside of xCELLigence® E-plate 16 well PET showing gold electrode arrangements. Group of electrodes under single well (red) is outlined and magnified with the arrow (orange) showing gap between the electrodes present. Bottom of the E-plate is constructed of plastic. **(B)** Image of underside of xCELLigence® E-plate 16 well VIEW showing gold electrode arrangements. Group of electrodes under single well (red) is outlined and magnified with the arrow (green) showing larger gap between the electrodes present compared to the PET E-plate electrode arrangement (orange). Bottom of the E-plate is constructed with glass making it suitable for imaging.

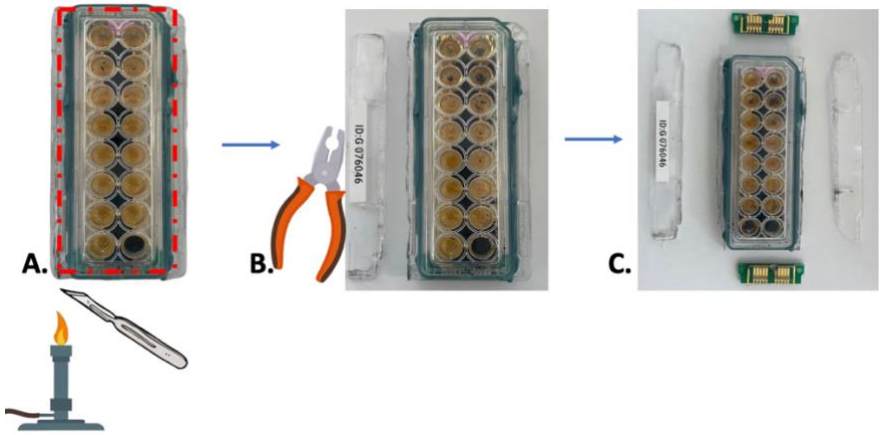

Figure 11: Schematic diagram of preparation of xCELLigence® E-plates for confocal imaging

(A) Open flame was used to heat up the scalpel to score the plastic xCELLigence® E-plate after completion of experiment (red dotted line) **(B)** Pliers were used to remove the sides of the E-plate along the scoring **(C)** Final result after all 4 sides of E-plate was removed in preparation for confocal microscopy

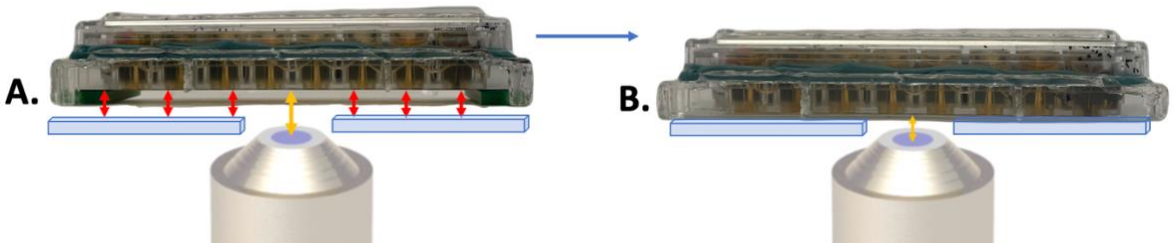

Figure 12: Comparison of xCELLigence® E-plate 16 well VIEW before and after customisation by removal of peripheral plastic

(A) Schematic diagram if the peripheral plastic of the E-plate was not removed and confocal microscopy was attempted to image the biofilm. The significant gap between the bottom of the wells and the confocal microscopy lens (red arrows) affected overall image quality due to greater distance between the two entities (yellow arrow). **(B)** Schematic diagram showing how customising the E-plates by removing the peripheral plastic allows for the glass bottom to sit flush with the confocal stage to reduce distance between the bottom of the wells and the microscopy lens (yellow arrow).

2.6.6 Confocal Imaging of xCELLigence® plates

After completion of experiment, each well of the xCELLigence® E-plate 16 VIEW was stained following manufacturer's instruction using the LIVE/DEAD™ Baclight™ Bacterial Viability Kit (Invitrogen™). One PBS wash was used to minimise dispersion and disruption of biofilms. Samples were then imaged using Confocal Laser Scanning Microscopy (CLSM) using the Olympus FV3000 at X40 magnification (Adelaide Microscopy, The University of Adelaide).

2.7 Statistics and analysis

Statistical analysis was conducted for appropriate data with help of Dr Tomas Sullivan (SAHMRI Biostatistics Unit). The results displayed as mean and standard deviations. Where applicable, data were analysed with Kruskal-Wallis test with Dunn's multiple comparison post-hoc test or unpaired t-tests. GraphPad Prism version 8.4.3 for OS X, GraphPad Software LLC, San Diego, California USA (Ivashchenko, 2020). To be noted that ns denotes no significant difference, * denotes significant difference compared to the control (* $p<0.05$, ** $p<0.01$, ***$p<0.001$, **** $p<0.0001$).

CHAPTER 3: RESULTS

3.1 Protocol optimisation to grow *F. nucleatum* in a spectrophotometer

3.1.1 Developing protocol for creating an anerobic environment *F. nucleatum* species in 96-well microtiter plates in a spectrophotometer

3.1.1.1 Growing F. *nucleatum* biofilm in a spectrophotometer

Several growth conditions were used to maximise the growth of different *F. nucleatum* subspecies in 96-well microtiter trays. With the spectrophotometer pre-heated to 37°C but in the absence of a mineral oil layer or AxySeal Plastic Sealing Film (Axygen®), FNP and FNA showed minimal growth over 10 hours (Figure 13). FNF and FNN differed as log phase growth occurred over 7 hours reaching an OD near 1.0 at 8 hours, this was followed by a rapid decrease in OD.

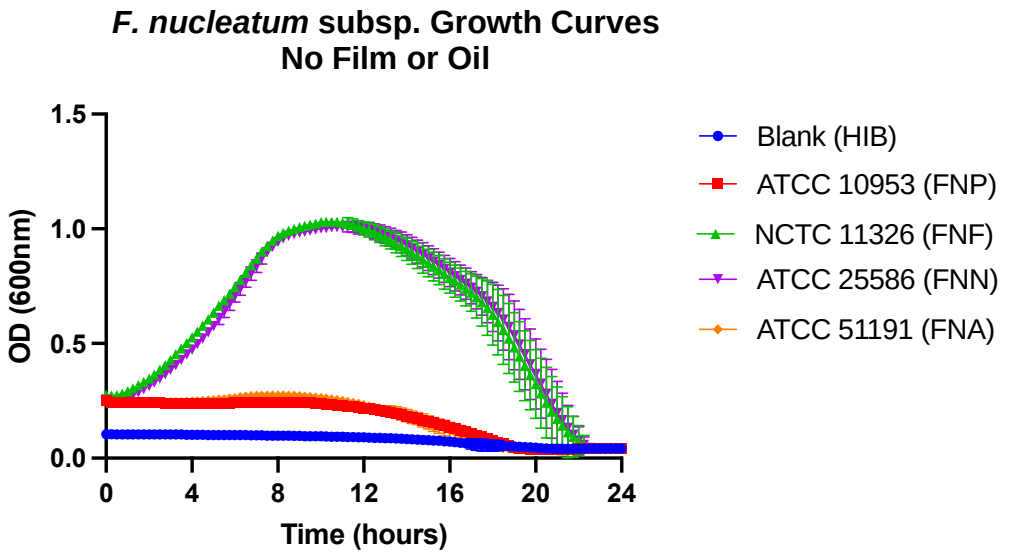

Figure 13: *F. nucleatum* growth curves in a 96-well plate with no film or oil layer
Growth curves for each *F. nucleatum* subspecies with no film or mineral oil layer. Sterile modified HIB served as blank. Each experiment was conducted in triplicate. Error bars represent standard deviation.

3.1.1.2 Effect of mineral oil overlay to create anaerobic conditions for growth of *F. nucleatum*

To create a more anerobic environment, sterile mineral oil was dispensed on the top of each well before the tray was placed into the spectrophotometer. Compared to the absence of mineral oil, FNP and FNA showed improved growth represented by an increase in OD_{600nm} reaching maximum OD of 0.789 and 0.669 compared to 0.246 and 0.279 respectively (Figure 14). In addition, the OD_{600nm} remained steady after 10 hours compared to the decrease in OD_{600nm} observed in the absence of mineral oil (Figure 14). Interestingly, the use of sterile mineral oil with FNN and FNF did not affect the log phase, however, the rapid decrease in OD_{600nm} after around 8 hours was absent (Figure 15).

3.1.1.3 Effect of mineral oil on growth of *F. nucleatum*

FNP, FNN and FNF followed similar growth curves after addition of either 50µl or 75µl sterile mineral oil (Figure 14 & 15). Only FNA showed improved growth over 24 hours with 75µl mineral oil (maximum OD 0.669) and an increase in generation time (log phase) in the first 4 hours of the experiment compared to 50µl (maximum OD 0.578) (Figure 14.B). For all subspecies, mineral oil maintained the OD_{600nm} over the 24-hour period. In conclusion, 75µl of sterile mineral oil created a sufficient anaerobic environment for the growth of all four subspecies (Figure 16).

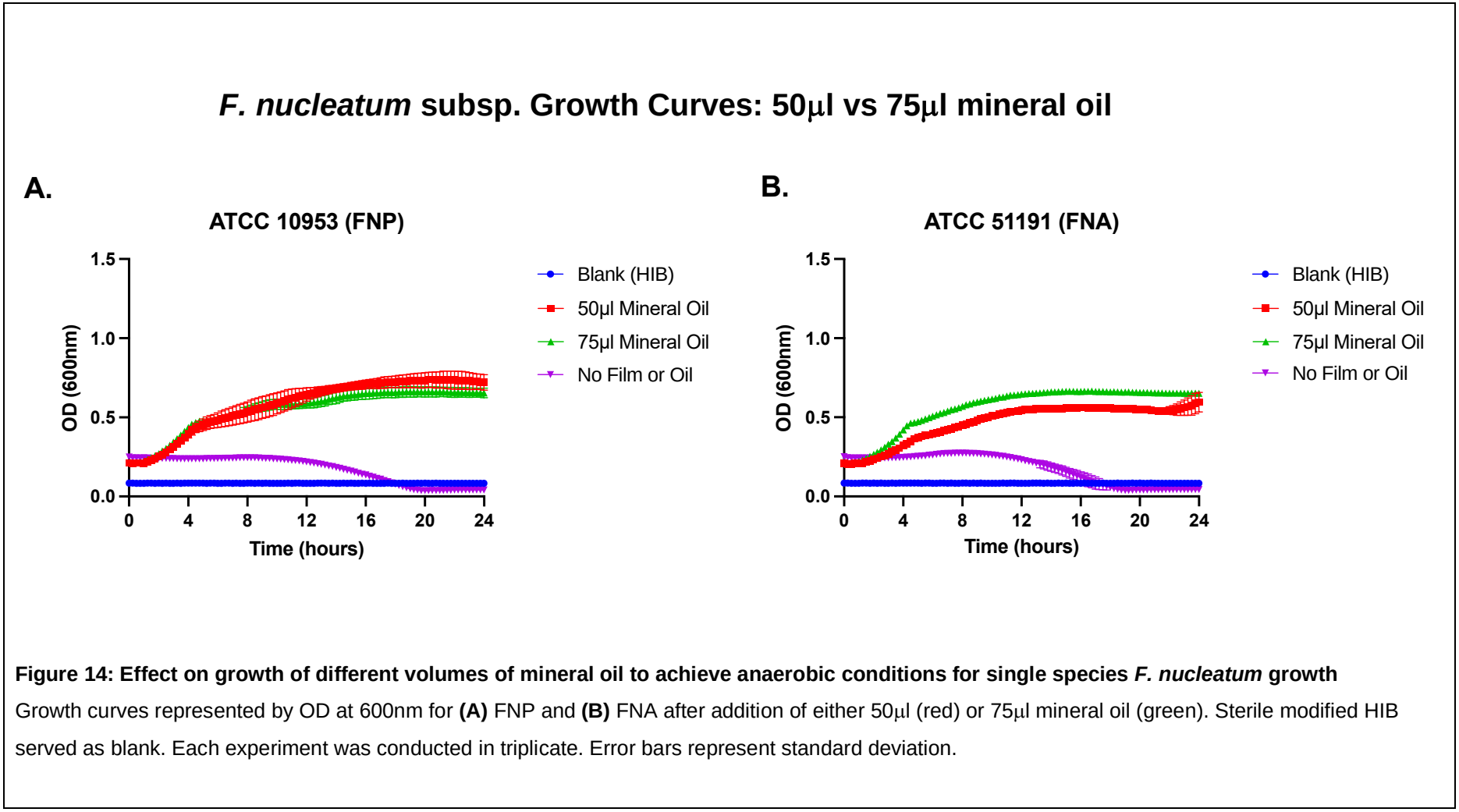

Figure 14: Effect on growth of different volumes of mineral oil to achieve anaerobic conditions for single species *F. nucleatum* growth

Growth curves represented by OD at 600nm for **(A)** FNP and **(B)** FNA after addition of either 50µl (red) or 75µl mineral oil (green). Sterile modified HIB served as blank. Each experiment was conducted in triplicate. Error bars represent standard deviation.

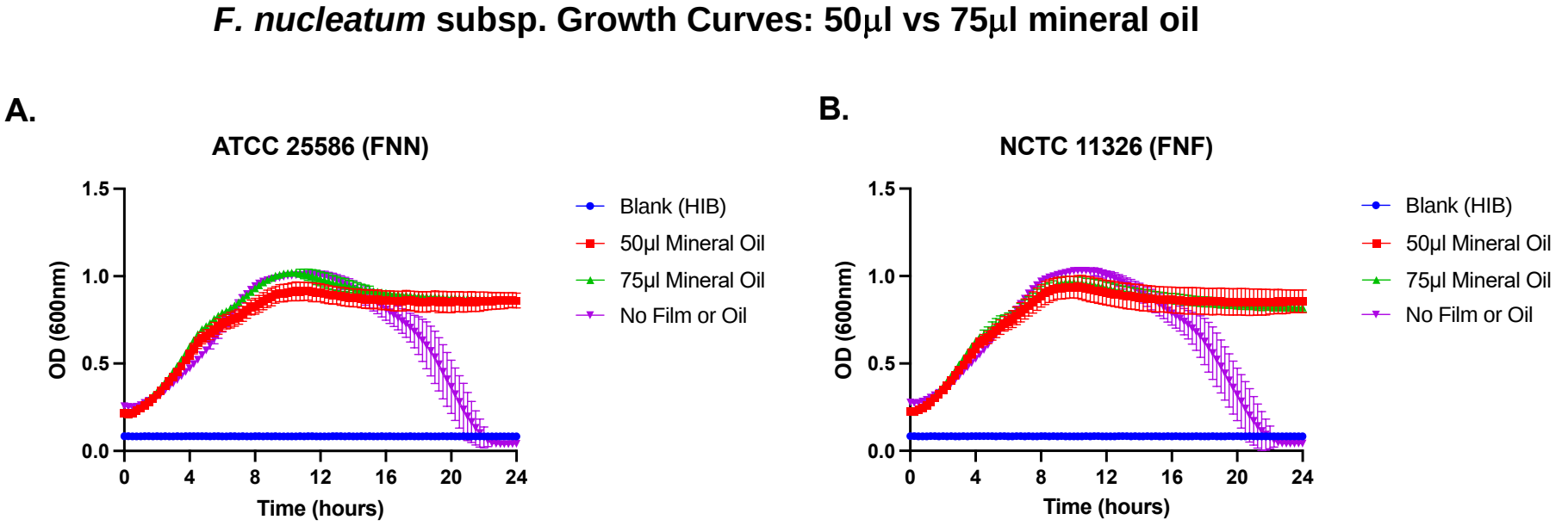

Figure 15: Effect on growth of different volumes of mineral oil to achieve anaerobic conditions for single-species *F. nucleatum*

Growth curves represented by OD at 600nm for **(A)** FNN and **(B)** FNF after addition of either 50µl (red) or 75µl mineral oil (green). Sterile modified HIB served as blank. Each experiment was conducted in triplicate. Error bars represent standard deviation.

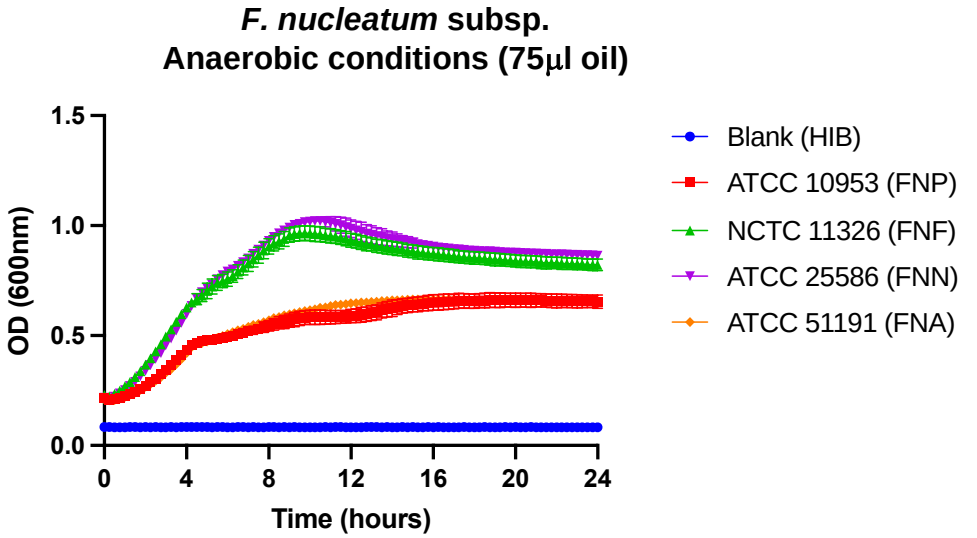

Figure 16: Single-species *F. nucleatum* growth curves using 75µl mineral oil

Growth curves represented by OD at 600nm for ATCC 10953 (red), NCTC 11326 (green), ATCC 25586 (purple) and ATCC 51191 (orange) with 75µl mineral oil over 24 hours. Sterile modified HIB served as blank. Each experiment was conducted in triplicate. Error bars represent standard deviation.

3.1.1.4 Effect of sealing 96-well microtiter plate with AxySeal Plastic Sealing Film to create anaerobic conditions for growth of *F. nucleatum* inoculum

The effectiveness of sealing the 96-well microtiter plate with AxySeal Plastic Sealing Film was also compared to adding mineral oil to create an anaerobic environment. Improved growth was observed in FNP, FNN and FNF with sealing the plate with AxySeal Plastic Sealing Film compared to the mineral oil overlay. This increase in OD reached a maximum of 0.893, 1.260 and 1.187, compared to mineral oil where the maximal OD reached 0.696, 1.040, and 0.985 respectively (Figure 17 and 18). FNA showed minimal difference between the use of AxySeal Plastic Sealing Film (maximum OD 0.766) and mineral oil only (maximum OD 0.671) (Figure 17). Interestingly, the combination of mineral oil and AxySeal Plastic Sealing Film did not have synergistic effects (Figure 17 and 18). Moreover, the use of film only appeared to have the greatest effect on improving growth (Figure 17 and 19).

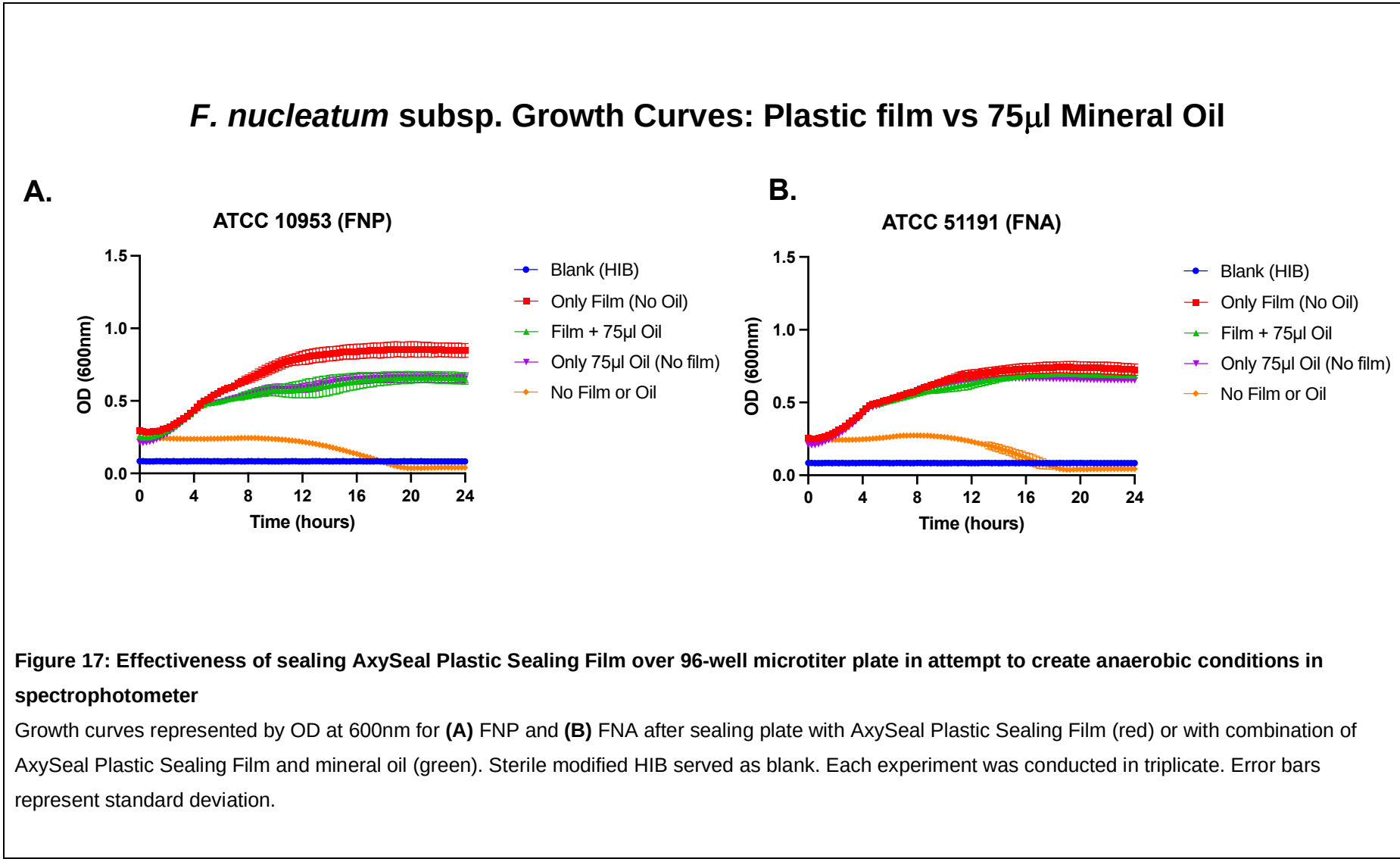

Figure 17: Effectiveness of sealing AxySeal Plastic Sealing Film over 96-well microtiter plate in attempt to create anaerobic conditions in spectrophotometer

Growth curves represented by OD at 600nm for **(A)** FNP and **(B)** FNA after sealing plate with AxySeal Plastic Sealing Film (red) or with combination of AxySeal Plastic Sealing Film and mineral oil (green). Sterile modified HIB served as blank. Each experiment was conducted in triplicate. Error bars represent standard deviation.

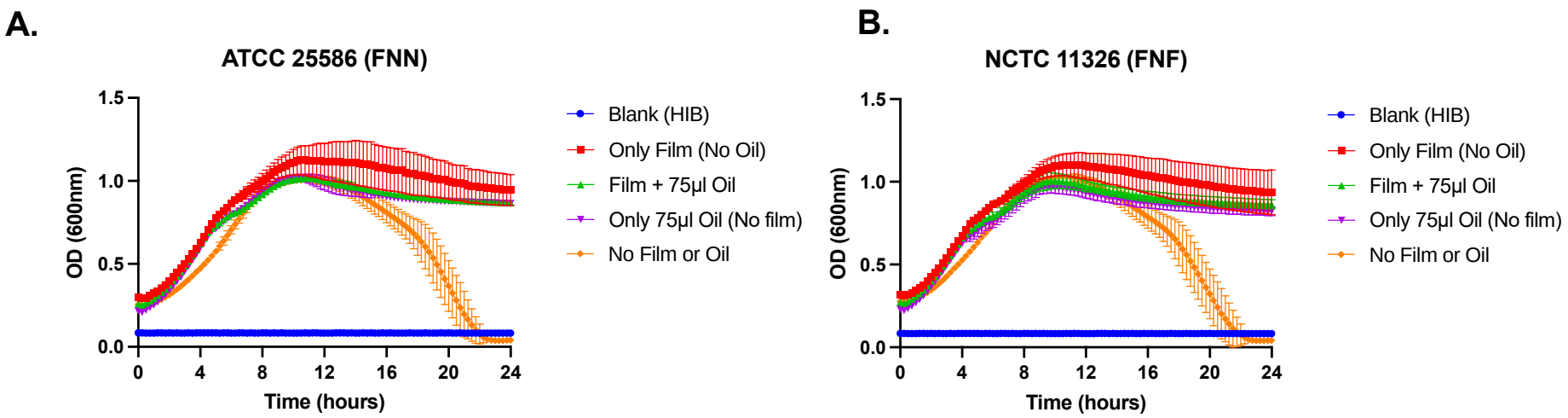

Figure 18: Effectiveness of sealing AxySeal Plastic Sealing Film over 96-well microtiter plate in attempt to create anaerobic conditions in a spectrophotometer

Growth curves represented by OD at 600nm for **(A)** FNN and **(B)** FNF after sealing plate with AxySeal Plastic Sealing Film (red) or with combination of AxySeal Plastic Sealing Film and mineral oil (green). Sterile modified HIB served as blank. Each experiment was conducted in triplicate. Error bars represent standard deviation.

3.1.1.5 Effect of combined use of AxySeal Plastic Sealing Film and anaerobic sachet material for growth of *F. nucleatum* in a spectrophotometer

Additionally, additional experiments were conducted to further improve *F. nucleatum* growth in a 96-well tray in the spectrophotometer. Oxioid™AnaeroGen™ (Thermo Scientific) anaerobic sachet material was dispensed into peripheral wells of 96-well microtiter plates before being sealed with AxySeal Plastic Sealing Film (Figure 19). Initial growth of FNP and FNA, represented by an increase in OD_{600nm}, was greater with the anaerobic sachet material sealed with film reaching maximum OD of 0.971 and 0.841 compared to film alone (maximum OD 0.893 and 0.768, respectively) (Figure 20). FNP improved the most of compared to the four subspecies with anaerobic sachet material and film (Figure 20). Interestingly, film only experimental samples showed slightly better growth in FNN and FNF, compared to the combination of sachet and film (Figure 21).

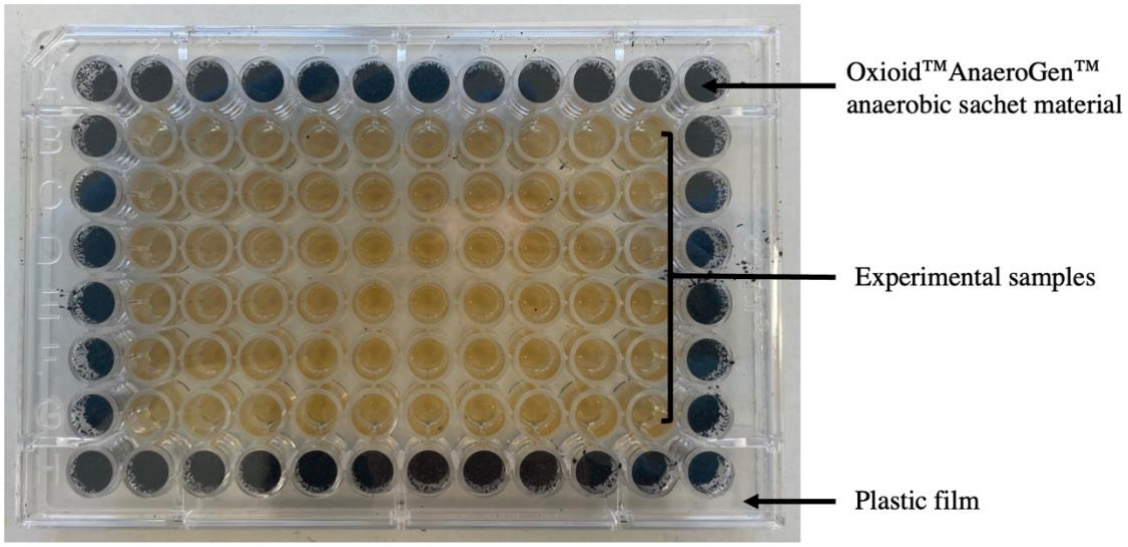

Figure 19: 96-well microtiter plate set up to create an anaerobic environment in wells while placed in the spectrophotometer. Experimental samples surrounded by AnaeroGen™(Thermo Scientific) anaerobic sachet material was dispensed into the peripheral wells of 96-well plates then sealed with a AxySeal Plastic Sealing Film before being placed into the spectrophotometer for 24 hours at 37°C.

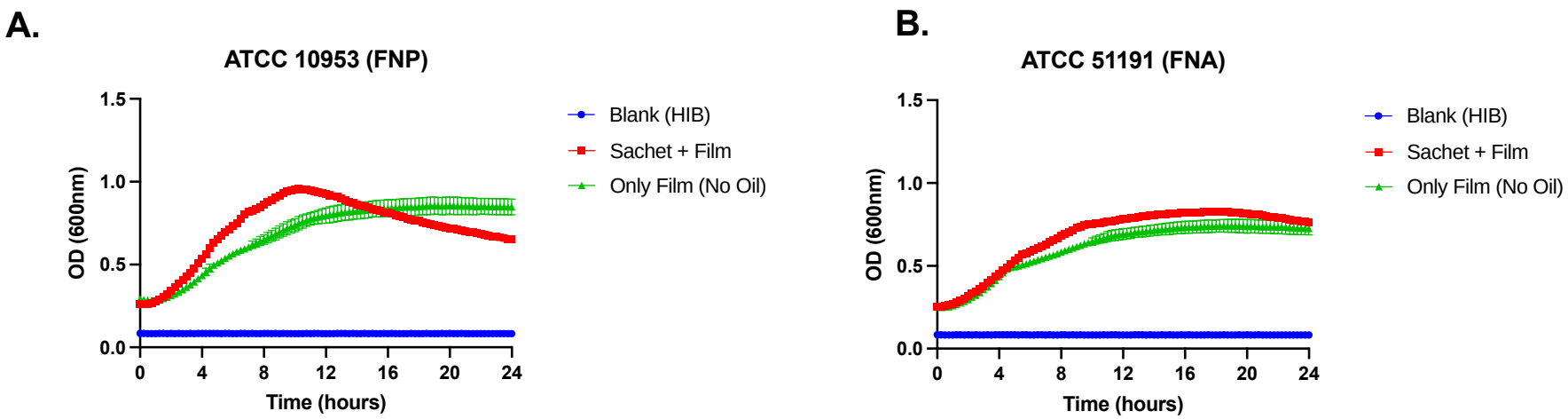

Figure 20: Comparison of effectiveness of sealing 96-well plates with AxySeal Plastic Sealing Film with or without AnaeroGen™ anaerobic sachet material

Growth curves represented by OD at 600nm for **(A)** FNP and **(B)** FNA after sealing plate with AxySeal Plastic Sealing Film only or with anaerobic sachet material. Sterile modified HIB served as blank. Each experiment was conducted in triplicate. Error bars represent standard deviation.

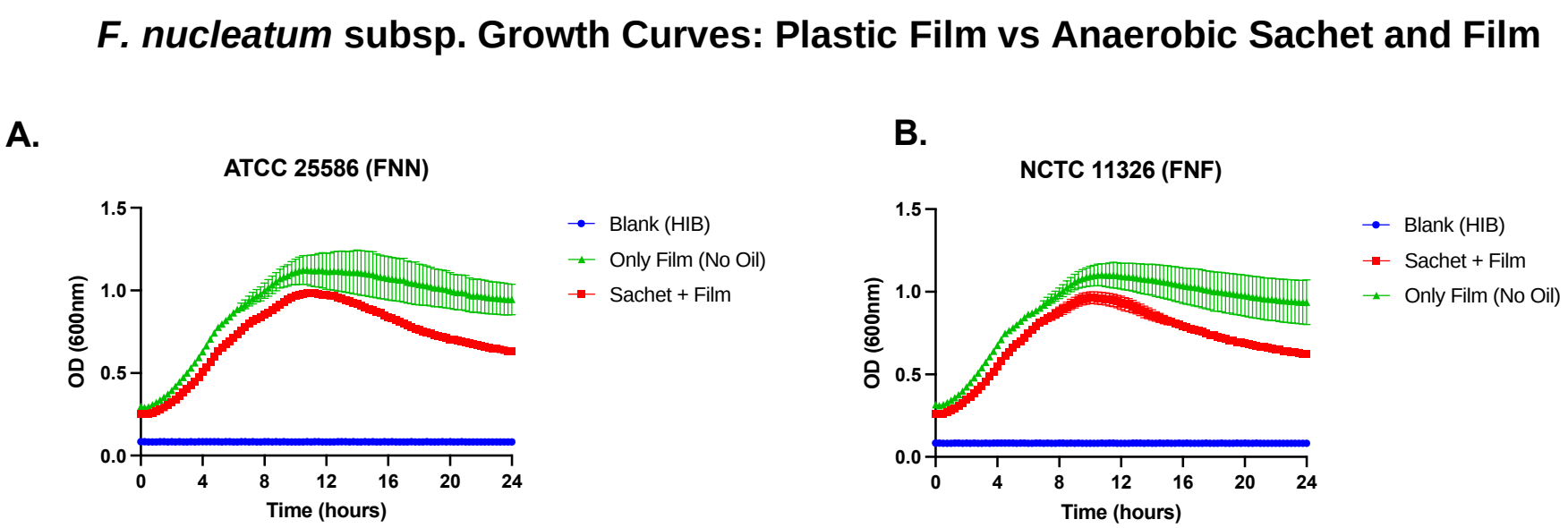

Figure 21: Comparison of effectiveness of sealing 96-well plates with AxySeal Plastic Sealing Film with or without AnaeroGen™ anaerobic sachet material

Growth curves represented by OD at 600nm for **(A)** FNN and **(B)** FNF after sealing plate with AxySeal Plastic Sealing Film only or with anaerobic sachet material. Sterile modified HIB served as blank. Each experiment was conducted in triplicate. Error bars represent standard deviation.

3.1.1.6 Growth curves of 4 subspecies of *F. nucleatum* over 24 hours in the spectrophotometer

All four subspecies of *F. nucleatum* was successfully grown under anaerobic conditions within the spectrophotometer created using anaerobic sachet material and plates sealed with AxySeal Plastic Sealing Film and growth curves were established for each subspecies of *F. nucleatum* (Figure 22). FNP, FNF and FNN all had similar growth curves while FNA appeared to have an increased doubling time during log phase. Doubling time was derived from these growth curves for all four subspecies (Supplementary Figure 1).

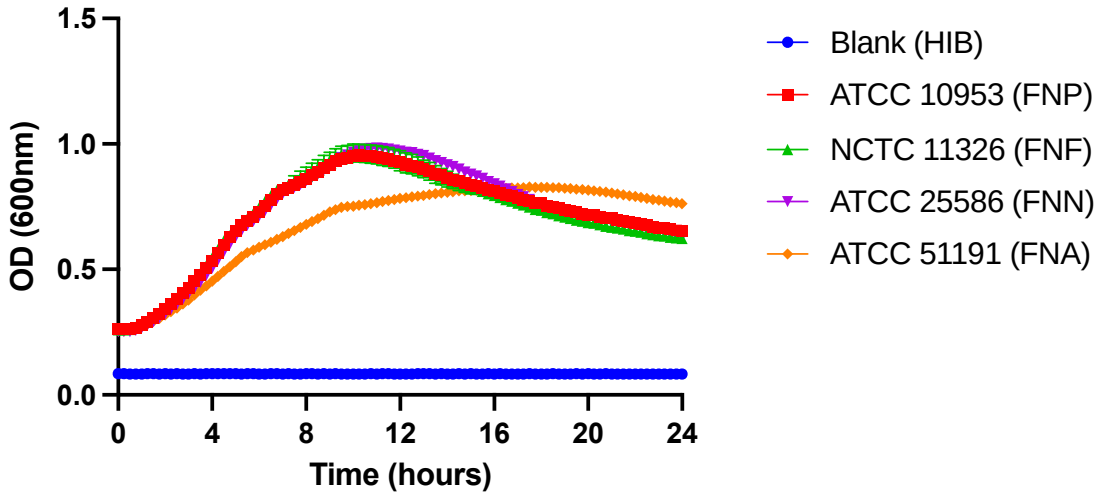

Figure 22: Single-species *F. nucleatum* growth curves using 96-well plates and anaerobic sachet material and sealing with AxySeal Plastic Sealing Film

Sterile modified HIB served as blank. Each experiment was conducted in triplicate. Error bars represent standard deviation.

3.1.2 Optimising the protocol for crystal violet staining in 96-well microtiter plates to assess *F. nucleatum* biofilm growth.

F. nucleatum biofilms grown in modified HIB were more resilient and could withstand multiple washing and staining steps during the CV protocol compared to DAA treated biofilms. DAA treated biofilms appeared to be loosely attached which caused excessive disruption during the multiple washing steps, leading to greater variability in the results. This suggests that DAAs were disrupting the biofilm. This was less obvious in control groups where *F. nucleatum* was grown in modified HIB where minimal variability in the results was observed (Figure 23). Therefore, for the following experiments, DAA treated *F. nucleatum* biofilms were used to optimise the protocol for CV staining to achieve more consistent results and minimise the disruption of the biofilm. Subspecies, FNN (ATCC 25586) was used for these experiments.

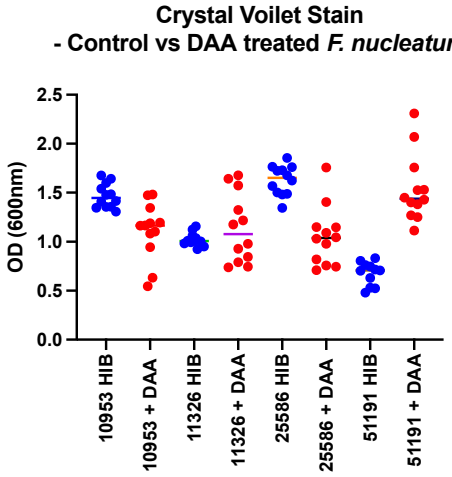

Figure 23: Scatter plot graph showing OD_{600nm} representing *F. nucleatum* control biofilm vs DAA treated biofilm

Distribution of results of four *F. nucleatum* subspecies comparing control (blue) and DAA treated (red) groups (n= 12) after crystal violet staining.

3.1.2.1 Effect of saliva coating 96-well microtiter plate wells on *F. nucleatum* subsp. *nucleatum* biofilm adhesion

Pre-coating the 96-well microtiter plate with sterile human saliva before growing the *F. nucleatum* biofilm treated with DAA did not improve the adhesion of biofilm. No significant differences (z-statistic for comparison = 0.07, p-value =0.47) in biofilm were observed between DAA treated FNN and DAA treated FNN grown in saliva coated 96-well plates (Figure 24). Saliva coating did not improve biofilm preservation during the CV staining protocol.

Method	DAA (positive control)	DAA+FA	DAA+PLL	DAA+PLL+FA	DAA + saliva	HIB+FA
DAA +FA	Z=-3.27 P=0.0005***					
DAA+PLL	-2.98 0.001***	0.29 0.38				
DAA+PLL + FA	-3.66 0.0001***	-0.38 0.35	-0.68 0.25			
DAA + saliva	0.07 0.47	3.34 0.0004***	3.05 0.001***	3.73 0.0001***		
HIB+FA	-0.42 0.34	2.85 0.002**	2.56 0.005**	3.24 0.0006***	-0.49 0.31	
HIB (negative control)	0.38 0.35	3.66 0.0001***	3.36 0.0004	4.04 <0.0001***	0.31 0.38	0.80 0.21

p, significance level; * p ≤ 0.05; ** p ≤ 0.01; *** p ≤ 0.001

KEY

DAA (Positive control)	F. nucleatum biofilm treated with DAA
DAA + Saliva	F. nucleatum biofilm treated with DAA Grown on saliva coated wells
DAA + PLL	F. nucleatum biofilm treated with DAA Grown on PLL coated wells
DAA + FA	F. nucleatum biofilm treated with DAA Fixed with formaldehyde
DAA + PLL + DA	F. nucleatum biofilm treated with DAA Grown on PLL coated wells and fixed with formaldehyde
HIB + FA	Modified HIB fixed with formaldehyde
HIB (negative control)	Modified HIB with no coating or fixing

Figure 24: Table summarising results comparing different methods to optimise the crystal violet staining protocol

Kruskal-Wallis test with Dunn's multiple comparison post-hoc test was conducted comparing DAA treated FNN biofilm and DAA treated FNN biofilm grown on saliva-coated wells (green highlighted). Top value represents z-statistic for comparison and the lower value represents p-value. Key is present on right hand side, which will be applicable for following Figures 25 and 27.

3.1.2.2 Effect of coating 96-well microtiter plate with Poly-L-Lysine on FNN biofilm development.

Pre-coating the 96-well microtiter plate with sterile 0.1% Poly-L-Lysine (PLL) before growing the *F. nucleatum* biofilm treated with DAA did improve the adhesion of biofilm. Significant differences (z-statistic for comparison = -2.98, p-value = 0.001) indicate that biofilm values were greater in the DAA treated FNN pre-coated with PLL compared to that of DAA treated FNN without PLL coating (Figure 25).

Method	DAA (positive control)	DAA+FA	DAA+PLL	DAA+PLL+FA	DAA + saliva	HIB+FA
DAA +FA	Z=-3.27 P=0.0005***					
DAA+PLL	-2.98 0.001***	0.29 0.38				
DAA+PLL + FA	-3.66 0.0001***	-0.38 0.35	-0.68 0.25			
DAA + saliva	0.07 0.47	3.34 0.0004***	3.05 0.001***	3.73 0.0001***		
HIB+FA	-0.42 0.34	2.85 0.002**	2.56 0.005**	3.24 0.0006***	-0.49 0.31	
HIB (negative control)	0.38 0.35	3.66 0.0001***	3.36 0.0004	4.04 <0.0001***	0.31 0.38	0.80 0.21

p, significance level; * p ≤ 0.05; ** p ≤ 0.01; *** p ≤ 0.001

Figure 25: Table summarising results comparing different methods to optimise crystal violet staining protocol.

Kruskal-Wallis test with Dunn's multiple comparison post-hoc test was conducted comparing DAA treated FNN biofilm and DAA treated FNN biofilm grown on Poly-L-Lysine coated wells (green highlighted). Top value represents z-statistic for comparison and the lower value represents p-value

3.1.2.3 Fixing the FNN biofilm with 4% formaldehyde solution

Additionally, DAA treated FNN biofilms were fixed with 4% formaldehyde (FA) to investigate if fixing the biofilm after the experiment would reduce biofilm dispersion during crystal violet staining. Significant differences (z-statistic for comparison = -3.27, p-value = 0.0005) indicate that biofilm values were greater in the DAA treated FNN fixed with 4% FA compared to that of DAA treated FNN without fixation (Figure 27). Furthermore, less variability was observed when DAA treated FNN was fixed with 4% FA (Figure 26).

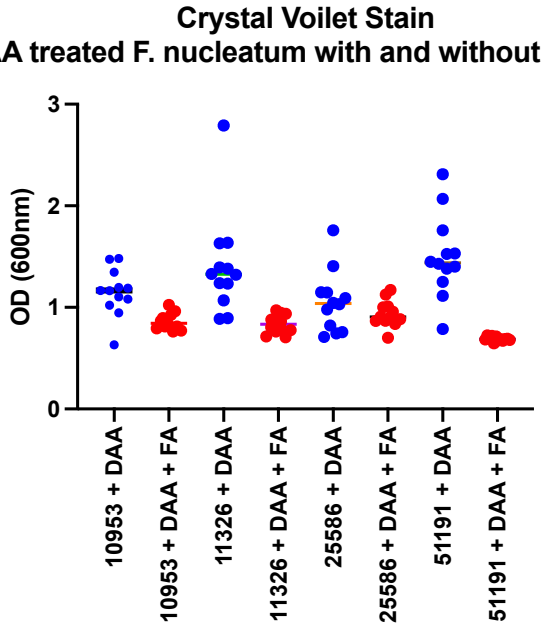

Figure 26: Scatter plot graph showing effect of fixing DAA treated *F. nucleatum* biofilm with FA for crystal violet staining experiment

Four *F. nucleatum* subspecies biofilm volume comparing DAA treated biofilm with and without FA fixation during crystal violet stain protocol (n= 12)

Furthermore, additional experiments were conducted where DAA treated FNN biofilm was grown on PLL coated wells and then fixed with 4% FA after the end of the experiment. Significant differences (z-statistic for comparison = -3.66, p-value = 0.0001) indicate that biofilm values were greater in the DAA treated FNN biofilm grown on PLL coated wells and post-experimental fixation with 4% FA compared to that of DAA treated FNN without fixation or coating (Figure 27).

Method	DAA (positive control)	DAA+FA	DAA+PLL	DAA+PLL+FA	DAA + saliva	HIB+FA
DAA +FA	Z=-3.27 P=0.0005***					
DAA+PLL	-2.98 0.001***	0.29 0.38				
DAA+PLL + FA	-3.66 0.0001***	-0.38 0.35	-0.68 0.25			
DAA + saliva	0.07 0.47	3.34 0.0004***	3.05 0.001***	3.73 0.0001***		
HIB+FA	-0.42 0.34	2.85 0.002**	2.56 0.005**	3.24 0.0006***	-0.49 0.31	
HIB (negative control)	0.38 0.35	3.66 0.0001***	3.36 0.0004	4.04 <0.0001***	0.31 0.38	0.80 0.21

p, significance level; * p ≤ 0.05; ** p ≤ 0.01; *** p ≤ 0.001

Figure 27: Table summarising results comparing different methods to optimise crystal violet staining protocol

Kruskal-Wallis test with Dunn's multiple comparison post-hoc test was conducted comparing DAA treated FNN biofilm to DAA treated FNN fixed with 4% FA (green highlighted) and to DAA treated FNN grown on PLL coated wells and fixed with 4% FA (yellow highlighted). Top value represents z-statistic for comparison and the lower value represents p-value

3.1.3 Optimising confocal imaging protocol

Initially two methods for growing *F. nucleatum* as a biofilm were performed before confocal imaging. Method 1 grew *F. nucleatum* biofilms on round glass coverslips placed into 24-well microtiter plates which were transferred onto glass slides after Live/Dead staining. This method showed extensive biofilm disruption during transferring the glass cover slips onto the glass slides and therefore gave variable results (Figure 28). Method 2 used µ-Slide 8 Well ibidiTreat plates as they allowed for immediate confocal imaging without transfer onto glass slides after Live/Dead staining (Figure 28). Furthermore, µ-Slide 8 Well ibidiTreat plates had more favourable qualities compared to normal glass slides such as having tissue culture treated well coatings for better adherence of the biofilm and a thinner polymer well base allowing for optimal confocal imaging (Figure 29).

Due to their advantages, µ-Slide 8 Well ibidiTreat plates were used to grow single subspecies FNN (ATCC 25586) to optimise confocal imaging to allow biofilm analysis with Imaris software.

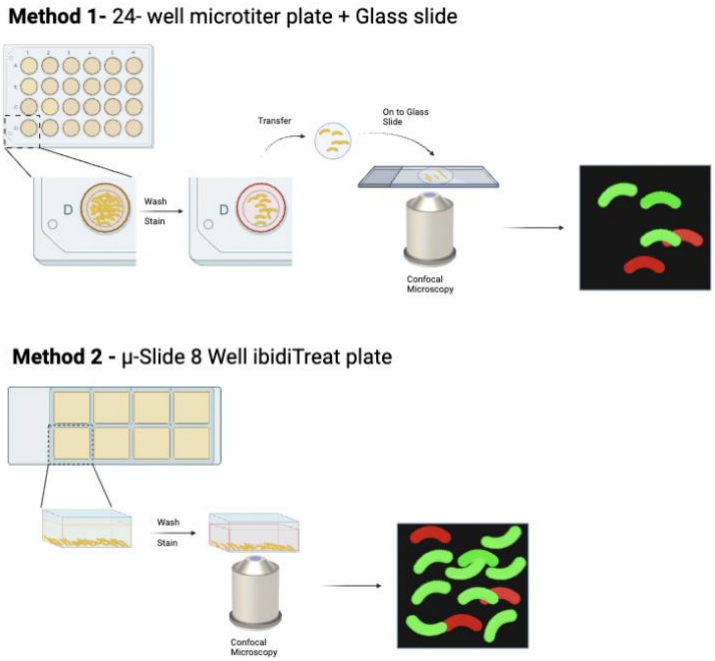

Figure 28: Schematic diagram showing workflow of Method 1 and Method 2

Method 1; *F. nucleatum* grown on 13mm glass coverslips in 24-well microtiter plate transferred onto glass slides for confocal imaging. Method 2; *F. nucleatum* grown in µ-Slide 8 Well ibidiTreat plate for confocal imaging

	Method 1	Method 2
	Coverslips in 24-well microtiter plate transferred onto Glass slides for imaging	**µ-Slide 8 Well ibidiTreat plate**
Max Volume	1ml	300µl
Well coating	Untreated	Tissue culture-treated
Thickness at the bottom of the wells	Glass slides 1mm	Polymer coverslip #1.5 180 µm (+10/–5 µm)

Figure 29: Table comparing Method 1 and Method 2 for confocal imaging *F. nucleatum* biofilms.

3.1.3.1 Effect of reducing cell numbers in the starting inoculum on cell density per confocal image

FNN was grown in µ-Slide 8 Well ibidiTreat plates (Ibidi) over 24 hours in an anaerobic jar to optimise Imaris analysis after Live/Dead florescent staining (Section 2.5.1). As expected, Live/Dead staining after 24 hours showed an abundance of live cells and minimal dead cells. However, there was no significant difference between samples, despite the 100-fold difference in OD of the starting inoculum (OD_{600nm} range 0.3 to 0.003) (Figure 30). Analysis of FNN biofilm volume and viability (%) could not be determined on these samples using Imaris software due to excessive cell density and morphology interfering with program's ability to identify each cell.

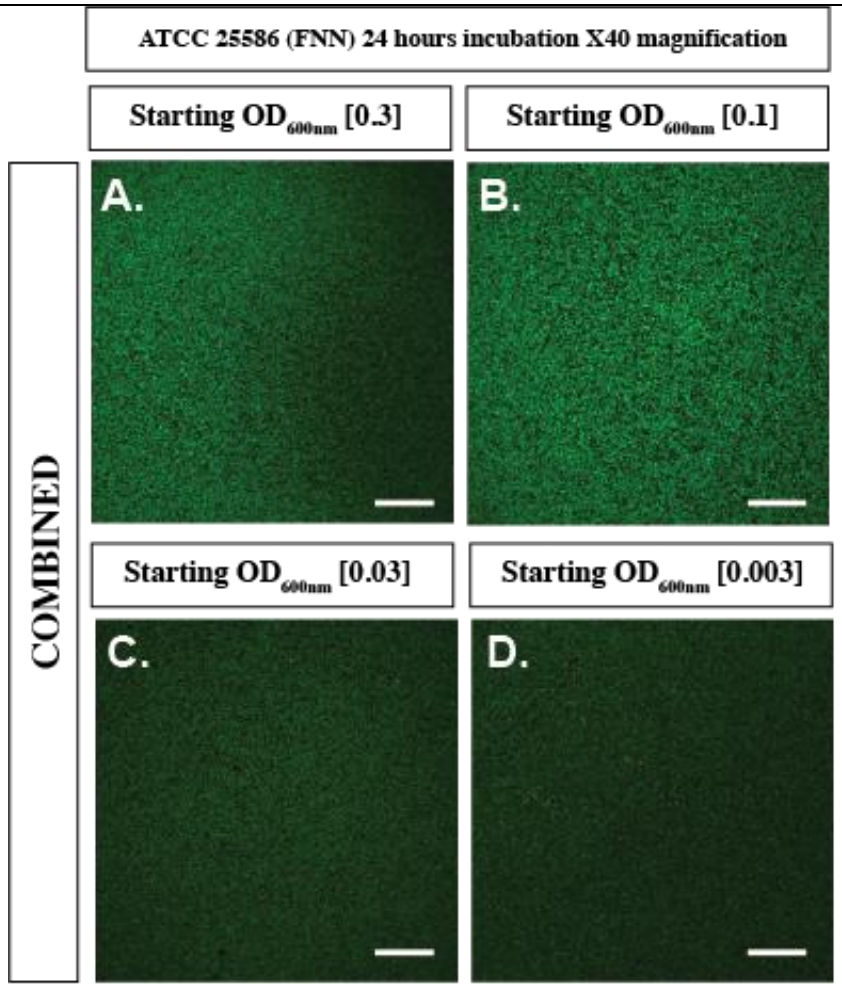

Figure 30: Live/Dead fluorescent staining of FNN biofilm after 24 hours incubation
Different starting OD_{600nm} of **(A)** 0.3, **(B)** 0.1, **(C)** 0.03 and **(D)** 0.003 showed similar cell density per confocal image after Live/dead staining. All images were taken at X40 magnification with both live (green) and dead (red) channels combined. Scale bars 50µm.

3.1.3.2 Reducing incubation time improved confocal imaging at at lower starting OD_{600nm}

The next parameter that was adjusted in an attempt to optimise the confocal microscopy protocol was modifying incubation time before Live/Dead staining and imaging. Incubation times of 7, 16 and 24 hours were assessed (Figure 31). Both starting OD_{600nm} of 0.03 and 0.003 showed similar trends where a decrease in incubation time from 24 hours to 16 and 7 hours showed a proportional decreased in cell density per confocal image. Analysis after 16 hours incubation using Imaris software was unable to be accurately completed due to the high cell density per confocal image (Figure 32). On the other hand, a more accurate analysis could be performed after 7 hours incubation where the software was able to identify and label each cell per confocal image more accurately (Figure 32). Henceforward, a starting inoculum of OD_{600nm} of 0.003 and 7 hours incubation before staining the biofilm with Live/Dead staining and confocal imaging was considered the optimal protocol.

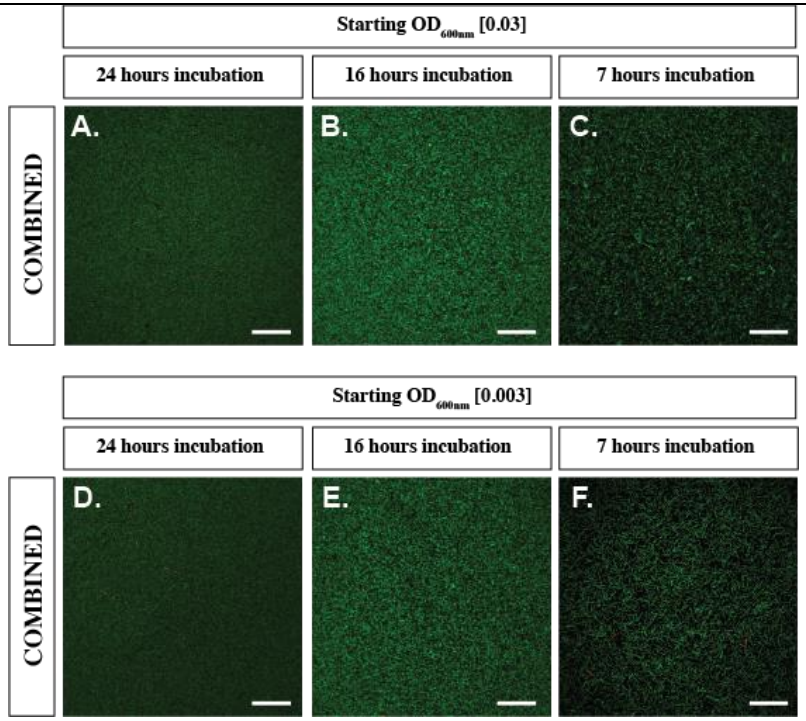

Figure 31: Live/Dead fluorescent staining of FNN biofilm after 7, 16 and 24 hour incubation at two different starting OD_{600nm}

Different starting OD_{600nm} of **(A-C)** 0.03 and **(D-F)** 0.003 incubated for 24 hours **(A and D),** 16 hours **(B and E)** or 7 hours **(C and F)**. All images were taken at X40 magnification with both live (green channel) and dead (red channel) stains combined. Scale bars 50μm.

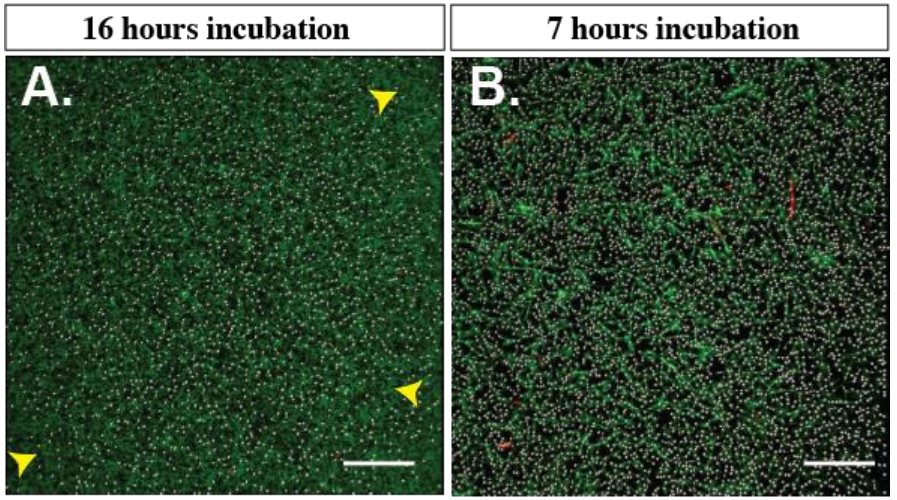

Figure 32: Snapshot of analysis tool interface on Imaris software

Each white dot represents Imaris software identifying each *F. nucleatum* cell. **(A)** At 16 hours incubation software is unable to identify each cell accurately, with many uncounted bacterial cells (yellow arrows). **(B)** At 7 hours incubation, Imaris software can more accurately identify each *F. nucleatum* bacterial cell. All images were taken at X40 magnification with both live (green channel) and dead (red channel) stains combined. Scale bars 50μm.

3.1.3.3 Biofilm volume was significantly different depending on incubation time

Another Imaris software analysis that aids in quantification of the biofilm is the calculation of biofilm volume through 3D rendering using CLSM Z-stack images after Live/Dead staining (Figure 33). There was a significant increase (p=0.0488) in biofilm volume after 24 hours incubation (mean biofilm volume 37.25 X10^4 μm^3; SD $\pm$10.11) compared to 7 hours incubation (mean biofilm volume 6.03 X10^4 μm^3; SD $\pm$ 0.49) (Figure 34) This can also be confirmed visually after 3D rendering the biofilm where biofilm incubated for 24 hours is thicker than the biofilm incubated for 7 hours (Figure 33).

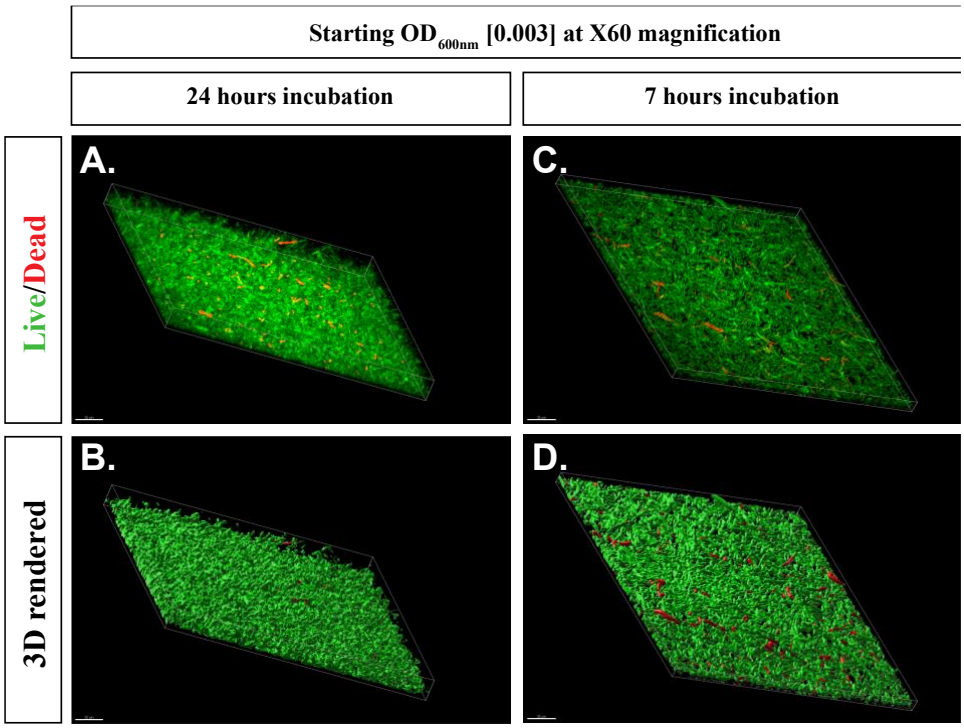

Figure 33: Z-stack image and 3D rendering of Live/Dead fluorescent stained FNN biofilm comparing biofilm volume after 7 and 24 hours incubation

Combined live (green) and dead (red) channels of FNN biofilm after **(A)** 24 hours incubation and **(C)** 7 hours incubation with **(B,D)** 3D rendered biofilm respectively. Scale bars 20μm.

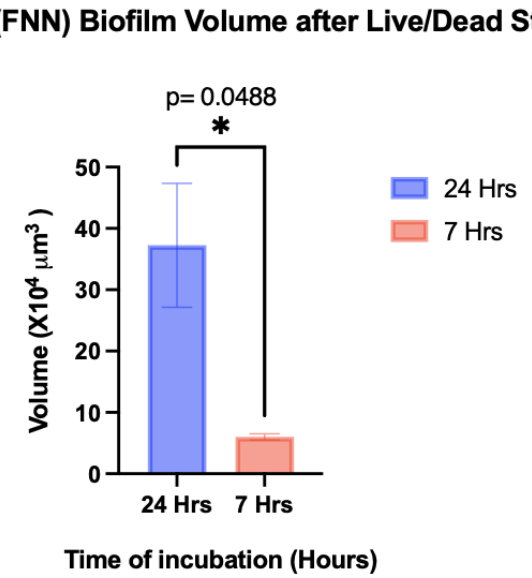

Figure 34: Comparison of volume of FNN biofilm incubated for 24 and 7 hours

Graph of FNN biofilm volume comparing 24 hours to 7 hours (mean±SD, n= 3); ns denotes no significant difference, * denotes significant difference compared to the control ($p < 0.05$) using unpaired t-test (* $p<0.05$, ** $p<0.01$, ***$p<0.001$).

3.1.3.4 Effect of using 4% Formaldehyde (FA) to fix FNN biofilm before live/dead staining

Furthermore, to minimise disruption of biofilm during staining process, FNN biofilms were fixed with 4% FA for 10 minutes before Live/Dead stain and imaging under confocal microscope (Figure 35). FA appeared to interfere with the dead channel (red), dampening down the overall signal compared to control samples that were not treated with FA where dead cells appeared to be more clearly imaged. This phenomenon was consistently observed in samples with a different starting inoculum OD_{600nm} of 0.03 and 0.003 (Figure 35).

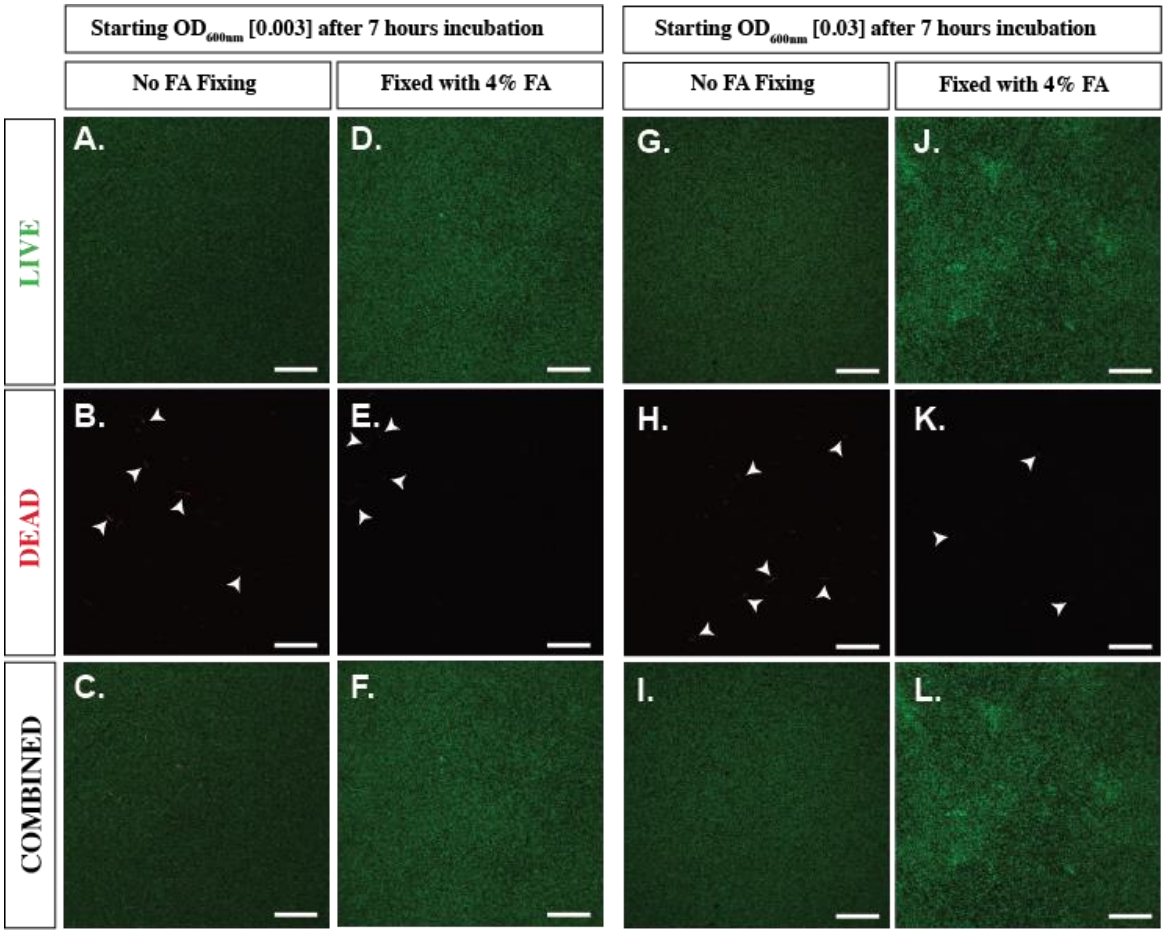

Figure 35: Effect of 4% FA on Live/dead fluorescent staining of FNN biofilm after 7 hours incubation

Confocal images comparing FNN biofilm with no fixing and fixing with 4% FA at two different starting inoculums (OD_{600nm} of 0.003 and 0.03). White arrows indicates where dead bacterial cells are present. Images separated into three channels: Live (green), Dead (red) and Combined. All images were taken at X40 magnification. Scale bars 50μm.

3.1.3.5 Magnification X60 is more suitable for Imaris analysis of Live/Dead stained FNN biofilm

The final parameter which was adjusted to improve confocal imaging protocol to permit Imaris software analysis was magnification of which the confocal images were taken. Originally all images were taken at X40 magnification, however after trial and error using Imaris software, a final decision was made to image at X60 magnification (Figure 36) which allowed for optimal cell density for the software to perform analysis more accurately (Figure 37).

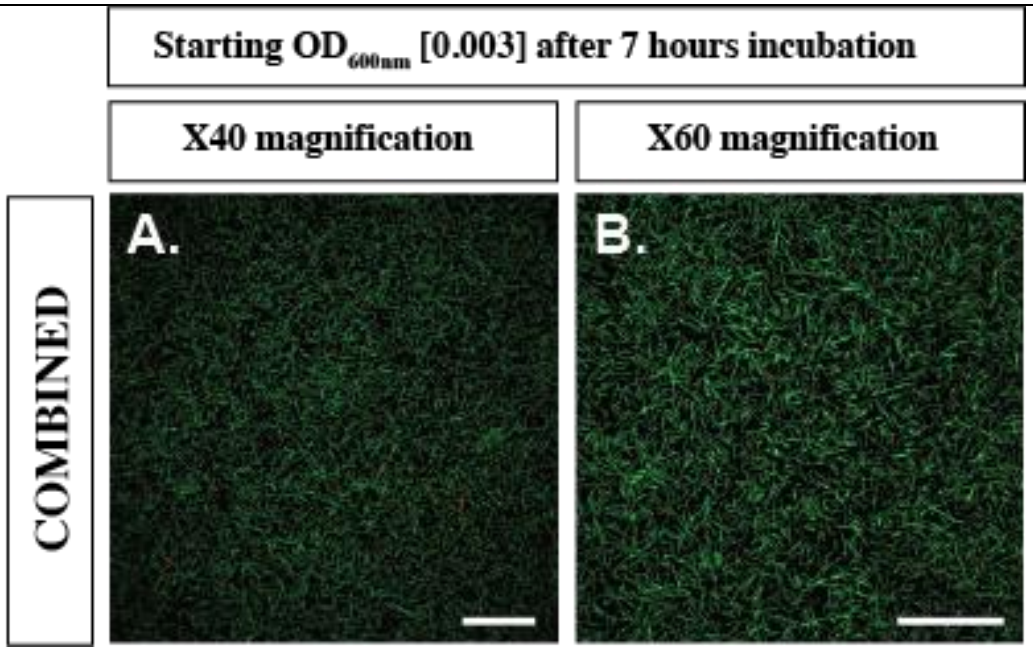

Figure 36: Confocal images of FNN biofilm after 7 hours incubation at two different magnifications

Starting OD_{600nm} of [0.003] and after 7 hours incubation, FNN biofilm was imaged at **(A)** X40 magnification and **(B)** X60 magnification. Scale bars 50μm.

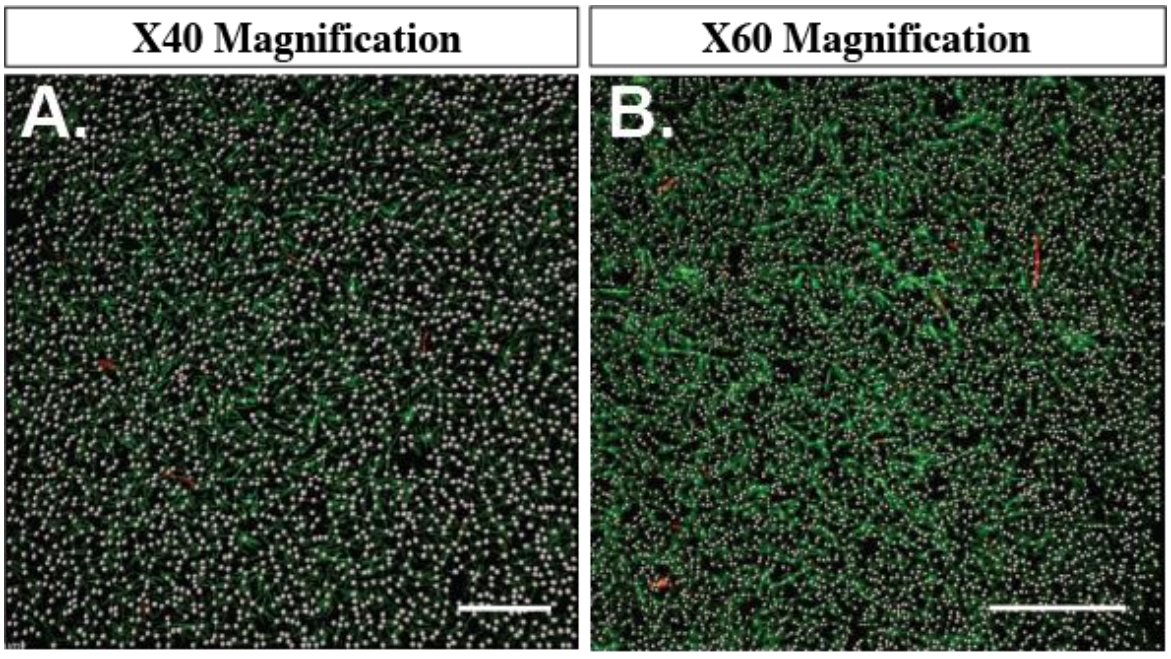

Figure 37: Snapshot of analysis tool interface on Imaris software

Each white dot represents Imaris software identifying each *F. nucleatum* bacterial cell at **(A)** at X40 magnification and **(B)** at X60 magnification. Both live (green channel) and dead (red channel) stains combined. Scale bars 50μm.

3.2 Optimising xCELLigence® platform protocol to grow single species *F. nucleatum* biofilm under anaerobic conditions

3.2.1 Use of anaerobic sachet material and dental impression material to create anaerobic conditions within xCELLigence® plate

Similarly, to creating a more anaerobic environment in the 96-well microtiter plates by using anaerobic sachet material and AxySeal Plastic Sealing Film (Axygen®), anaerobic sachet material was added into the evaporation wells of the xCELLigence® plates followed by sealing of the lid with dental impression material (Figure 9). This adequately created an anaerobic environment, as seen from the colour change of the anaerobic indicator from pink to white over 24 hours (Figure 38).

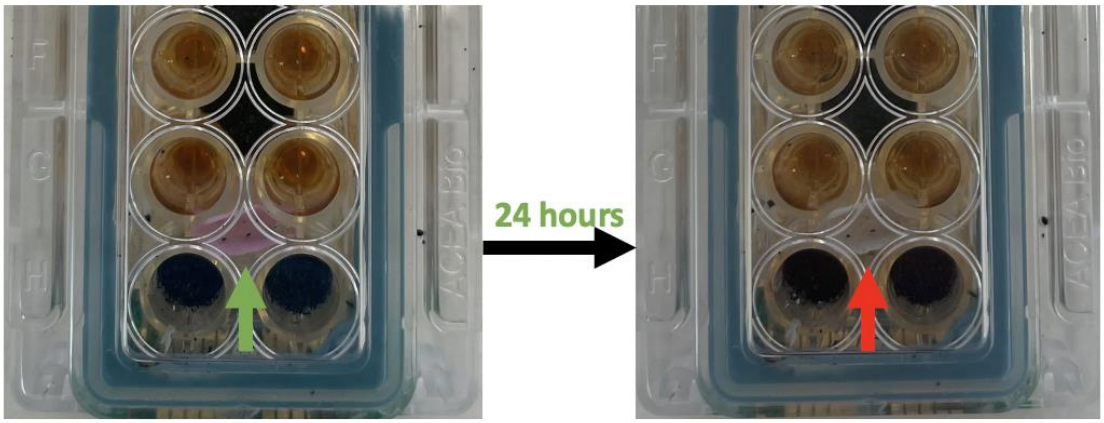

Figure 38: Assessing anaerobicity of xCELLigence® plate

(A) Photo of xCELLigence® E-plate before experiment was placed in the incubator for 24 hours. Anaerobic indicator strip (green arrow) indicates oxygen was still present within the E-plate. **(B)** Photo of xCELLigence® E-plate after 24 hours in the incubator. Anaerobic indicator strip (red arrow) indicates sufficient anaerobicity of E-plate.

3.2.2 *F. nucleatum* biofilm growth in the xCELLigience® platform over 24 hours

Electrical impedance detected between electrodes embedded within the xCELLigence® plate is proportional to biofilm formation and is expressed as an arbitrary unit called Cell Index (CI). Biofilm formation was therefore represented by an increase in CI. Although FNP, FNF and FNN appeared to form biofilm initially in the first hour, represented by increase CI (maximum CI 0.045, 0.068, 0.06 respectively), this was followed by decrease in CI to below zero. On the other hand, FNA immediately dropped and remained below. It is to be noted that CI curves for FNA were highly variable as reflected by large standard deviation error bars (Figure 41). Over 24 hours, all 4 subspecies of *F. nucleatum* (FNP, FNF, FNN, FNA) produced CI values below zero (Figure 39 and 40).

Furthermore, to ensure that the negative impedance was not due to a technical error, FNA biofilm was grown under anaerobic conditions alongside *Streptococcus mutans* and *Streptococcus sobrinus*, both facultative anaerobes which produce biofilms that are known to be detected by the xCELLigence® platform. Both *S. mutans* and *S. sobrinus* produced increases in CI which correlated to formation of biofilm, whilst FNA showed negative CI as previously observed (Figure 41).

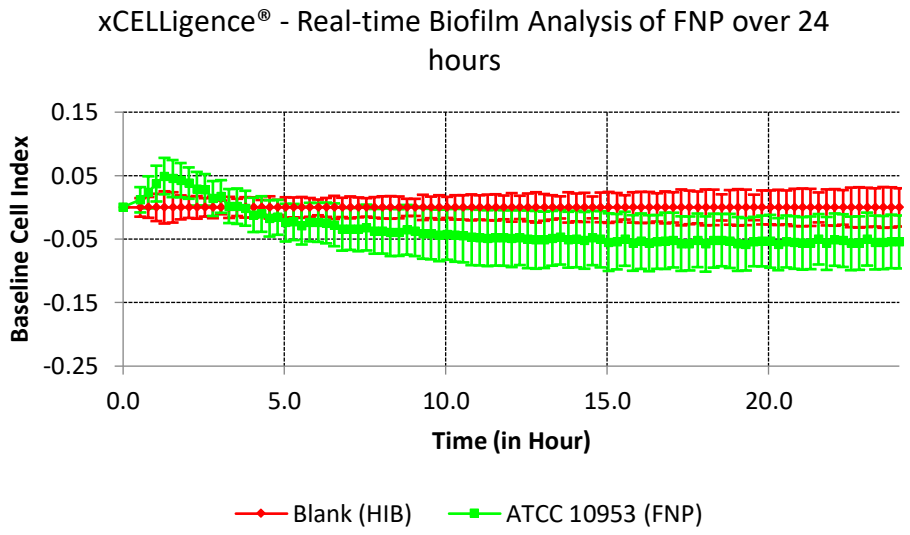

Figure 39: Real-time Biofilm Analysis of FNP over 24 hours

Experiments conducted in triplicate. Mean and SD of a single experiment shown and normalised to the control (Modified HIB).

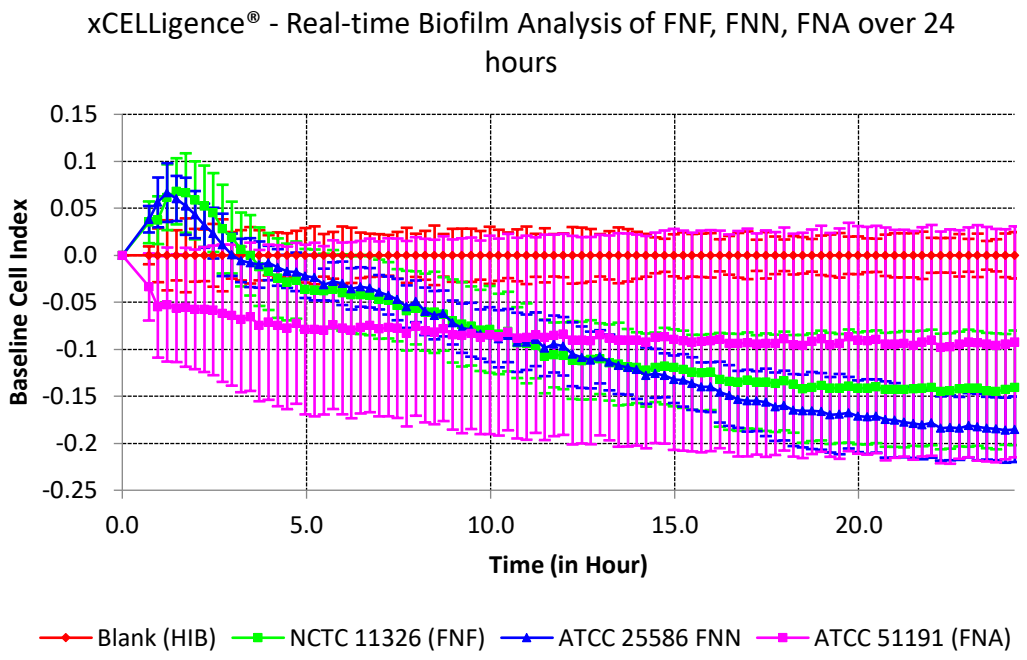

Figure 40: Real-time Biofilm Analysis of FNF, FNN and FNA over 24 hours

Experiments conducted in triplicate. Mean and SD of a single experiment shown and normalised to the control (Modified HIB).

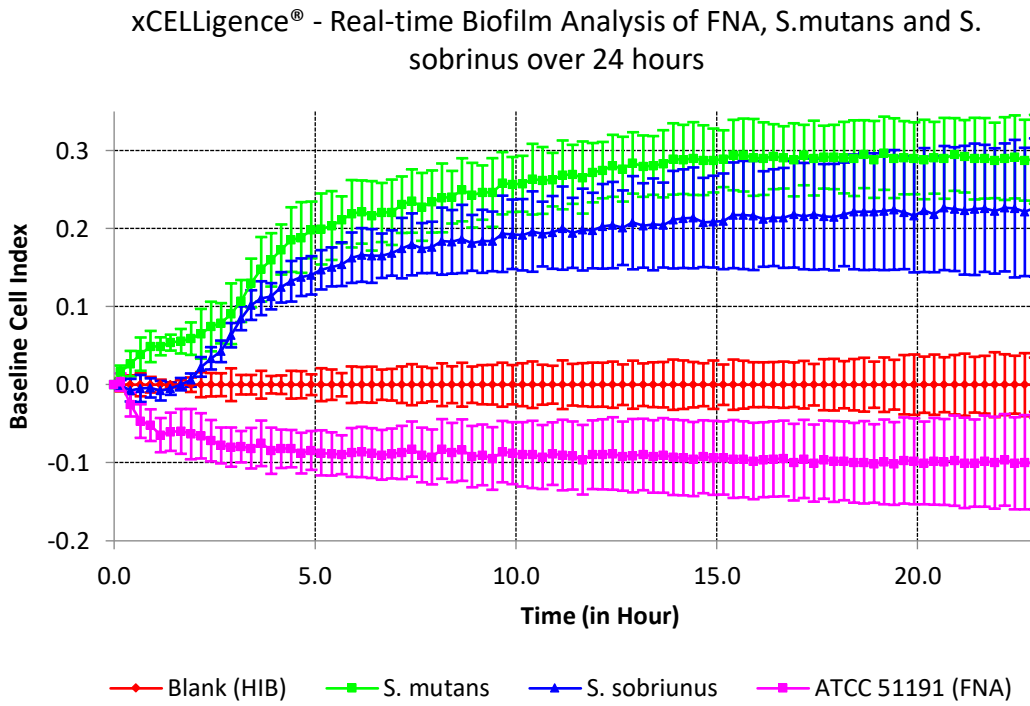

Figure 41: Real-time Biofilm Analysis of FNA, *S. mutans* and *S. sobrinus* over 24 hours

Experiments conducted in triplicate. Mean and SD of a single experiment shown and normalised to the control (Modified HIB).

3.2.3 Effect of increasing the duration of the experiment longer than 24 hours

To investigate if longer incubation period within the xCELLigence® platform will affect the CI readings of FNP biofilms, incubation time was extended to 48 hours (Figure 42). Although a slight increase in CI can be observed after 20 hours incubation, FNP CI remained negative, and biofilm remained undetected for the duration of the experiment (Figure 42).

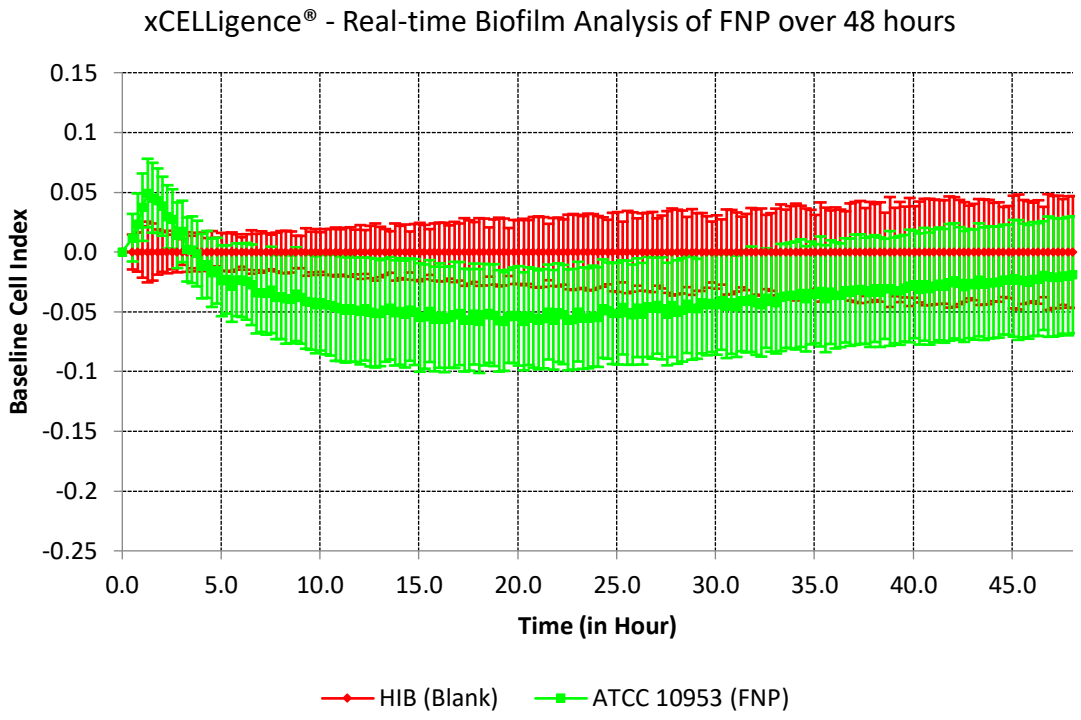

Figure 42: Real-time Biofilm Analysis of FNP over 48 hours

Experiments conducted in triplicate. Mean and SD of a single experiment shown and normalised to the control (Modified HIB).

3.2.4 Effect of different starting inoculum

FNP at two different starting inoculums of OD_{600nm} 0.3 and 0.6 were tested to investigate if starting inoculum could potentially resolve the issue with the negative CI readings (Figure 43). No apparent differences were observed even after doubling the starting inoculum. Therefore, it can be concluded that different starting inoculum does not contribute to the issue of negative CI reading on the xCELLigence® platform.

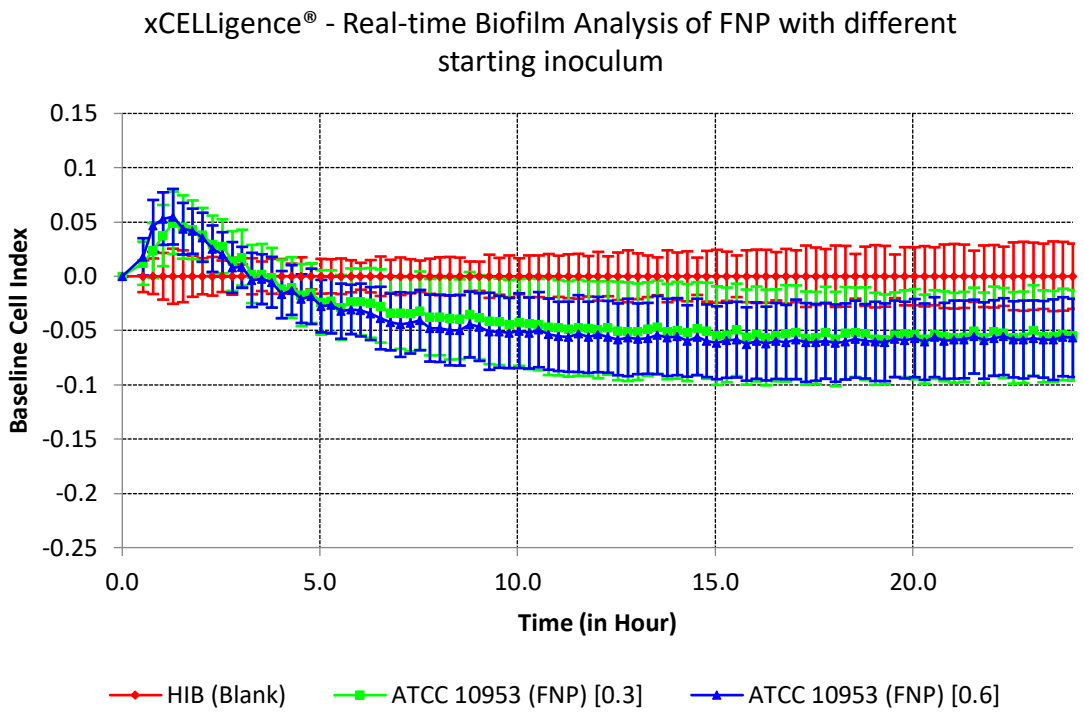

Figure 43: Effect of different starting OD_{600nm} of 0.3 and 0.6 on Real-time Biofilm Analysis of FNP over 24 hours

Experiments conducted in triplicate. Mean and SD of a single experiment shown and normalised to the control (Modified HIB).

3.2.5 Effect of saliva coating xCELLigence® plates

Furthermore, xCELLigence® plate wells were coated with sterile human saliva to investigate if coating the wells could potentially resolve the issue with the negative CI readings (Figure 44). However, similar CI curve patterns were observed between the saliva coated and non-saliva coated wells where FNP CI remained in the negative values and biofilm grown was not detected through real-time biofilm analysis on the xCELLigence® platform. Saliva pre-

coating the xCELLigence® plate wells did not contribute to improving FNP biofilm detection of the platform.

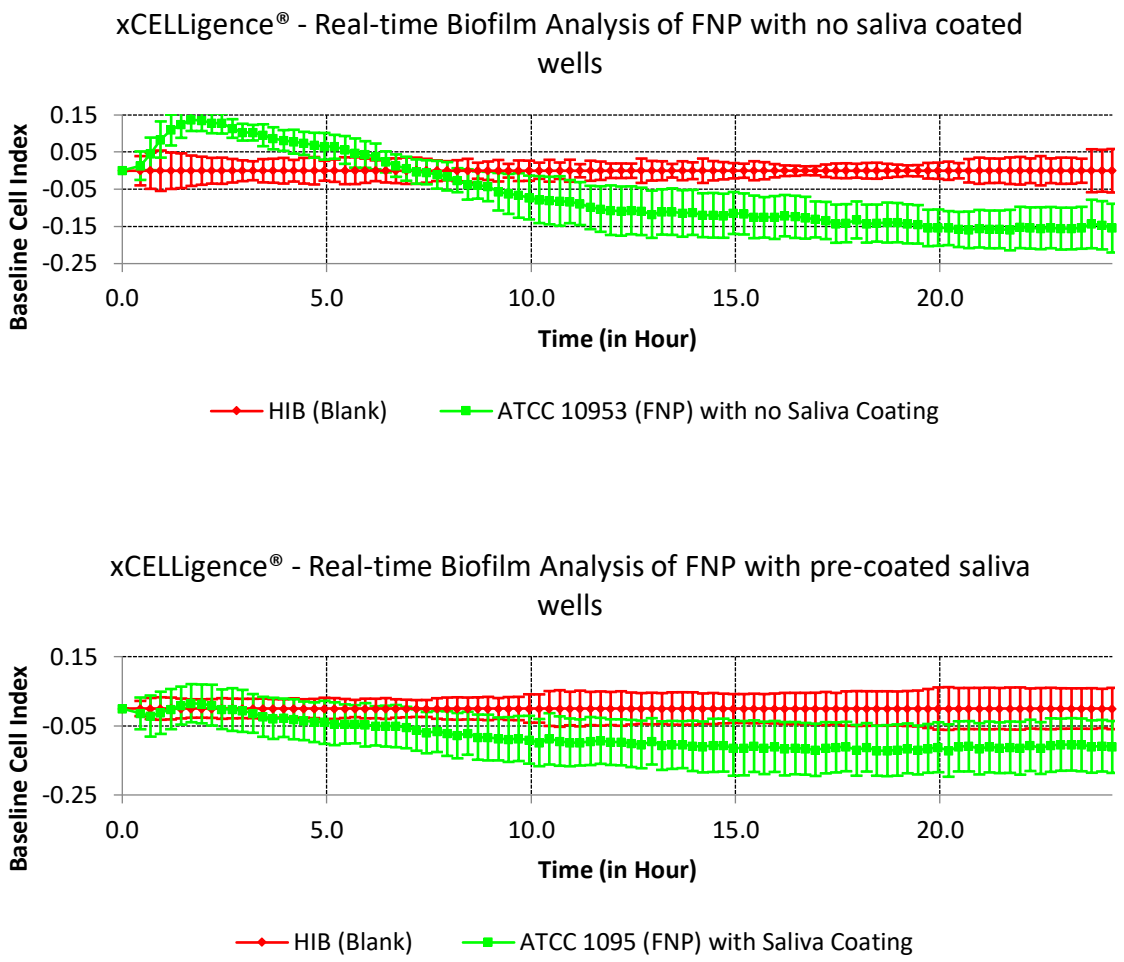

Figure 44: Real-time Biofilm Analysis of FNP on Saliva Coated wells over 24 hours
Experiments conducted in triplicate. Mean and SD of a single experiment shown and normalised to the control (Modified HIB).

3.2.6 Confocal images of *F. nucleatum* biofilm after 24 hours

From previous experiments, *F. nucleatum* is known to have formed biofilm after 24 hours, which is not reflected in the real-time biofilm monitoring system in the xCELLigence® platform where the CI remained constantly negative. Therefore, to confirm that *F. nucleatum* biofilm was forming over 24 hours in the xCELLigence® E-plate, confocal imaging using Live/Dead staining was conducted. To make the xCELLigence® E-plate 16 VIEW suitable for

confocal microscopy, the plates were modified to ensure adequate adaptation of the bottom of the bottom of the E-plate to the confocal microscope lens (Figure 11).

Although the resolution of the confocal image is low, FNN biofilm can be visualised with mixture of live cells (green) and dead cells (red), as expected in a biofilm (Figure 45). After further investigations through contacting the manufacturer, xCELLigence® E-plate 16 VIEW was deemed not suitable for confocal microscopy imaging (Figure 45).

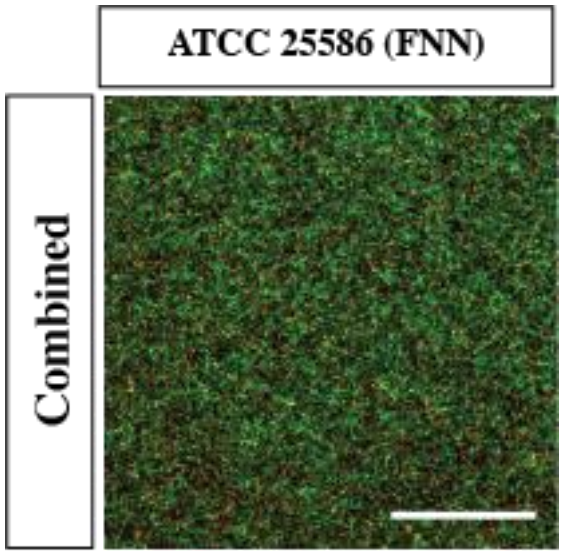

Figure 45: Confocal image of FNN biofilm after 24 hours incubation with in xCELLigence® platform

FNN biofilm was imaged at X10 magnification. Both Live (green) and Dead (red) channels are imaged. Scale bar 25μm.

3.3 Novel antimicrobials and their effects on *F. nucleatum*

3.3.1 Effect of D-amino acids on *F. nucleatum*

3.3.1.1 Visual changes of *F. nucleatum* biofilm after DAA treatment

All 4 subspecies of *F. nucleatum* were treated with DAA to investigate their effect on biofilm formation. After 24 hours incubation, the biofilms in the presence of DAA consistently showed a different appearance which was visually observed in microtiter plates (Figure 46). For all 4 subspecies, *F. nucleatum* biofilm grown in modified HIB and LAA appeared visually similar. Interestingly, FNF and FNN biofilm had a sunray appearance which differed from its modified HIB and LAA biofilm counterparts (Figure 46). This phenomenon was less obvious with FNP and FNA.

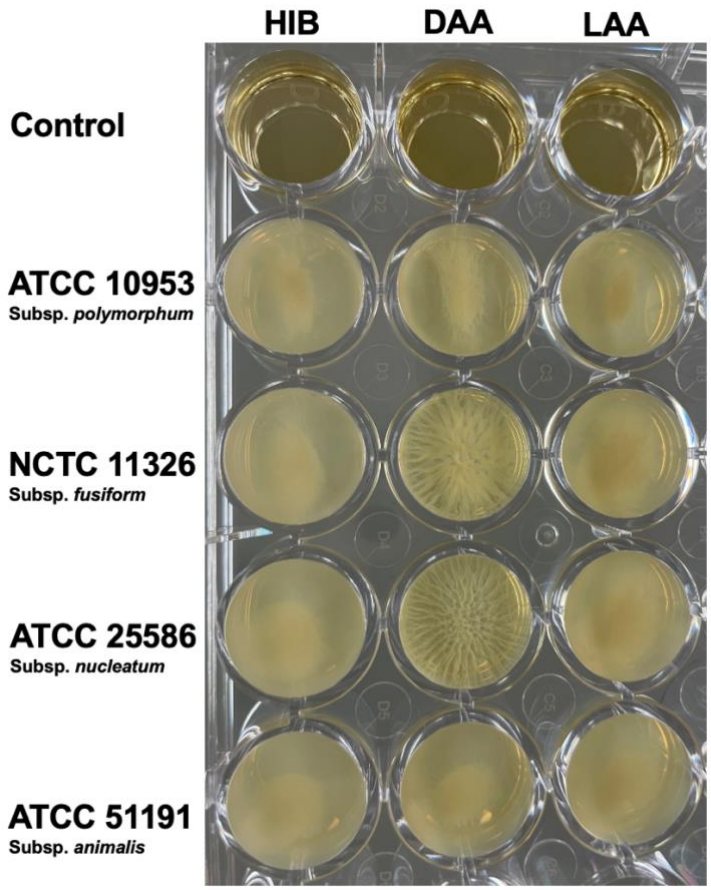

Figure 46: Picture of *F. nucleatum* grown in 24-well microtiter plate
Subspecies **(A)** FNP, **(B)** FNF **(C)** FNN **(D)** FNA grown in modified HIB (Control), DAA (treatment) and LAA for 24 hours

3.3.1.2 Concentration dependant effect of DAA on *F. nucleatum* growth

DAAs used in experiments were dissolved in modified HIB and diluted to 50%, 25% and 12.5% (Figure 47). A concentration dependant inhibitory effect was seen for FNP, FNF and FNN, but was less pronounced for FNA (Figure 47). While the concentration dependant effect of DAAs were most pronounced during log phase for FNF and FNN affecting the doubling time which decreased the maximum OD_{600nm} reached, this was less obvious in FNP growth curves. No concentration dependant effect of DAAs were observed for FNA (Figure 47). DAAs used at previously described concentration of 25mM for D-Leu, D-Met, D-Trp and 0.25mM for D-Tyr (Zilm et al., 2017) had greatest effects on FNP, FNF and FNN growth and was used for future experiments, further discussed in the following section.

3.3.1.3 Effect of DAA on growth of *F. nucleatum*.

All four subspecies of *F. nucleatum* were grown in the spectrophotometer over 24 hours to investigate the effect of DAAs on growth under anaerobic conditions (Section 2.1.3). For all subsequent experiments, DAAs were used at concentration of 25mM for D-Leu, D-Met, D-Trp and 0.25mM for D-Tyr (Zilm et al., 2017). DAAs had similar effects on the growth of FNF and FNN where both the log phase and stationary phase were affected. Growth of FNF and FNN over the first 6 hours produced an increase in doubling time by 2-fold (log phase) and stationary phase was reached earlier near 4 hours in the DAA treated groups (Figure 48). DAA treated FNP, FNF and FNN groups showed a reduced capacity to grow, reflected in a reduction of the maximum OD_{600nm} reached (0.96, 0.96 and 0.98 for control groups and 0.59, 0.51 and 0.53 for DAA treated groups respectively). For FNF and FNN, the maximum OD_{600nm} occurred at around 7 hours compared to *ca.* 10 hours for the control (Figure 48).

On the contrary, minimal differences were observed between the control and DAA treated growth curves for FNA, which was consistently observed throughout the experiment repeated in triplicate. The final OD_{600nm} after 24 hours were 0.76 and 0.66 for the control and DAA treated group respectively (Figure 48). Overall, DAA increased the doubling time and reduced maximum OD_{600nm} for FNP, FNF and FNN. However, DAA treated FNA only reduced the maximum OD_{600nm} seen at a lesser extent over 24 hours in a spectrophotometer (Figure 48).

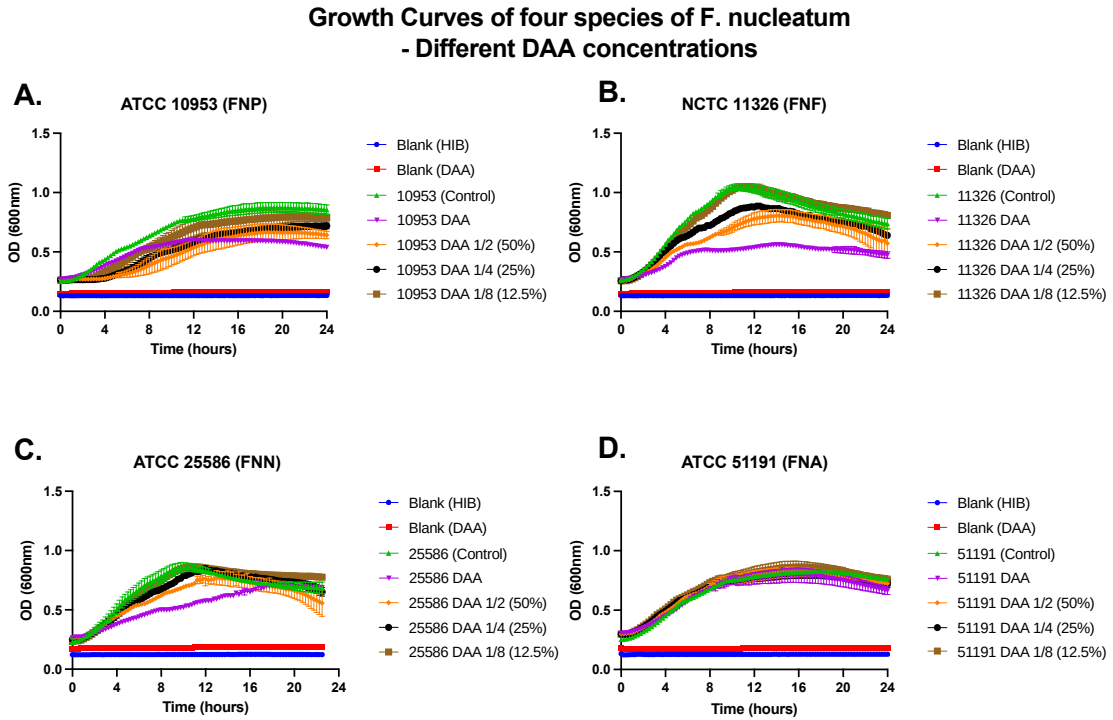

Dilutions	D-Leu, D-Met, D-Trp concentrations	D-Tyr concentrations
Original Concentration (DAA)	25mM	0.25mM
DAA ½ (50%)	12.5mM	0.125mM
DAA ¼ (25%)	6.25mM	0.063mM
DAA $^{1}/_{8}$ (12.5%)	3.13mM	0.031mM

Figure 47: Growth curves of *F. nucleatum* treated with different concentrations of DAAs at concentration of 25mM for D-Leu, D-Met, D-Trp and 0.25mM for D-Tyr

Growth curves represented by OD at 600nm for **(A)** FNP **(B)** FNF, **(C)** FNN and **(D)** FNA comparing control group and DAA treated groups. Sterile modified HIB and DAA in modified HIB served as blanks. Each experiment was conducted in triplicate. Error bars represent standard deviation.

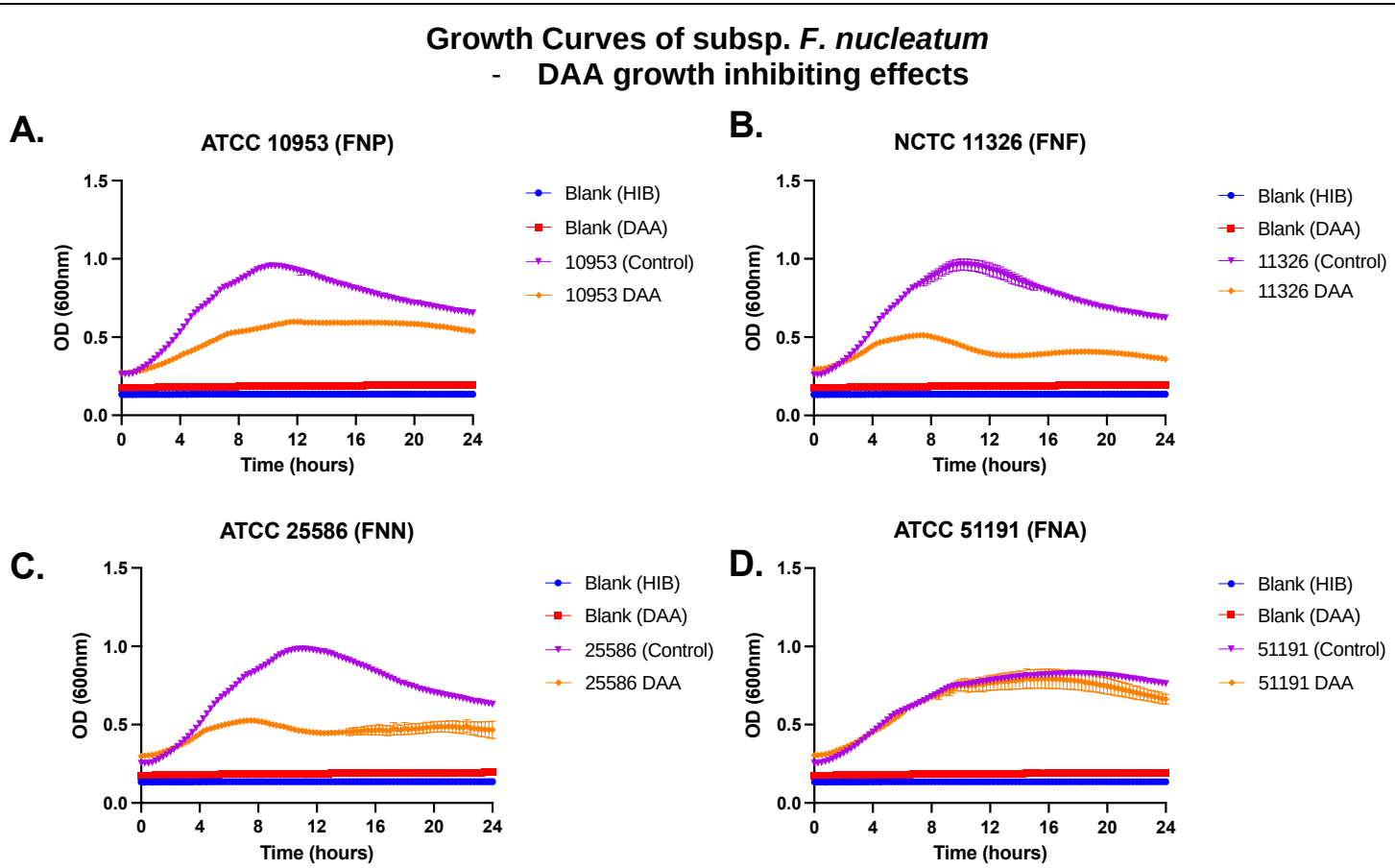

Figure 48: Growth curves of *F. nucleatum* in the presence of DAAs at concentration of 25mM for D-Leu, D-Met, D-Trp and 0.25mM for D-Tyr

Growth curves represented by OD at 600nm for **(A)** FNP **(B)** FNF, **(C)** FNN and **(D)** FNA comparing control group (purple) and DAA treated group (orange). Sterile modified HIB and DAA in modified HIB served as blanks. Each experiment was conducted in triplicate. Error bars represent standard deviation.

3.3.1.4 The effect of DAAs on biofilm formation by *F. nucleatum* subspecies using crystal violet staining

Crystal violet staining was used for *F. nucleatum* biofilm quantification in the presence of DAAs at a concentration of 25mM for D-Leu, D-Met, D-Trp and 0.25mM for D-Tyr (Section 2.4) add at the start of the experiment. After 24 hours, FNP and FNF treated with DAAs had a significant decrease in biofilm (Figure 49). FNP and FNF controls had a mean OD_{600nm} of 0.86 (SD± 0.09) and 1.02 (SD± 0.07) compared to DAA treated group of 0.67 (SD± 0.12) and 0.83 (SD± 0.09) respectively. On the contrary, the effect of DAA treatment of FNN and FNA was not significant (Figure 49).

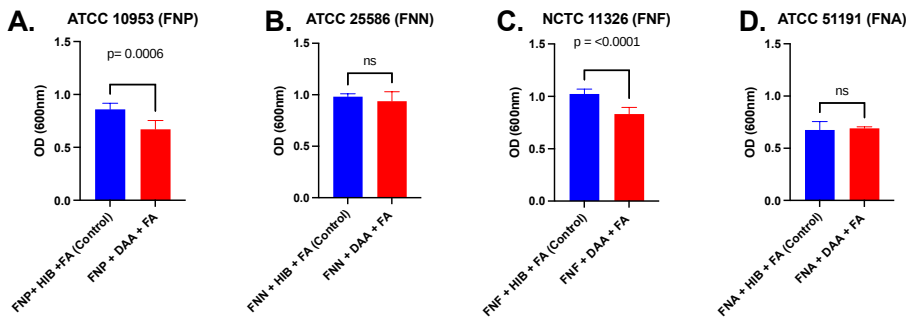

Figure 49: Effect of DAA on *F. nucleatum subspecies* biofilm formation using crystal violet staining

DAA treatment (concentration of 25mM for D-Leu, D-Met, D-Trp and 0.25mM for D-Tyr) was added at the start of the experiment. Graph comparing DAA treated and control (modified HIB) **(A)** FNP, **(B)** FNN **(C)** FNF and **(D)** FNA biofilm using crystal violet staining (mean± SD, n= 12); ns denotes no significant difference, * denotes significant difference compared to the control (p< 0.05) using unpaired t-test (* p<0.05, ** p<0.01, ***p<0.001, **** p<0.0001).

3.3.1.5 Cellular morphology of *F. nucleatum* grown as a biofilm

To assess *F. nucleatum* biofilm architecture, SEM imaging was performed after growing *F. nucleatum* in modified HIB on glass cover clips in 24 well microtiter plates for 24 hours in an anaerobic jar (Section 2.5.2). SEM images shows the fusiform shaped bacterial cells. Interesting, FNP and FNF showed the appearance of an extrapolymeric substance (EPS) on the bacterial surface which was not seen on FNN and FNA where coaggregation of bacterial cells were seen without EPS (Figure 50).

3.3.1.6 DAA treated *F. nucleatum* shows changes in cellular morphology

Subsequently, DAAs (concentration of 25mM for D-Leu, D-Met, D-Trp and 0.25mM for D-Tyr) were added at the start of the experiment which then *F. nucleatum* biofilms were imaged under SEM to assess changes in cellular morphology after 24 hours incubation in an anaerobic jar. EPS which was prominent in the FNP and FNF control group (as seen previously) was no longer present in the DAA treated groups although some extra-cellular material was present (Figure 50, yellow arrowhead). For all subspecies treated with DAAs, the biofilm appeared to have almost vesicular looking irregularities on the surface of the bacteria (Figure 50, red arrowhead). Interestingly, after DAA treatment, FNA cells became elongated (Figure 50.)

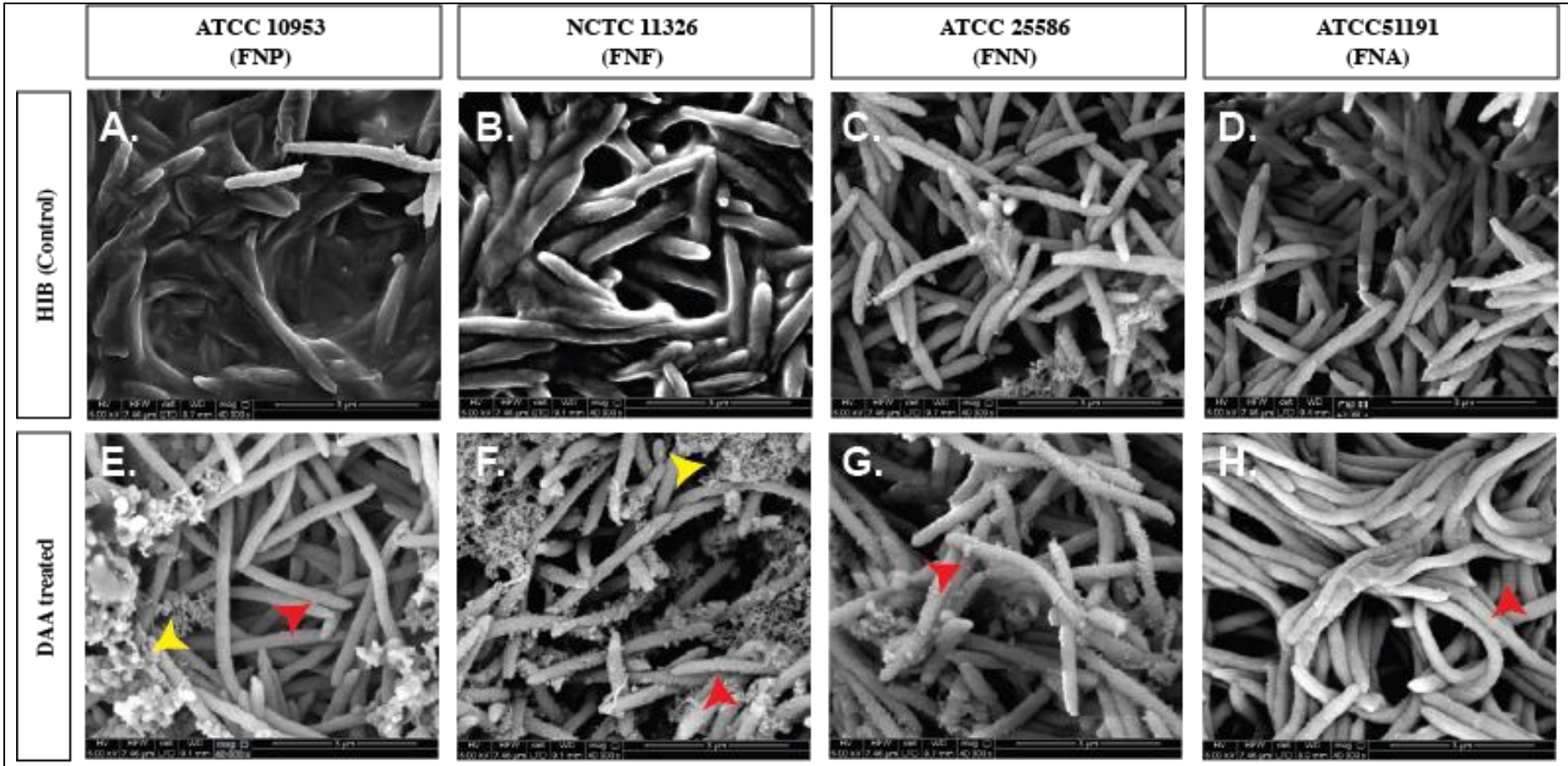

Figure 50: SEM imaging of four *F. nucleatum* subspecies grown as a biofilm

SEM images of **(A)** FNP, **(B)** FNF, **(C)** FNN and **(D)** FNA biofilms and DAA treated counterparts **(E-H)** grown on glass slides over 24 hours. DAAs at concentrations of 25mM for D-Leu, D-Met, D-Trp and 0.25mM for D-Tyr were added at the start of the experiment. Red arrow heads indicate vesicular looking structures and yellow arrowhead indicates extracellular material. Imaged at 40,000X magnification, scale bar 3μm. Three random points of glass slides imaged.

3.3.1.7 Confocal imaging and 3D analysis of *F. nucleatum* biofilms treated with DAAs

Confocal imaging of *F. nucleatum* biofilms grown in modified HIB was conducted using µ-Slide 8 Well ibidiTreat plates (Ibidi) grown in an anaerobic jar, where the biofilm was then Live/Dead stained for confocal microscopy (Section 2.5.1). A decrease in bacterial cell numbers after DAA treatment (25mM for D-Leu, D-Met, D-Trp and 0.25mM for D-Tyr) was added at the start of the experiment can be observed for all 4 subspecies. This observation is reflected in the density of cells (Figure 51 and 52). Both live and dead cells are present in both control and DAA treated groups for all 4 subspecies. Interestingly, as seen in DAA treated FNA using SEM imaging, DAA treated FNP also appeared to show elongated cellular morphology (Figure 51). This was less prominent in the other DAA treated groups for FNF, FNN and FNA.

Furthermore, after 3D rendering the Z-stack confocal images, there was a decrease in biofilm volume after DAA treatment for all four *F. nucleatum* subspecies (Figure 53 and 54).

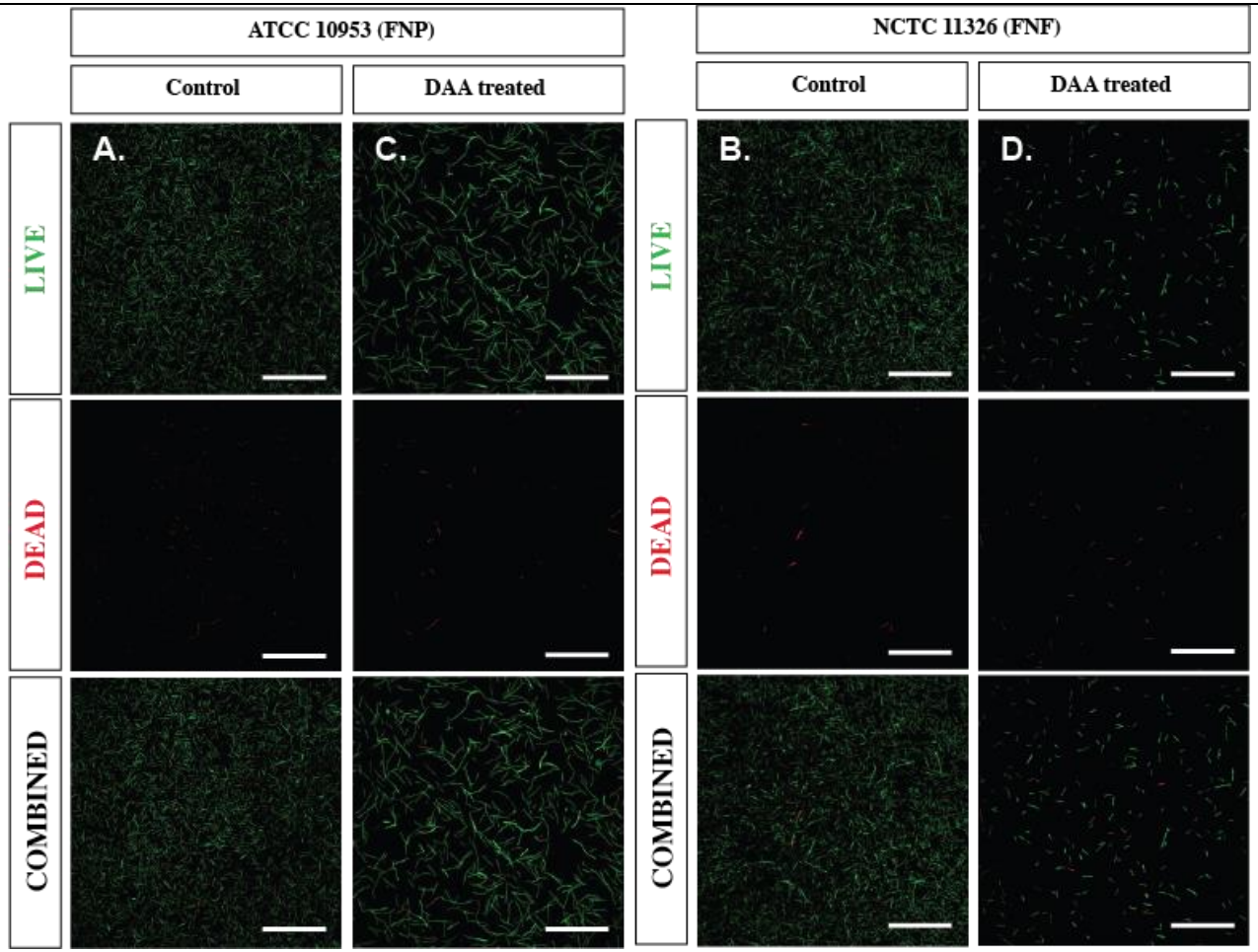

Figure 51: Confocal images of *F. nucleatum* biofilm comparing control and DAA treated group after Live/dead staining

(A) FNP and **(B)** FNF control biofilm and DAA treated counterparts **(C and D)** were imaged at X60 magnification. DAAs at concentrations of 25mM for D-Leu, D-Met, D-Trp and 0.25mM for D-Tyr were added at the start of the experiment. Both Live (green) and Dead (red) channels were imaged. Scale bar 50μm.

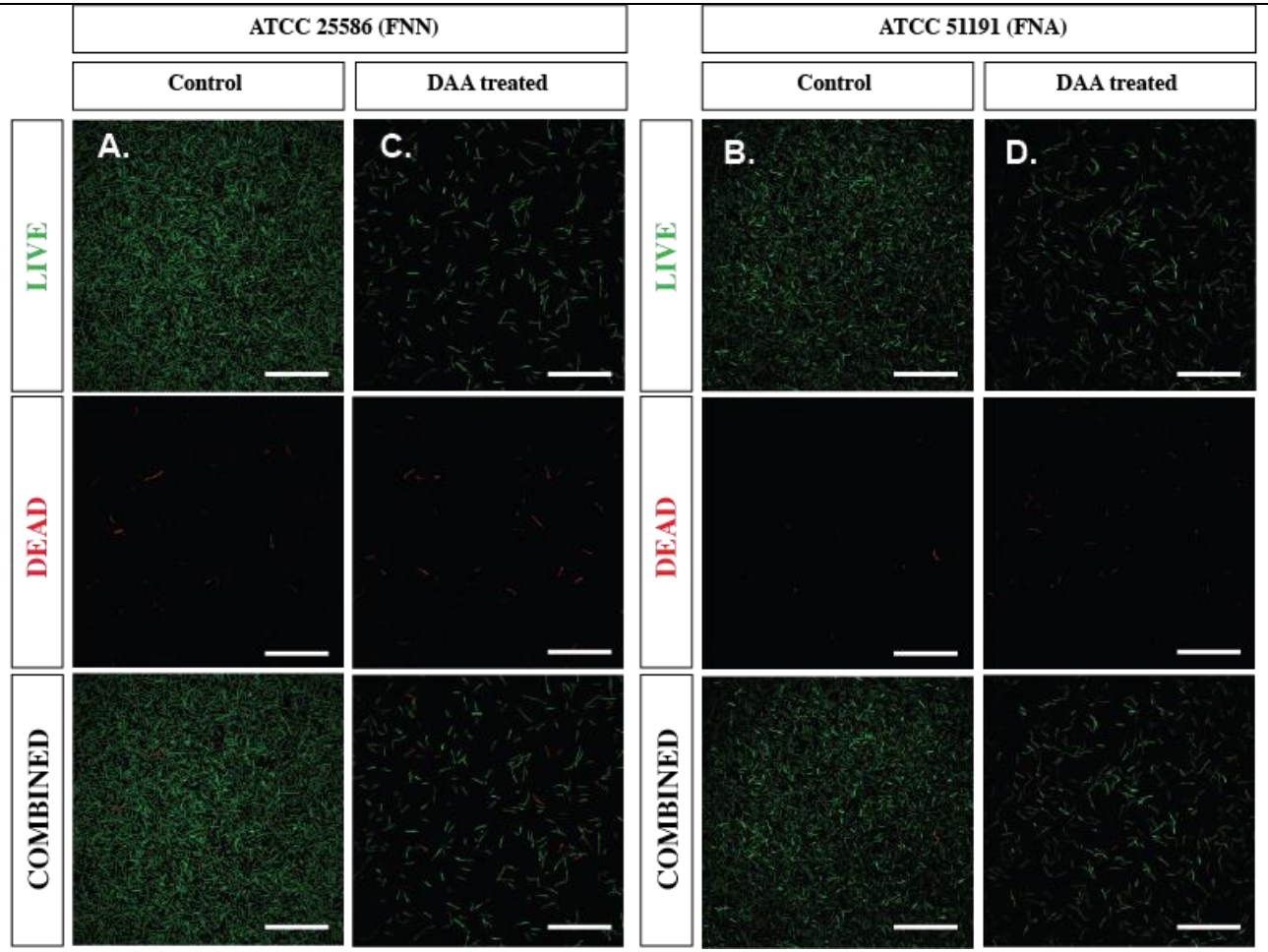

Figure 52: Confocal images of *F. nucleatum* biofilm comparing control and DAA treated group after Live/dead staining

(A) FNN and **(B)** FNA control biofilm and DAA treated counterparts **(C and D)** were imaged at X60 magnification. DAAs at concentrations of 25mM for D-Leu, D-Met, D-Trp and 0.25mM for D-Tyr were added at the start of the experiment. Both Live (green) and Dead (red) channels were imaged. Scale bar 50μm.

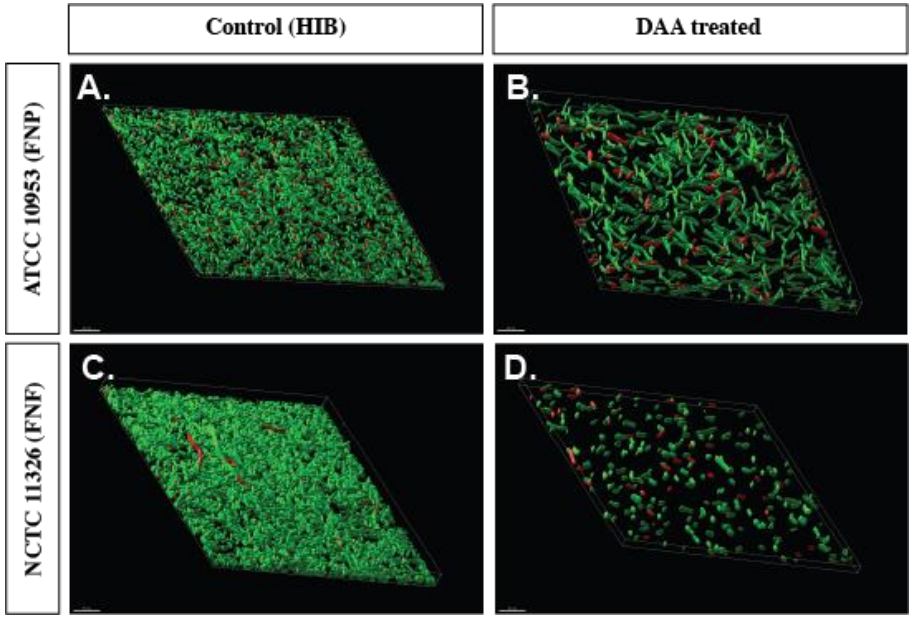

Figure 53: 3D rendering of Live/Dead fluorescent stained FNP and FNF biofilm comparing control and DAA treatment

3D rendered combined live (green) and dead (red) channels of **(A,C)** control and **(B,D)** DAA treated FNP and FNF. DAAs at concentrations of 25mM for D-Leu, D-Met, D-Trp and 0.25mM for D-Tyr were added at the start of the experiment. Scale bars 20μm.

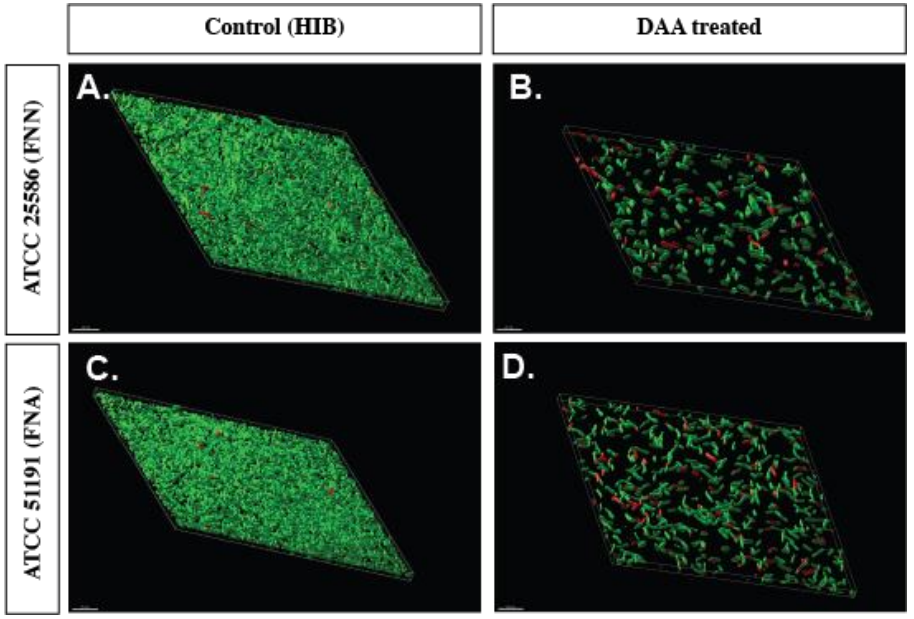

Figure 54: 3D rendering of Live/Dead fluorescent stained FNP and FNF biofilm comparing control and DAA treatment

3D rendered combined live (green) and dead (red) channels of **(A,C)** control and **(B,D)** DAA treated FNN and FNA. DAAs at concentrations of 25mM for D-Leu, D-Met, D-Trp and 0.25mM for D-Tyr were added at the start of the experiment. Scale bars 20μm.

3.3.1.8 *F. nucleatum* biofilm volume after DAA treatment

The Imaris Analysis tool was used after confocal images were obtained for 3D rendering of the biofilm to compare the biofilm volume after DAA treatment was added at the start of the experiment. Due to the experiment conducted in duplicate, statistical analysis was not performed to conclude significance of the results. A decrease in volume was seen for FNF, FNN and FNA after DAA treatment compared to the control. DAA treated FNF and FNN biofilm showed almost 4-fold decrease in mean volume ($1.95X10^4$ μm^3; SD$\pm$ 0.61 and 1.58 $X10^4$ μm^3; SD$\pm$ 0.49 respectively) compared to the control group ($7.53X10^4$ μm^3; SD$\pm$ 0.85 and 6.03 $X10^4$ $\mu m^{3;}$ SD$\pm$ 0.49 respectively). DAA treated FNA showed an almost 3-fold decrease in mean volume ($2.09X10^4$ μm^3; SD$\pm$ 0.29) compared to the control group ($5.92X10^4$ μm^3; SD$\pm$ 1.55). On the other hand, DAA treated FNP showed an increase in mean volume ($5.21X10^4$ μm^3; SD $\pm$ 0.06) compared to the control ($4.12X10^4$ μm^3; SD $\pm$ 1.30) (Figure 55).

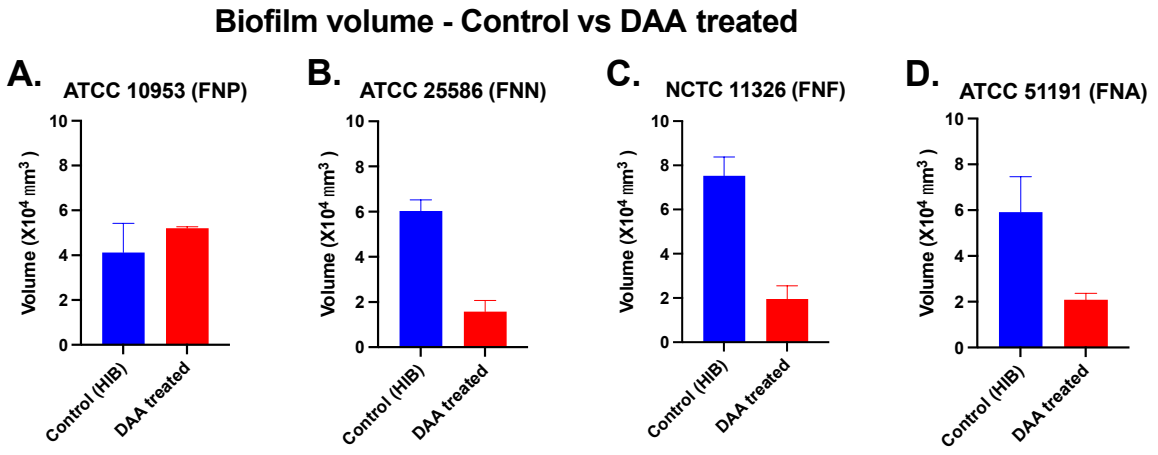

Figure 55: Effect of DAA on *F. nucleatum* biofilm volume

Graph of **(A)** FNP, **(B)** FNF, **(C)** FNN and **(D)** FNA biofilm volume comparing control and DAA treated groups (mean$\pm$SD, n= 2). DAAs at concentrations of 25mM for D-Leu, D-Met, D-Trp and 0.25mM for D-Tyr were added at the start of the experiment.

3.3.1.9 *F. nucleatum* viability after DAA treatment

Imaris Software was also used to compare the viability (%) of *F. nucleatum* after DAA treatment was added at the start of the experiment (Section 2.5.1). Due to the experiment conducted in duplicate, statistical analysis was not performed to conclude significance of the results. Mean viability (%) and SD showed DAA treatment produced a slight decrease and greater variability in the viability compared to controls, ranging from 84.64% (SD± 4.19) to 94.42% (SD± 0.20). FNP biofilm had a decrease in viability of 1.73% (control group mean viability 96.15% SD± 4.46 and DAA treated group mean viability 94.42% SD± 0.20) compared to FNN biofilm which had a decrease in viability of 13.68% (control group mean viability 98.32% SD± 1.52 and DAA treated group mean viability 84.64% SD± 4.19). FNF biofilm had 8.79% decrease in viability (control group mean viability 97.57% SD± 2.64 and DAA treated group mean viability 88.79% SD±5.42) and FNA biofilm had 10.32% decrease in viability (control group mean viability 99.79% SD± 0.06 and DAA treated group mean viability 89.47% SD±0.51). In the control group, the viability of all 4 subspecies was between 96.15% to 99.79% (Figure 56).

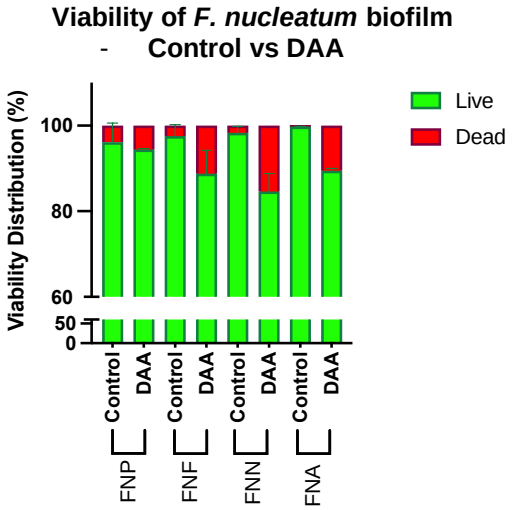

F. nucleatum subspecies	Live (%) Control	Live (%) DAA treated	Decrease in viability (%)
FNP	96.15 SD± 4.46	94.42 SD± 0.20	**1.73**
FNF	97.57 SD± 2.64	88.78 SD± 5.42	**8.79**
FNN	98.32 SD± 1.52	84.64 SD± 4.19	**13.68**
FNA	99.79 SD± 0.06	89.47 SD± 0.51	**10.32**

Figure 56: Effect of DAA at concentration of 25mM for D-Leu, D-Met, D-Trp and 0.25mM for D-Tyr on *F. nucleatum* biofilm viability (%)

Viability (%) calculated after analysis using Imaris software tool of FNP, FNF, FNN and FNA control groups compared to its DAA treated counterparts (mean±SD, n= 2). DAAs at concentrations of 25mM for D-Leu, D-Met, D-Trp and 0.25mM for D-Tyr were added at the start of the experiment.

Furthermore, the viability of *F. nucleatum* after DAA treatment was added at the start of the experiment was also assessed using viable cell counts after 24 hours (Section 2.3). Due to the experiment conducted in duplicate, statistical analysis was not performed to conclude significance of the results. All four subspecies showed a decrease in viable cells compared to their control counterparts. DAA treated FNP showed 1.7-fold decrease (mean viable cell count of control $3.18X10^9$ CFU/ml; SD± 0.95 and DAA treated, $1.80X10^9$ CFU/ml; SD± 0.42). FNA and FNF showed 3- and 4-fold decrease in the viable cell count after DAA treatment ($1.37\ X10^9$ CFU/ml; SD± 1.60 and $1.20\ X10^9$ CFU/ml; SD±1.41 respectively) compared to the control group ($4.15\ X10^9$ CFU/ml; SD± 0.57 and $4.88X10^9$ CFU/ml; SD± 1.38 respectively). FNN showed greatest decrease in viability of cells after DAA treatment with a 6-fold decrease where the control group had mean viable cells value of $4.15\ X10^9$

CFU/ml; SD± 0.28 compared to DAA treated mean value of 6.00 X10^8 CFU/ml; SD± 0.72 (Figure 57).

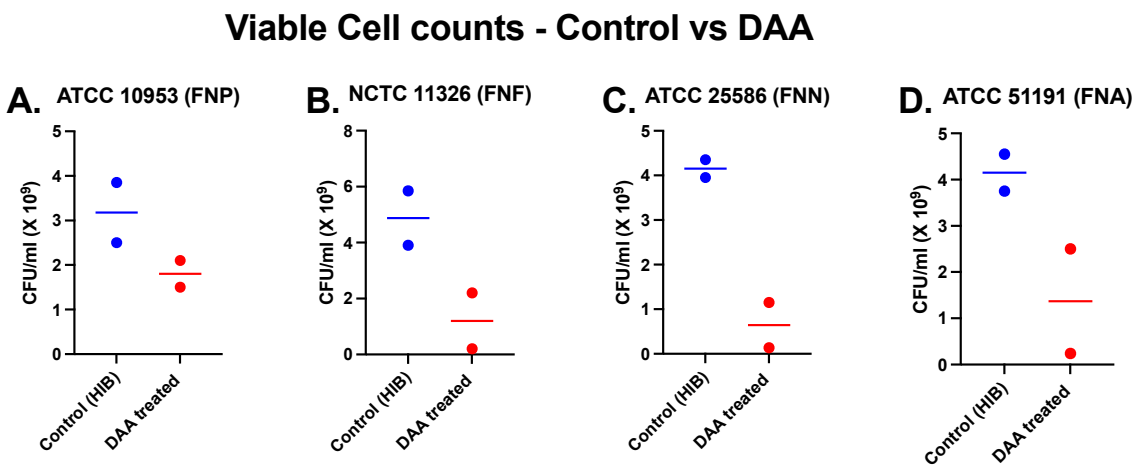

F. nucleatum subspecies	Control (mean value CFU/ml)	DAA treated (mean value CFU/ml)	Effect
FNP	3.18X10^9 CFU/ml SD± 0.95	1.80 X10^9 CFU/ml SD± 0.42	**1.7-fold decrease**
FNF	4.88X10^9 CFU/ml SD± 1.38	1.20 X10^9 CFU/ml SD± 1.41	**4-fold decrease**
FNN	4.15 X10^9 CFU/ml SD± 0.28	6.00 X10^8 CFU/ml SD± 0.72	**6-fold decrease**
FNA	4.15 X10^9 CFU/ml SD± 0.57	1.37 X10^9 CFU/ml SD± 1.60	**3-fold decrease**

Figure 57: Viable cell counts and table comparing *F. nucleatum* growth between control and DAA treated groups

Graph of **(A)** FNP, **(B)** FNF **(C)** FNN and **(D)** FNA growth after viable cell counts comparing control with DAA treated samples in two separate experiments. DAAs at concentrations of 25mM for D-Leu, D-Met, D-Trp and 0.25mM for D-Tyr were added at the start of the experiment.

3.3.2 Effect of D-amino acids on established *F. nucleatum* biofilms

3.3.2.1 Effect of DAA on *F. nucleatum* biofilm dispersion

Crystal violet staining and viable cell count experiments were also performed to investigate the ability of DAA to disperse an established biofilm (Section 2.1.3). DAAs used at concentrations of 25mM for D-Leu, D-Met, D-Trp and 0.25mM for D-Tyr to treat already established *F. nucleatum* biofilm (previously incubated for 24 hours in an anaerobic jar), which was then further incubated for another 24 hours in an anaerobic jar (Section 2.1.3).

There was a significant decrease in biofilm (crystal violet staining) after DAA treatment of biofilms for FNP, FNF and FNN with mean OD_{600nm} readings of 0.96, 1.19 and 0.77 compared to the control groups with mean OD_{600nm} readings of 1.06, 1.60 and 1.36 (Figure 58). The FNA biofilm showed a significant increase in biofilm, (mean value of OD_{600nm} 0.63 for control to 0.72 for the DAA treated group - Figure 58).

Effect of DAA on established *F. nucleatum* biofilm dispersion - Crystal voilet staining

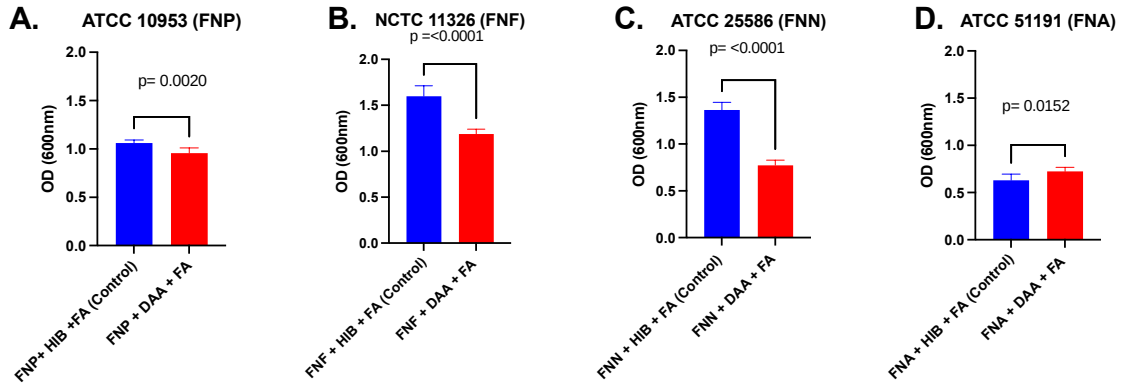

***F. nucleatum* subspecies**	Control (Mean OD_{600nm})	DAA treated (Mean OD_{600nm})	P- value
FNP	1.06 SD±0.05	0.96 SD±0.08	0.0020**
FNF	1.60 SD±0.17	1.19 SD±0.08	<0.0001****
FNN	1.36 SD±0.12	0.77 SD±0.08	<0.0001****
FNA	0.63 SD±0.10	0.72 SD±0.15	0.0152*

Figure 58: Effect of DAA treatment on established *F. nucleatum* biofilms using crystal violet staining

Graph of **(A)** FNP, **(B)** FNF, **(C)** FNN and **(D)** FNA biofilm after DAA treatment at 24 hours (mean± SD, n= 12). DAAs at concentrations of 25mM for D-Leu, D-Met, D-Trp and 0.25mM for D-Tyr were added to already established *F. nucleatum* biofilms; ns denotes no significant difference, * denotes significant difference compared to the control (p< 0.05) using unpaired t-test (* p<0.05, ** p<0.01, ***p<0.001).

For all four subspecies, there were no obvious changes in viability compared to the control seen from viable cell count results (Figure 59). Due to the experiment conducted in duplicate, statistical analysis was not performed to conclude significance of the results.

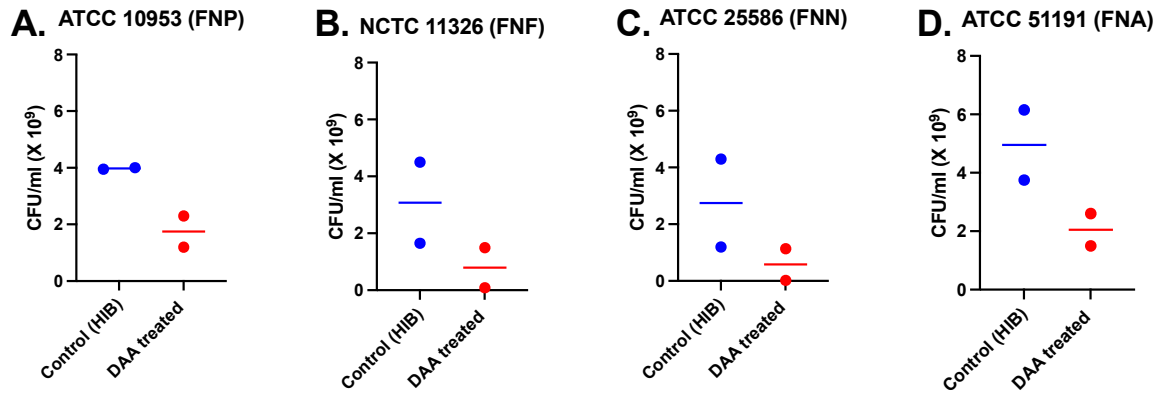

Figure 59: Scatter plot showing viable cell counts comparing *F. nucleatum* growth between control and DAA treated groups

Graph of **(A)** FNP, **(B)** FNF **(C)** FNN and **(D)** FNA viable cell counts comparing effect of DAA to the control in two separate experiments. DAAs at concentrations of 25mM for D-Leu, D-Met, D-Trp and 0.25mM for D-Tyr were added to already established *F. nucleatum* biofilms

3.3.3 Effect of Polycationic Silver nanoparticles (AgNPs)

3.3.3.1 Effect of AgNPs on the growth of *F. nucleatum*

Another novel antimicrobial agent that was used to investigate the effect on *F. nucleatum* growth was polycationic AgNPs (Section 2.2.2). Similar, to the DAA experiments, various concentrations (ranging from 10µg/ml- 60µg/ml) of pre-prepared AgNPs were added to a culture of each four subspecies of *F. nucleatum* grown in modified HIB at the start of the

experiment and incubated for 24 hours. The effect on the growth was evaluated by viable cell counts (Section 2.3).

AgNPs at concentrations ranging from 10-60µg/ml were used. Viable cell counts showed a concentration dependant trend for all four subspecies, where the concentration of AgNPs was inversely proportional to viability (Figure 60). Due to the experiment conducted in duplicate, statistical analysis was not performed to conclude significance of the results. FNP and FNA showed a decrease in viable cell numbers at a AgNP concentration of 40µg/ml (mean of 5.74; SD±5.67 and 7.37 $X10^9$ CFU/ml; SD±3.03 respectively) compared to the control (mean of 1.01; SD±1.30 and 1.28 $X10^{10}$ CFU/ml; SD±0.85 respectively). FNF showed a decrease in viable cell numbers at a AgNP concentration of 20µg/ml (mean of 0.18$X10^9$ CFU/ml; SD± 0.13) compared to control (mean of 16.93 $X10^9$ CFU/ml; SD±3.78) while FNN showed decrease at AgNP concentration 10µg/ml (mean of 5.57 $X10^9$ CFU/ml; SD±3.04) compared to control (mean of 16.97; SD± 3.78 and 21.43 $X10^9$ CFU/ml; SD±0.75 respectively). FNN was the most sensitive to AgNP treatment (Figure 60).

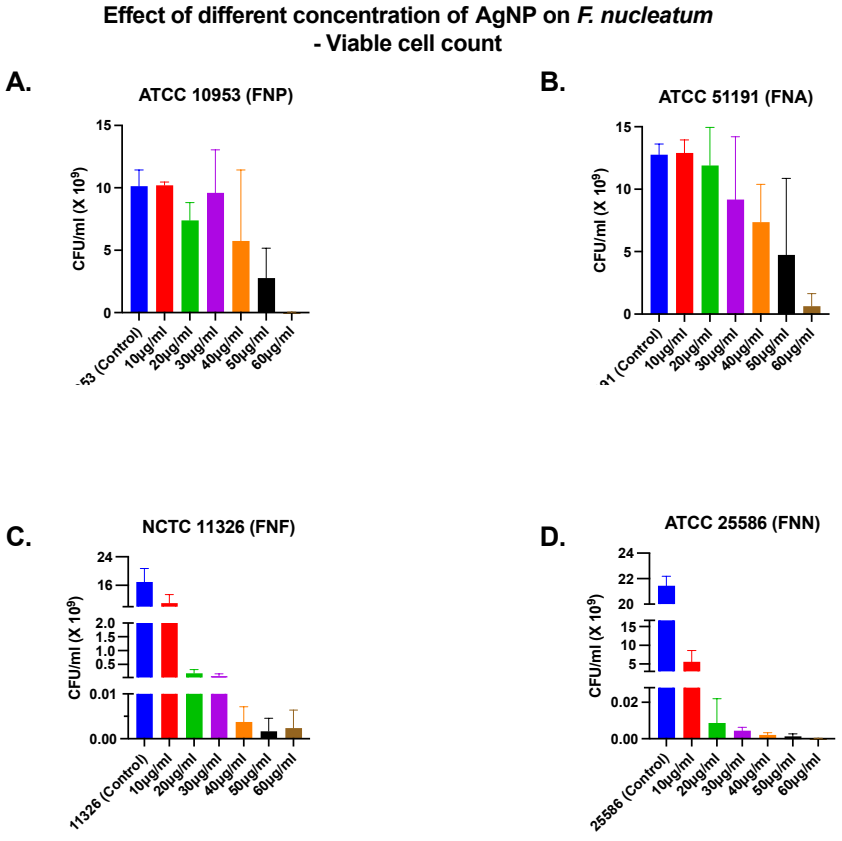

Figure 60: Viable cell count of *F. nucleatum* treated with polycationic AgNP

Viable cell counts of AgNP treated **(A)** FNP, **(B)** FNA **(C)** FNF and **(D)** FNN (mean± SD, n= 2).

3.3.3.2 Confocal imaging of Live/Dead stained *F. nucleatum* biofilms treated with AgNP

Confocal imaging was performed on *F. nucleatum* biofilms after Live/Dead staining. *F. nucleatum* subspecies were treated with AgNPs (60μg/ml) added at the start of the experiment (Section 2.5.1). Due to AgNPs being used at a high concentration of 60μg/ml, it formed clumps which was visually observed when added into the μ-Slide 8 Well ibidiTreat plates (Ibidi) with *F. nucleatum*. Morphological differences between *F. nucleatum* and AgNPs can be seen as fusiform cells against the spherical clumps of AgNPs (Figure 61 and 62). All four subspecies of *F. nucleatum* showed a significant reduction in bacterial cell number after being treated with 60μg/ml AgNPs, represented by decrease in number of rod-shaped bacteria per confocal image (Figure 61 and 62). These were all qualitative observations, due to difficulty for Imaris analysis tool to differential between *F. nucleatum* and AgNPs.

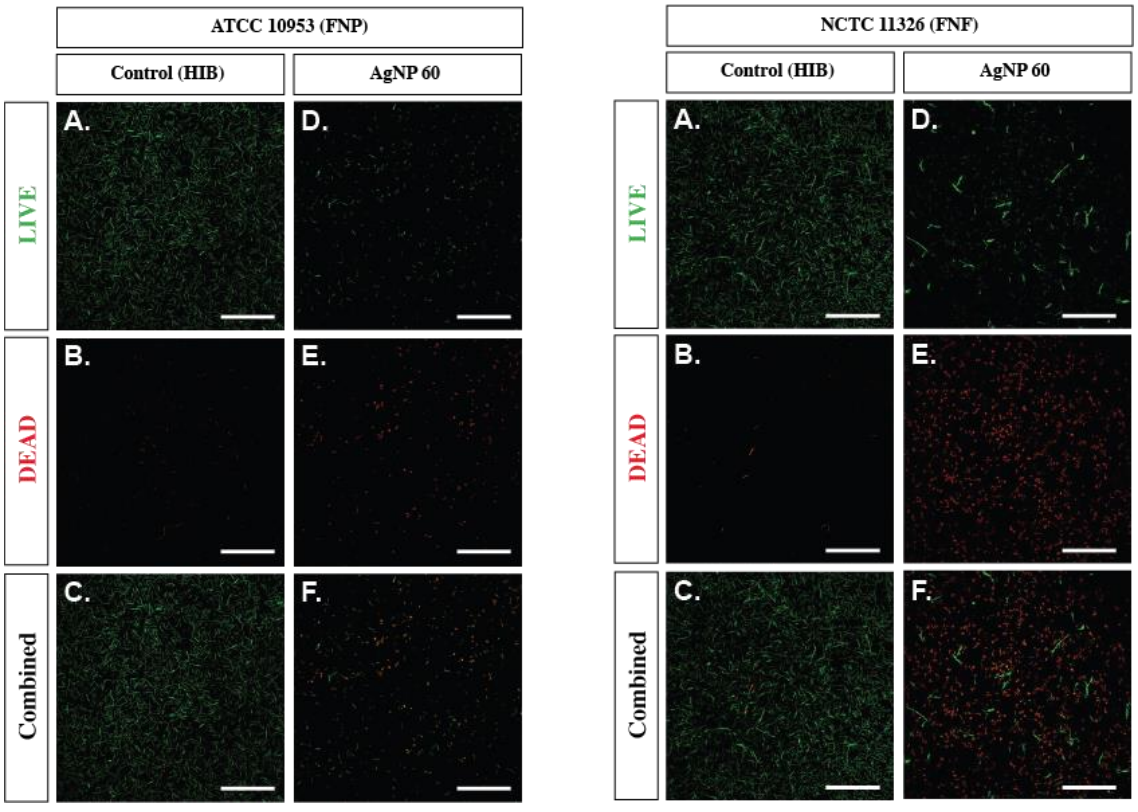

Figure 61: Confocal images of FNP and FNF biofilm comparing control and AgNP treated biofilm after Live/dead staining

(C) FNP and FNF control biofilm and AgNP 60μg/ml treated counterparts **(F)** were imaged at X60 magnification. AgNPs at concentrations of 60μg/ml were added at the start of the experiment. Both Live (green) and Dead (red) channels are imaged **(A-F)**. Scale bar 50μm.

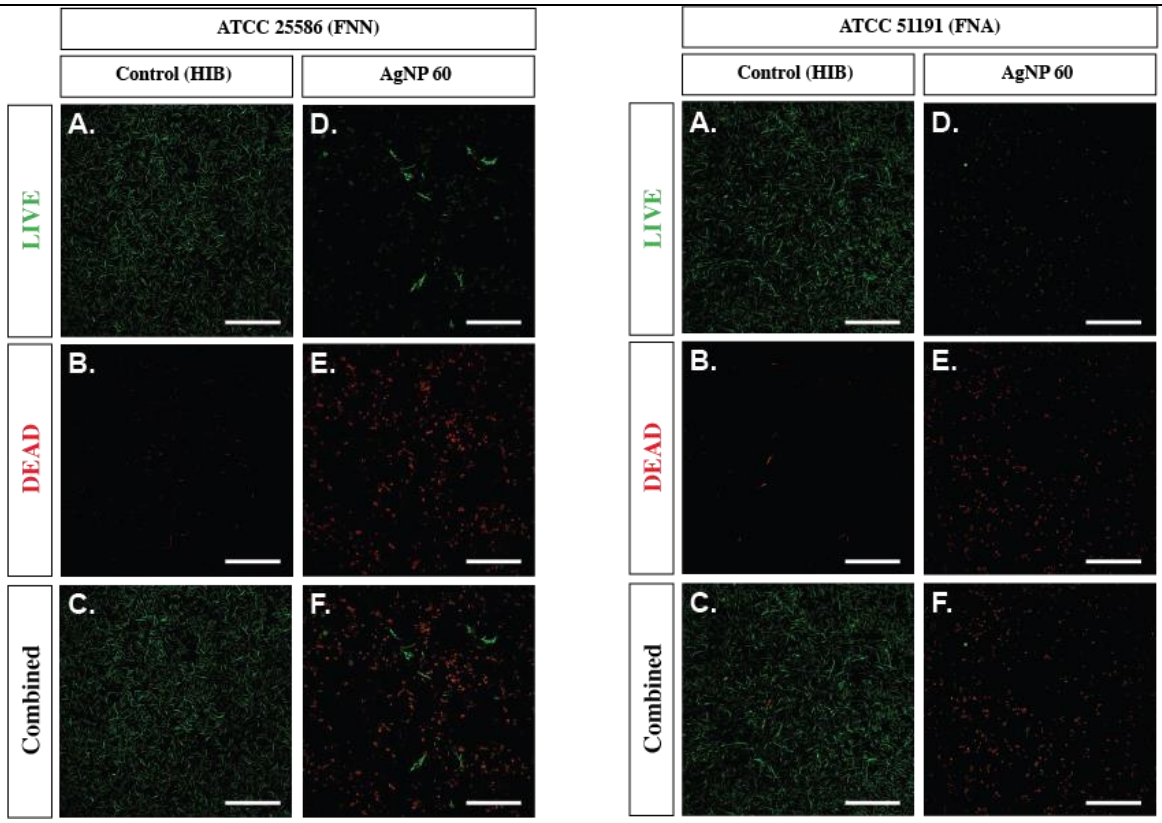

Figure 62: Confocal images of FNN and FNA biofilm comparing control and AgNP treated biofilm after Live/dead staining

(C) FNN and FNA control biofilm and AgNP 60μg/ml treated counterparts **(F)** were imaged at X60 magnification. AgNPs at concentrations of 60μg/ml were added at the start of the experiment. Both Live (green) and Dead (red) channels are imaged **(A-F)**. Scale bar 50μm.

3.3.3.3 Effect of *F. nucleatum* biofilm volume after AgNPs (60μg/ml) treatment

Due to the Imaris analysis tool's inability to differentiate between *F. nucleatum* and AgNPs, this interfered with the analysis of the biofilms. Therefore, biofilm viability (%) and volume ($X10^4$ μm^3) were unable to be assessed after AgNPs were added at the start of the experiment. However, through Z-stack confocal imaging, all four subspecies showed a dramatic reduction in biofilm volume which can be visually seen from the dispersion of bacterial cells after 3D rendering (Figure 63 and 64). Moreover, AgNPs non-specifically bound to both the Live (green) and Dead (red) stain, appearing orange in colour due to colocalization of the stain (Figure 63 and 64).

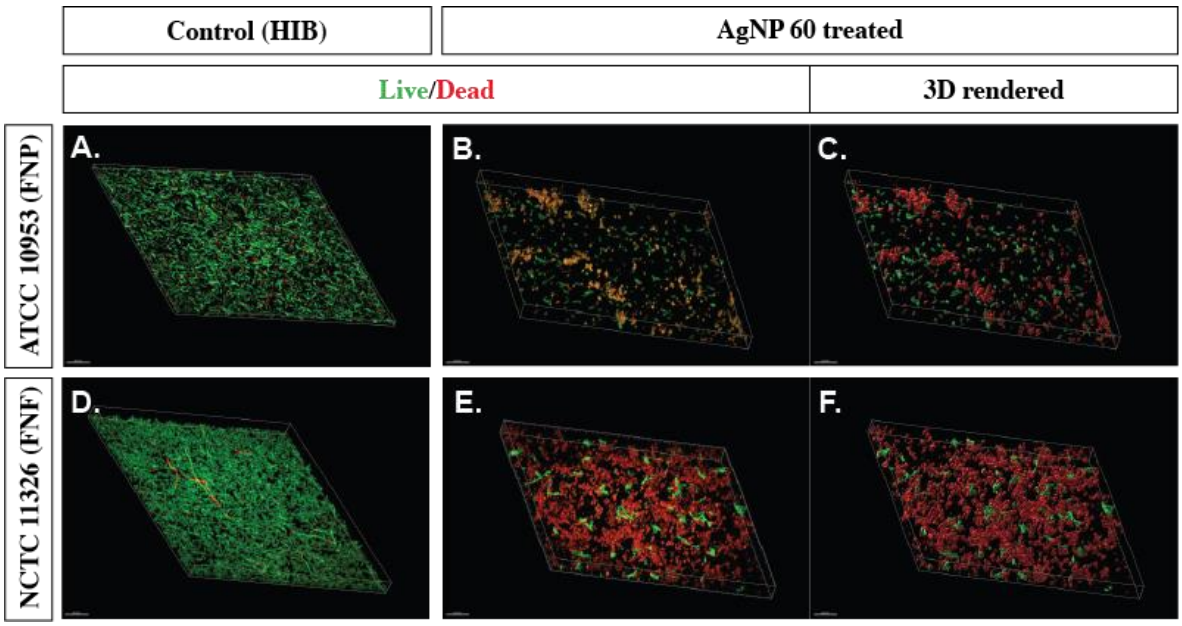

Figure 63: Z stack images and 3D rendering of Live/Dead fluorescent stained FNP and FNF biofilm comparing control and AgNP 60 treated biofilm volume

Comparison of confocal images of **(A)** FNP and **(D)** FNF control groups and AgNP 60 treated **(B,E)** biofilm with **(C,F)** 3D rendering. Combined live (green) and dead (red) channels are imaged. AgNPs at concentrations of 60μg/ml were added at the start of the experiment. Scale bars 20μm.

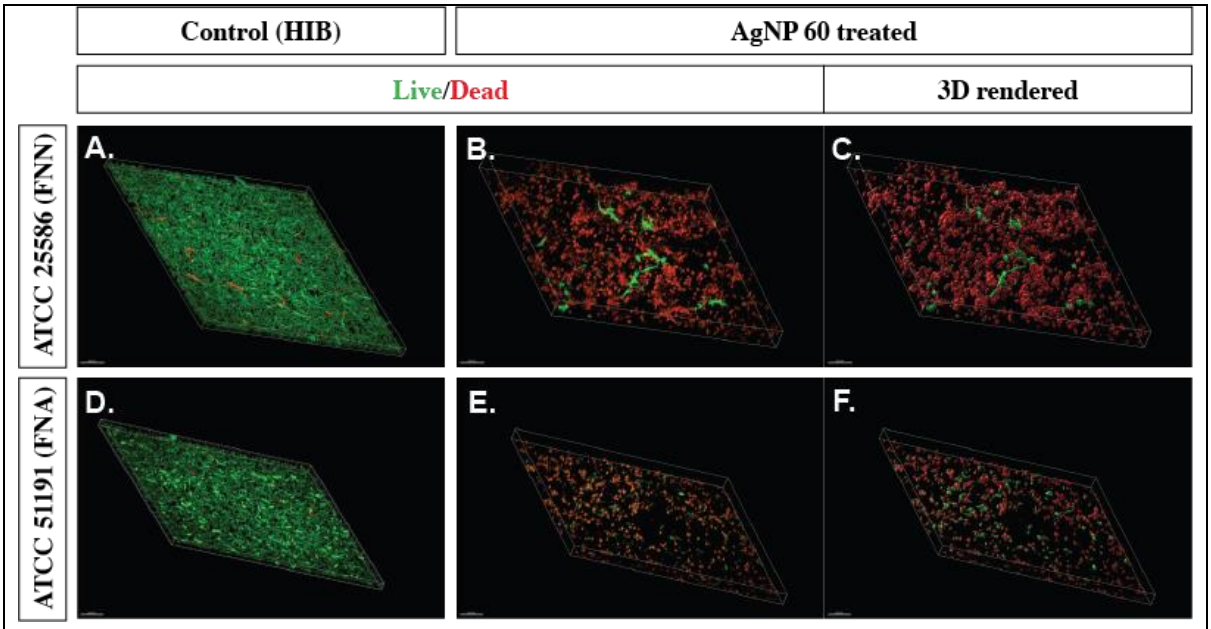

Figure 64: Z stack images and 3D rendering of Live/Dead fluorescent stained FNN and FNA biofilm comparing control and AgNP 60 treated biofilm volume

Comparison of confocal images of **(A)** FNN and **(D)** FNA control groups and AgNP 60 treated **(B,E)** biofilm with **(C,F)** 3D rendering. Combined live (green) and dead (red) channels are imaged. AgNPs at concentrations of 60μg/ml were added at the start of the experiment. Scale bars 20μm.

3.3.4 Effect of Gold Nanoparticles (AuNPs)

3.3.4.1 Effect of AuNPs on the growth of FNN

The final novel antimicrobial agent tested was AuNPs. AuNPs were added to FNN inoculum at the start of the experiment, which was then incubated over 24 hours before undergoing viable cell counting (Section 2.1.3). Due to time constraints, only FNN subspecies was used for the following experiments.

AuNPs at concentrations ranging from 10-60μg/ml were investigated. AuNPs followed a similar result to AgNPs where viable cell numbers decrease as the concentration of AuNPs increased (Figure 65). Due to the experiment conducted in duplicate, statistical analysis was not performed to conclude significance of the results. At AuNP concentration of 10μg/ml, there was a 4.4-fold decrease in viable cell numbers (mean value of 4.95 $X10^9$ CFU/ml; SD±4.03) compared to the control (mean value of 22.0 $X10^9$ CFU/ml; SD±0.71). There was a greater decrease in viability when FNN was treated with AuNP at a concentration 20μg/ml or greater (Figure 65).

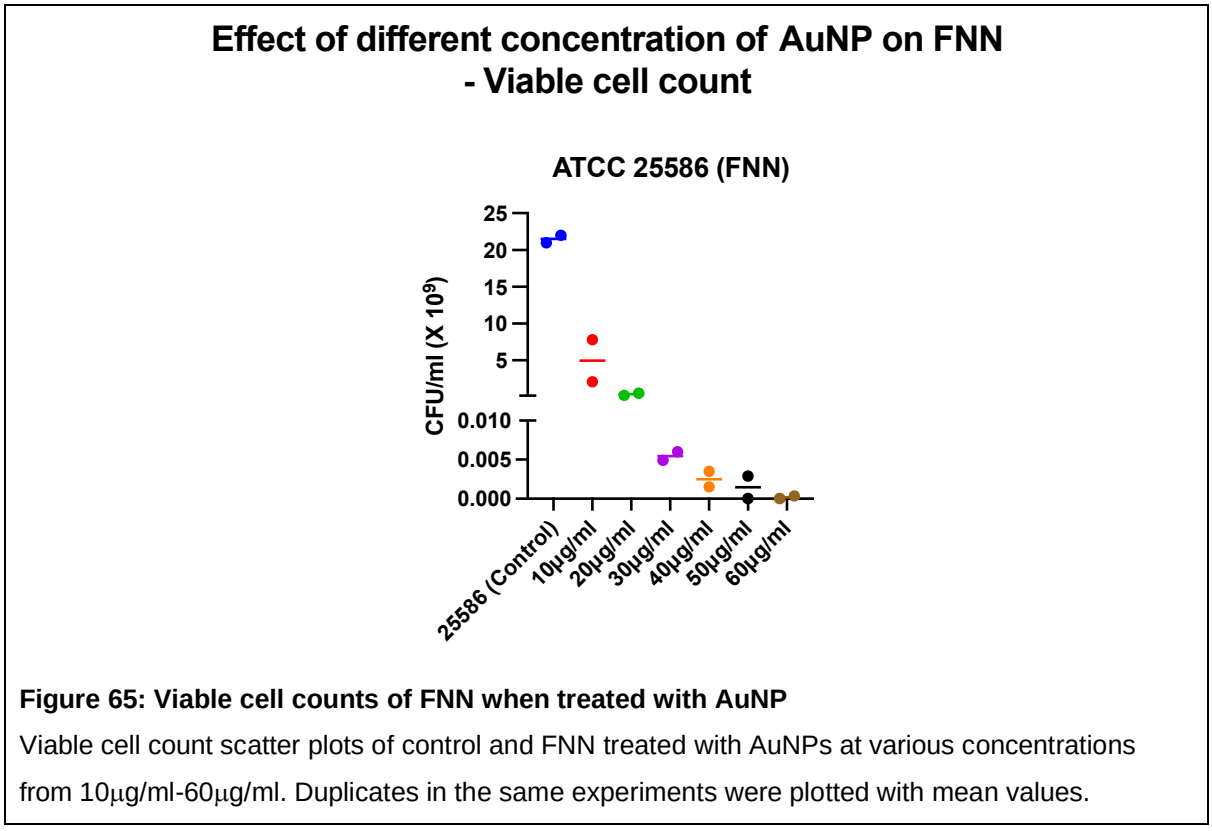

Figure 65: Viable cell counts of FNN when treated with AuNP

Viable cell count scatter plots of control and FNN treated with AuNPs at various concentrations from 10μg/ml-60μg/ml. Duplicates in the same experiments were plotted with mean values.

CHAPTER 4: DISCUSSION AND CONCLUSION

4.1 Protocol optimisation

4.1.1 Overcoming difficulties creating an anaerobic environment in the spectrophotometer to measure growth of *F. nucleatum*

Early in the project, a major issue was faced in creating an anaerobic environment to facilitate growth of *F. nucleatum*, an obligate anaerobe, within the spectrophotometer at 37°C. When the four subspecies of *F. nucleatum* were grown without any interventions to achieve anaerobic conditions, FNP and FNA showed minimal growth as expected. Surprisingly, although *F. nucleatum* is known to only grow under strict anaerobic conditions and can be susceptible to atmospheric oxygen (Spaulding and Rettger, 1937), FNN and FNF showed significant growth (Figure 13).

Although there is no current literature on using mineral oil to grow *F. nucleatum* specifically, sterile mineral oil is a well-known method used to create anaerobic conditions (Hall, 1929; Hanisakova et al., 2022; Jacobson et al., 2004). Therefore, sterile mineral oil was overlayed on samples in each well to achieve anaerobic conditions. However, although growth of FNP and FNA improved as seen by the increase in log phase and decrease in doubling time, growth was still not comparable to FNN and FNF (Figure 14). In this project we have shown that there are sub-species specific differences in *F. nucleatum* growth. FNP and FNA showed increase sensitivity to oxygen compared to FNN and FNF, current literature has not addressed these differences, however, it could be possibly to due to in genetic differences (Gharbia and Shah, 1989; Kim et al., 2010; Kook et al., 2013; Nie et al., 2015). The ability for the four subspecies to produce NADH oxidases to remove oxygen differed. Further examination of their genetic sequences may provide clarification. For all four subspecies, the volume of mineral oil (50µl vs 75µl) had minimal effects on the growth (Section 3.1.1.2-3). The mineral oil overlay also provided technical challenges when adding antimicrobial/antibiofilm treatments to established biofilms.

Mineral oil was therefore replaced with AxySeal Plastic Sealing Film. At experimental completion, if further experiments were needed, samples were able to be accessed by making a small opening through the plastic film with a sterile surgical blade and re-sealed with AxySeal Plastic Sealing Film. FNP and FNA showed improved growth when a combination

of anaerobic sachet material and AxySeal Plastic Sealing Film was used (Figure 19). While other creative methods such as OVAMO (use of Oxyrase enzyme to remove dissolved oxygen, applying a partial VAcuum to remove oxygen in the air and Mineral Oil) has been suggested to generate an *in situ* anaerobic environment within the 96-well microtiter plate (Lam et al., 2018), the combination of anaerobic sachet material and AxySeal Plastic Sealing Film was deemed more appropriate and effective (Section 3.1.1.5). Furthermore, it is to be noted that to reduce static and risk of anaerobic sachet material dispersing into samples when sealing the plate, spraying the AxySeal Plastic Sealing Film lightly with 80% alcohol before sealing was very effective.

Moreover, this may be less of a problem for spectrophotometers that enable the lid to be placed on the microtiter tray. If so, the use of a mineral oil overlay and sealing the lid with a thin layer of Vaseline may be effective.

4.1.2 Optimisation of the Crystal Violet (CV) staining protocol to minimise disruption of the *F. nucleatum* biofilm

As previously discussed in Section 3.1.2, *F. nucleatum* biofilms grown in modified HIB resisted multiple washing and staining steps during the CV protocol. However, DAA treated biofilms were loosely attached, displaying excessive and unpredictable dispersion during the CV protocol, leading to greater variability in the results (Figure 23). Similar observations with the difficulty of staining *F. nucleatum* biofilms was reported by Muchova et al. (2022). Therefore, this study used different well preparations including sandblasting glass surface, artificial saliva, fibronectin, gelatine, and Poly-L-Lysine to investigate if adhesion of the biofilm improves. They concluded that Poly-L-Lysine and sandblasting glass surface was the most effective. Furthermore, due to time constraints, one subspecies FNN (ATCC 25586) was chosen to develop the protocol.

Kruskal Wallis test with Dunn's multiple comparison post-hoc test comparing DAA treated FNN and DAA treated FNN with well coatings (sterile human saliva or Poly-L-lysine and/or fixation with 4% formaldehyde) showed that Poly-L-lysine showed significantly better adhesion of FNN biofilm (Section 3.1.2.2). Poly-L-lysine coating has been recommended to promote bacterial adhesion in *E. coli* (Benn et al., 2019; Cowan et al., 2001) and *F.*

nucleatum (Muchova et al., 2022). Furthermore, fixating DAA treated FNN biofilms with 4% formaldehyde reduced the variability within the sample groups (Figure 26).

While the PLL well coating showed a significant decrease in the dispersal of biofilm, fixing the DAA treated biofilm with 4% formaldehyde post-experiment for 10 minutes gave the best results (Section 3.1.2.3). Therefore, this method was chosen for CV staining and was just as effective amd less time consuming as PLL coating microtiter plates as PLL coating can take more than an hour to prepare (Section 2.4.2). It was concluded that fixating biofilm with 4% formaldehyde at the end of the experiment for 10 minutes sufficiently increased reproducibility of the results and reduced detachment of the *F. nucleatum* biofilm.

4.1.3 Optimising the confocal imaging protocol for Imaris analysis of *F. nucleatum* biofilms

Optimising the confocal imaging process was time consuming but important to visually assess the quality as well as quantify the biofilm through viability (%) and volume ($X10^4$ μm^3) analysis using Imaris Software. This was performed after the biofilm was Live/Dead stained and Z-stack images were captured. Due to time limitations, FNN was chosen to optimise the confocal imaging protocol.

Initially, biofilms with and without DAA treatments were grown on 13mm glass cover slips in a 24-well microtiter plate which were then prepared for confocal imaging following Live/Dead staining (Elliott, 2020). However, as previously discussed in Section 3.1.2, DAA biofilms were unable to withstand the multiple washing and staining stages as well as the physical transfer onto glass slides for confocal imaging, leading to large variability in the biofilm analysis (Figure 28 – Method 1).

Therefore, µ-Slide 8 Well ibidiTreat plates (Ibidi) were investigated. The ibidiTreat (tissue culture-treated) surface allowed for optimal cell adhesion and the smaller well size allowed for more controlled washing and staining with minimal disruption to the biofilm (Figure 29) Furthermore, this method allowed for a better optical quality image due to its very thin 180µm polymer coverslip base which could immediately be used for confocal microscopy without the need to transfer elements to glass slides (Figure 28- Method 2).

An additional challenge was to try to achieve representative Z- stack confocal images of the biofilm which enables the Imaris Analysis software to quantify the viability (%) and biofilm volume ($X10^4$ μm^3). For the software to be able to analyse these parameters, it needs to be able to detect and count each bacterial cell (Figure 32 and 37). High cell density per confocal image and fusiform shape of the bacteria interferes with the software function, leading to inaccurate results in measuring the number of live and dead cells.

Reducing the incubation time from 24 hours to 7 hours as well as reducing the initial inoculum to OD_{600nm} 0.003 produced the best outcome (Figure 36), allowing the Imaris Software to count individual bacterial cells accurately and perform quantitative analysis of the biofilm (Figure 37).

While fixation of samples is common in SEM imaging, it is not routinely carried out for confocal imaging. However, fixating the biofilm with 4% formaldehyde (FA) was carried out to investigate if disruption to the biofilm during Live/Dead staining could be minimised (Section 3.1.3.4), following a similar to protocol to Muchova et al. (2022). Initial concerns were that fixation of the biofilm with 4% FA may kill the cells and over represent dead cells after Live/Dead staining, however this was not the case as samples fixed and not fixed with 4% FA showed similar live to dead ratio per confocal image, 4% FA appeared to interfere with the dead channel (red), dampening down the overall signal (Figure 35). Therefore, 4% FA fixation was chosen not to be used.

Finally, X60 magnification was more suitable than X40 magnification, as greater magnification of the field allows for Imaris software to identify each cell and perform quantitative analysis more accurately (Figure 37). For subsequent confocal microscopy experiments using novel anti-microbial compounds, the *F. nucleatum* inoculum (OD_{600nm} of 0.003) in modified HIB was incubated for 7 hours in µ-Slide 8 Well ibidiTreat plates in anaerobic jars. Live/Dead staining was conducted, and confocal microscopy was performed at X60 magnification. To date, there are no such detailed protocol that has been described in the literature investigating optimisation for *F. nucleatum* biofilm analysis on Imaris Software, making this a novel protocol.

4.1.4 Optimising the xCELLigence® protocol to facilitate *F. nucleatum* growth for real-time biofilm analysis

The xCELLigence® platform is a microfluidic cell analyser that integrates impendence-based technology, revolutionising biofilm research in the recent years (Mira et al., 2019). Unlike standard end-point cell assays, it is designed to allow continuous real-time cell analysis to monitor biofilm growth in a non-invasive and label free manner as well as producing accurate and reproducible results. While extensive studies have been conducted for growing aerobic biofilms for *Streptococcus mutans, Streptococcus sanguinis, Candida albicans* and *lactobacilli* spp. (Abrantes and Africa, 2020; Martinez et al., 2020; Mira et al., 2019; Muras et al., 2018) in the xCELLigence® platform, to date, there is limited data for anaerobic oral bacteria, including *F. nucleatum*. This is most likely due to the fact that creating an adequate anaerobic environment within the xCELLigence® platform is difficult and has not yet been investigated. Therefore, one of the aims of this project was to grow *F. nucleatum* biofilm in the xCELLigence® platform under anaerobic conditions.

Due to previous challenges creating an anaerobic condition within the spectrophotometer (Section 4.1.1) similar methods were used to create an anaerobic environment in the xCELLigence® platform. Anaerobic sachet material was dispensed into evaporation wells before the lid was sealed with dental impression material (Section 2.6.2). Anaerobicity was confirmed through the use of an anaerobic indicator strip (Oxoid) (Figure 38).

Although FNP, FNF and FNN appeared to form biofilms in the first hour of the experiment, the CI soon dropped below zero. Usually, a decrease in CI indicates the dispersion of the biofilm. This is a phenomenon that has not yet been documented in other studies on oral bacteria (Abrantes and Africa, 2020; Martinez et al., 2020; Mira et al., 2019; Muras et al., 2018). FNA had the most variable CI readings and the CI fell below zero at the start of the experiment. CI of all four subspecies of *F. nucleatum* remained below zero over 24 hours. While coating surfaces with sterile human saliva is a common method *in vitro* to mimic host environment and to increase growth and adherence of the biofilm (Vyas et al., 2022), coating the E-plate wells with sterile human saliva nor changing the inoculum concentration improved this issue (Section 3.2.4 and 3.2.5).

Further discussion occurred with Dr Alex Mira from the Oral Microbiome Laboratory at the FISABIO foundation in Spain who has extensive experience and knowledge in the use of xCELLigence® platform. However, it was concluded that possibly the xCELLigence® platform is unable to register the forming *F. nucleatum* biofilm where it could be attributed to the organism producing metabolites that may interfere with the electric current, affecting the CI readings.

The crystal violet experiments demonstrated that biofilm formed for all four subspecies (Figurer 49) and *F. nucleatum* biofilm was also visualised in the E-plate 16 VIEW at experimental completion. To further confirm this using the xCELLigence® platform, E-plate 16 VIEW plates with a glass bottom and bigger viewing window between the gold electrodes for imaging were used (Section 2.6.5). FNN was used for this investigation, however, without adjustments to the E-plate (Figure 11) confocal imaging was not possible due to the bottom of the well being too far away from the confocal microscope lens, making focusing on the image impossible. This was overcome by customising the E-plate to sit flush with the confocal stage (Figure 12).

In addition, biofilm analysis was impossible as the final confocal image resolution was too low. However, the FNN biofilm was visualised with a mixture of both live and dead cells, confirming biofilm formation in the xCELLigence® platform (Figure 45). However, magnification greater than 10 times was unable to be used due to low image resolution. The manufacturer of the xCELLigence® E-plates was contacted and further investigation revealed that neither xCELLigence® E-plates PET nor VIEW are suitable for confocal imaging due to the thickness of the bottom of the E-plates being greater than 1mm which is too thick for confocal imaging (Elliott, 2020). Therefore, further investigation using confocal imaging was not able to be conducted.

From these findings, it can be concluded that *F. nucleatum* biofilm is forming under anaerobic conditions in the xCELLigence® E-plates but is not being recognised as increased CI readings. Although one of my aims of this project was to grow *F. nucleatum* biofilm in the xCELLigence® platform and investigate the effect of novel antimicrobials, difficulties encountered getting the xCELLigence® platform to recognise *F. nucleatum* biofilms meant further experiments were not pursued.

4.2 Effect of novel anti-biofilm compounds on *F. nucleatum* – D-amino acids

DAAs have previous been reported to be an effective biofilm dispersing agent in dental unit waterlines (Ampornaramveth et al., 2018) as well as potential antibiofilm agent to be used in endodontic treatment mixed into medicaments (Khider et al., 2021; Rosen et al., 2016; Zilm et al., 2017). However, currently literature has not investigated the effect of DAAs on *F. nucleatum* growth inhibition and biofilm dispersion.

Interestingly, when DAAs were added to *F. nucleatum* at the start of the experiment, biofilms were visually different compared to the control, more obviously in FNF and FNN, having a sun ray appearance. For all subspecies DAA treated biofilm appeared to be loosely attached compared to the control (Figure 46) indicating a role of DAA's in disrupting the biofilm.

While various concentrations of DAAs ranging from 12.5mM of D-Leu, D-Met, D-Trp and and 0.125mM of D-Tyr (dissolved and diluted to 50% of original concentration) to 6.25mM of D-Leu, D-Met, D-Trp and 0.063mM for D-Tyr (dissolved and diluted to 12.5% of original concentration) were tested, the concentration of 25mM each for D-Leu, D-Met, D-Trp and 0.25mM for D-Tyr as previously published by Zilm et al., (2017) was deemed most effective (Section 3.3.1.3). Therefore, for all experiments, this concentration of DAAs were used to treat *F. nucleatum* to investigate its antibiofilm effects. This combination of DAAs presents promising antibiofilm effects as seen in this project (Section 3.3) and previously published studies (Ampornaramveth et al., 2018; Zilm et al., 2017).

Biofilm volume analysis supported by 3D rendering using Imaris software generally showed a decrease in biofilm volume, with exception of FNP, which will be further discussed in Section 4.2.1. Due to time constraints the experiment was only repeated twice, statistical analysis was not able to be conducted to conclude its significance. Nevertheless, 3D rendered images showed a decrease in biofilm volume therefore it can be assumed that DAAs were successful in biofilm dispersal. The differences in biofilm volume between the DAA treated *F. nucleatum* and the control were less obvious using crystal violet staining (Figure 49). However, this may be due to the longer incubation time of 24 hours for CV staining (Section 2.4).

Viability (%) through Imaris software analysis and viable cell counts showed similar results for all four subspecies where there were minimal effects on the viability after DAA treatment

at the start of the experiment. It is of note that even with the decrease in number of cells that can be seen after DAA treatment in the confocal images (Figure 53 and 54), viability remained unchanged where it consisted of mostly live cells (green) with minimal dead cells (red) (Section 3.3.1.7). This further emphasises the fact that DAAs are biofilm breakers and do not have bactericidal effects, shown through results from viable cell counts and viability (%) analysis suggesting DAAs reduced growth was only several fold difference and not significant log-fold differences. This is to be expected as DAAs are commonly found in nature being produced by Gram-negative bacteria such as *Vibrio cholera* and *Pseudomonas putida* (Espaillat et al., 2021; Radkov and Moe, 2018) as well as being routinely found as a constituent in the peptidoglycan (PG) cell wall in bacteria (Vollmer et al., 2008). Therefore, it is not surprising that DAAs do not have an effect on viability of cells after treatment. Therefore, in the DAA experiments, MIC and MBC was not determined as the biofilm dispersing ability was investigated over their bactericidal effects.

While DAAs effect on *F. nucleatum* is unclear, current literature suggest that DAAs have various mechanism of action (Vahdati et al., 2022). Firstly, through inhibition of EPS production (Yu et al., 2016). This can be supported by our observation through SEM imaging where extra-cellular debris appeared to be found in the FNP and FNN biofilm after DAA treatment, possibly due to the breakdown of EPS which supports the biofilm (Figure 50). Secondly, through interference of peptidoglycan synthesis (Kolodkin-Gal et al., 2010). SEM images show changes in the surfaces of all four subspecies where vesicular looking structures appeared to be more prominent in the DAA treated *F. nucleatum* compared to controls (Figure 50). The third mechanism is through inhibition of quorum sensing (Autoinducer-2) which will be further discussed in Section 4.2.1. The differences in the results of this study may be related to the genetic differences among *F. nucleatum* subspecies (Gharbia and Shah, 1989; Kim et al., 2010; Kook et al., 2013; Nie et al., 2015). Data presented in this project showed for the first time that DAA appears to be an effective biofilm inhibiting compound that could be used to inhibit *F. nucleatum* biofilms when added at the start of the experiment and used as an adjunct for potential periodontitis treatment if similar effects are seen with multispecies biofilms.

4.2.1 ATCC 10953 (FNP)

Interestingly, FNP biofilm volume appeared to be unchanged after DAA treatment compared to the control using Imaris software analysis (Figure 55). Compared to the other three subspecies, FNP appeared to have the least amount of biofilm volume. Similar observations were observed in the study by Muchova et al. (2022) where FNP failed to form a detectable and continuous layer of biofilm possibly due to having the least conservation of adhesion proteins investigated *in silico*. Moreover, from the confocal imaging and 3D rendering it appeared as though FNP cells became more elongated which is consistent with *F. nucleatum* experiencing stress (Diaz et al., 2000b; Silva et al., 2005).

Furthermore, as discussed in Section 4.2, one of the proposed mechanism of action of DAA having antibiofilm effects is through inhibiting AI-2 (Autoinducer-2), which is an important signalling molecule for bacteria communication and biofilm formation (Li and Nair, 2012; McNab et al., 2003). Interestingly, D-Try has been shown to inhibit mixed culture biofilm formation through inhibition of AI-2 synthesis (Xu and Liu, 2011a; Xu and Liu, 2011b). FNP possesses the LuxS gene which is responsible for encoding for AI-2 synthase (Schauder et al., 2001), while FNF and FNP lacks in this gene. Therefore, in the case of FNP biofilm disruption, this could be a unique target that could potentially be affecting bacterial communication leading to biofilm breakdown.

4.2.2 NCTC 11326 (FNF) and ATCC 25586 (FNN)

Previous genomic sequencing performed by Kapatral et al., (2002, 2003) showed that FNF and FNN have over 85% synergy and shared similar metabolic capabilities. This can be supported by our observation where DAA treated FNF and FNN appeared visually similar with a sunray appearance (Figure 46) and showed similar growth curves (Figure 47) when DAAs were added at the start of the experiment. Furthermore, both showed an almost 4-fold decrease in biofilm volume after DAA treatment (Section 3.3.1.8) and although signifiance was not able to be tested, they had greater proportion of dead cells compared the other two subspecies (FNP and FNA) after Imaris Software Analysis of viability (%) (Section 3.3.1.9).

4.2.3 ATCC 51191 (FNA)

While FNA growth was least affected by DAA treatment, SEM images showed FNA biofilm cells becoming elongated and formed a woven-like structure (Figure 50). This has been previous documented where this change in cell morphology may be associated with oxidative stress which was achieved through aeration of continuous culture (Diaz et al., 2000a) and by atmospheric oxygen exposure (Silva et al., 2005).

Currently, there is limited published research on the genomic sequencing of FNA and its comparison to other *F. nucleatum* subspecies. Of note, interestingly FNP and FNA appeared to have similar biofilm morphology (Figure 46), similar sensitivity to environmental oxygen and similar growth curves (Section 3.1.1.1). It would be interesting to see if FNP and FNA have genetic similarities.

4.2.4 Dispersion Effects of DAAs on established *F. nucleatum* biofilms

DAA treatment on established *F. nucleatum* biofilms grown over 24 hours showed a significant decrease in the biofilm volume through biofilm dispersion for all 4 subspecies (Figure 58). As seen in Section 4.2, viability was not affected (Figure 59). Due to time constraints, further investigations were not undertaken.

4.3 Effect of polycationic AgNPs and AuNPs on *F. nucleatum* growth and biofilm formation

4.3.1 AgNPs

Recent research shows the effectiveness of silver nanoparticles on reducing the viability of aerobic oral microorganisms (He et al., 2023) as well their use as an intracanal medicament (AlGazlan et al., 2022). The novelty of the polycationic silver nanoparticles synthesised within our laboratory is that the AgNPs have a positive surface charge, which allows for better interaction with bacteria cells due to enhanced electrostatic interactions with the negative surface charge of the bacteria (He et al., 2023). However, to date, there is no current literature investigating the effect of the AgNPs on *F. nucleatum*. Therefore, this a novel aspect of this project.

While biofilm analysis was attempted to measure the effects of *F. nucleatum* biofilm volume after AgNP treatment, both crystal violet stain and real-time biofilm analysis using the xCELLgience® platform ran into technical complications. Crystal violet stain was attempted after AgNP treatment added at the start of the experiment, but the silver nanoparticles visibly clumped amongst the biofilm, influencing the crystal violet staining. Furthermore, due the complication of growing *F. nucleatum* in the xCELLgience® platform (Section 3.2), the biofilm could not be further assessed.

Viable cell counts showed a concentration dependant effect for all four subspecies, with the concentration of AgNPs being inversely proportional to viability (Section 3.3.3.1). Interestingly, the FNN appeared to be most sensitive to AgNP treatment where a AgNP concentration of 10μg/ml showed significant decrease in viable cell counts. FNP, FNA, FNF also showed a decrease in viability, with significant falls at a concentration of 40μg/ml, 40μg/ml and 20μg/ml respectively (Figure 60). Differences in sensitivity to AgNPs may be due to subspecies variability in membrane composition and metabolic activity (Gharbia and Shah, 1989; Kim et al., 2010; Kook et al., 2013; Nie et al., 2015). At a concentration of 60μg/ml, AgNPs exhibited a bactericidal effect (Figure 60). This was supported through confocal Z-stack images where the proportion of red (dead) stained cells increased (Figure 61 and 62). This was a qualitative observation, due to difficulty for Imaris software to differential between *F. nucleatum* and AgNPs (Section 3.3.3.2). Some caution should be taken with interpretation of the results as AgNPs contributed to both red and green stains (live and dead). Due to this, Imaris analysis to quantify the viability (%) and biofilm volume ($X10^4$ μm^3) was unable to be performed.

Interestingly, He et al., (2023) demonstrated for both aerobically grown *S. mutans* and *S. sobrinus* the MIC and MBC were 5μg/ml and 10μg/ml respectively. On the contrary, MIC and MBC were not able to be determined for *F. nucleatum* even at the high concentration of AgNPs (60μg/ml) for all subspecies. This may be due to differences in structure in bacterial cell wall between Gram positive (*S. mutans* and *S. Sobrinus)* and Gram negative (*F. nucleatum)* bacteria (Beveridge, 1999). Current literature supports the mechanism of antibacterial action of AgNPs acting to penetrate the outer peptidoglycan layer to destabilize and damage the membrane (Dakal et al., 2016; Marambio-Jones and Hoek, 2010; Qing et al., 2018). It may be due to the unique permeability of the barrier created by the outer membrane

of the Gram-negative bacteria, possibly making it more challenging for small molecules to cross and have an effect (Lam et al., 2016b)

4.2.3 AuNPs

Recent published research demonstrate that AuNPs have antimicrobial effects on *F. nucleatum, Staphylococcus aureus, Staphylococcus epidermis, Bacillus subtilis* and *E. coli in vitro* (Chen et al., 2021; Wang et al., 2021; Zheng and Xie, 2020). Chen et al., (2021) propose that AuNPs have antibacterial effects *on F. nucleatum* through a combination of oxidative stress and membrane damage. While exact mechanism of the effect AuNPs was not explored in this project, similar results were observed where a decrease in viability of FNN was observed as the concentration of AuNPs increased (Figure 65). However, due to time limitations, further investigations were not carried out.

4.4 Limitation of investigations

There are several aspects that can be considered limitations of this project. Firstly, this project focused on one species of bacteria: *Fusobacterium nucleatum*. As discussed throughout the thesis, oral biofilm is known for their complex architecture and relationship between over 700 species of bacteria (Paster et al., 2006). Therefore further *in vitro* experiments must be conducted to replicate a subgingival biofilm model including early colonisers and late colonisers. Due to subgingival biofilm being very difficult to collect from patients, if this model is successfully grown *in vitro,* it will revolutionise periodontal treatment research and will allow better understanding of the architecture and the complex interactions of the subgingival biofilm.

This leads onto the second limitation of this project where *F. nucleatum* biofilms were grown on polystyrene microtiter trays. While microtiter plates are commonly used to grow biofilms *in vitro* (Azeredo et al., 2017), they do not accurately simulate the tooth surface. Throughout the project, reoccurring issues of *F. nucleatum* biofilm being easily disrupted during experimental procedures was encountered. While different surface coatings such as sterile human saliva and Poly-L-lysine was investigated in this project, they had minimal improvement of *F. nucleatum* biofilm adhesion. Perhaps, other dental tissue substrates such as hydroxyapatite disks or dentine and cementum slices may have increased biofilm adhesion.

Thirdly, this project used a static biofilm model, which is not entirely representative of the oral environment which has number of different intraoral niches. The oral environment is dynamic where there are various factors present including different surfaces of bacterial attachment, changes in saliva flow and nutrient availability. Therefore, future studies may use an open system such as the flow cell which more closely resembles *in vivo* conditions.

Lastly, due to the complications experienced when using the xCELLigence® platform, real-time biofilm analysis was unable to be completed. Therefore, more conventional methods such as crystal violet staining, viable cell counts, Live/Dead staining and confocal microscopy had to be performed. Perhaps future studies will continue exploring the xCELLigence® platform, providing a more accurate system to study real time biofilm formation.

4.5 Conclusion

4.5.1 Growing *F. nucleatum*

Protocol optimisation for growth curves in spectrophotometer, crystal violet staining, xCELLigence® platform and confocal microscopy had its challenges. This was not only because *F. nucleatum* is an obligate anaerobe and sufficient anaerobic conditions had to be created, but also due to its loosely attached biofilm making working with it a very delicate process even when grown in modified HIB. Therefore, protocol optimisation was necessary to improve the workflow and allow reproducibility.

In conclusion, all four subspecies of *F. nucleatum* was successfully grown and sub-species specific differences were observed. For *F. nucleatum* growth curves in the spectrophotometer, method using anaerobic sachet material and AxySeal Plastic Sealing Film was optimal. Future experiments may include the maintenance of a controlled anaerobic environment using an anaerobic chamber as a positive control. This would allow the precise determination of the redox potential of the environment and how changes in this parameter may influence the growth of *F. nucleatum*. For crystal violet protocol fixing the *F. nucleatum* biofilm with 4% formaldehyde post-experiment for 10 minutes showed best results in minimising biofilm dispersion during experimental washes. Furthermore, successful Imaris software analysis was performed at X60 magnification using a defined cell number as an

inoculum (OD_{600nm} 0.003). The protocol also used modified HIB as the growth medium and biofilms were grown for 7 hours using the µ-Slide 8 Well ibidiTreat plates (Ibidi) incubated in anaerobic jars. Lastly, *F. nucleatum* biofilm growth was unable to be successfully detected by the xCELLigence® platform.

4.5.2 D-Amino Acids

DAAs showed promising results as a potential antibiofilm compound as they successfully inhibited biofilm formation for all four subspecies of *F. nucleatum* (FNP, FNF, FNN and FNA) when added at the start of the experiment. FNA appeared to be the least affected by DAA treatment. When DAAs were added later to already established *F. nucleatum* biofilm, it had biofilm dispersing effects. DAAs as expected, showed minimal changes in viability. This is no surprise as DAAs are abundantly present in nature (Lam et al., 2009; Matsumoto et al., 2018). Given the important role of *F. nucleatum* in periodontitis, the inhibition or dispersion of biofilms by DAAs may have importance in the treatment of periodontitis.

4.5.3 AgNPs and AuNPs

While AgNPs and AuNPs both appeared to have promising antibacterial effects, due to inability to perform biofilm analysis using crystal violet and the xCELLigence® platform, further investigation is needed to evaluate the effectiveness of these nanoparticles on *F. nucleatum* biofilms.

4.5.4 Clinical Significance

Although *F. nucleatum* has a central role in the development of periodontitis, it has also been a focal point of research due to its association with other systemic effects such as adverse pregnancy outcomes (Han, 2011), arthritis (Ebbers et al., 2018) and colorectal cancer (Koliarakis et al., 2019; Tjalsma et al., 2012). However, antibiotics resistance is a major problem in the health industry, leading to reduced efficacy of periodontal treatment (Sukumar et al., 2020; Teoh et al., 2018). Therefore, the use of novel antibiofilm and antimicrobial compounds such as DAAs, AgNPs and AuNPs will have a very important role in treatment of periodontitis.

4.6 Future directions

While this project provides us with useful protocols to grow *F. nucleatum* using unique methods to create an anerobic environment and show promising initial results investigating the effects of novel antimicrobial compounds such as DAAs and AgNPs and AuNPs, further investigations are necessary.

Future work will involve a detailed analysis of the published sequences of each subspecies to further understand the differences observed in this project. Another aspect to consider is to investigate utilising dental specific substrates such as hydroxyapatite or cementum slices where subgingival biofilm is known to form.

Further studies of effectiveness of DAAs, AgNPs and AuNPs must be investigated to ensure biocompatibility and to investigate possible host immune interactions. Future studies may be conducted on investigating effects of combinations of these novel antimicrobials and antibiofilm compounds on *F. nucleatum* biofilms.

SUPPLEMENTARY FIGURES

5.1 Doubling time for each *F. nucleatum* subspecies grown in modified HIB

F. nucleatum subspecies	Doubling Time (Hours)
ATCC 10953 (FNP)	12.71 hours
NCTC 11326 (FNF)	12.69 hours
ATCC 25586 (FNN)	12.76 hours
ATCC 51191 (FNA)	16.70 hours

APPENDICES

5.2 Calculation of CFU/ml for viable cell counts

$$\boldsymbol{CFU/ml} = \frac{\boldsymbol{Colonies\ formed\ X\ Total\ dilution\ factor}}{\boldsymbol{volume\ of\ culture\ plated\ (ml)}}$$

Example: after plating 0.01ml (10µl) from 10^6 dilution, 72 colonies grew. Therefore

$$\boldsymbol{CFU/ml} = \frac{(\mathbf{72}\ \boldsymbol{colonies\ X}\ \mathbf{10^6})}{\mathbf{0.01}\ \boldsymbol{ml}}$$

$$= 7.2\ X\ 10^8\ CFU/ml$$

REFERENCES

Aas, J.A., Paster, B.J., Stokes, L.N., Olsen, I., Dewhirst, F.E., 2005. Defining the normal bacterial flora of the oral cavity. J Clin Microbiol 43, 5721-5732.

Abed, J., Emgard, J.E., Zamir, G., Faroja, M., Almogy, G., Grenov, A., Sol, A., Naor, R., Pikarsky, E., Atlan, K.A., Mellul, A., Chaushu, S., Manson, A.L., Earl, A.M., Ou, N., Brennan, C.A., Garrett, W.S., Bachrach, G., 2016. Fap2 Mediates Fusobacterium nucleatum Colorectal Adenocarcinoma Enrichment by Binding to Tumor-Expressed Gal-GalNAc. Cell Host Microbe 20, 215-225.

Abrantes, P., Africa, C.W.J., 2020. Measuring Streptococcus mutans, Streptococcus sanguinis and Candida albicans biofilm formation using a real-time impedance-based system. J Microbiol Methods 169, 105815.

AlGazlan, A.S., Auda, S.H., Balto, H., Alsalleeh, F., 2022. Antibiofilm Efficacy of Silver Nanoparticles Alone or Mixed with Calcium Hydroxide as Intracanal Medicaments: An Ex-Vivo Analysis. J Endod 48, 1294-1300.

Almeida-da-Silva, C.L.C., Morandini, A.C., Ulrich, H., Ojcius, D.M., Coutinho-Silva, R., 2016. Purinergic signaling during Porphyromonas gingivalis infection. Biomed J 39, 251-260.

Altshuler, G., Hyde, S., 1988. Clinicopathologic considerations of fusobacteria chorioamnionitis. Acta Obstet Gynecol Scand 67, 513-517.

Ampornaramveth, R.S., Akeatichod, N., Lertnukkhid, J., Songsang, N., 2018. Application of D-Amino Acids as Biofilm Dispersing Agent in Dental Unit Waterlines. Int J Dent 2018, 9413925.

Amy, P., Thayalan, K., 2020. Resistance to change: how much longer will our antibiotics work? Faculty Dental Journal 9.

Arimatsu, K., Yamada, H., Miyazawa, H., Minagawa, T., Nakajima, M., Ryder, M.I., Gotoh, K., Motooka, D., Nakamura, S., Iida, T., Yamazaki, K., 2014. Oral pathobiont induces systemic inflammation and metabolic changes associated with alteration of gut microbiota. Sci Rep 4, 4828.

Armitage, G.C., 1999. Development of a classification system for periodontal diseases and conditions. Ann Periodontol 4, 1-6.

Azeredo, J., Azevedo, N.F., Briandet, R., Cerca, N., Coenye, T., Costa, A.R., Desvaux, M., Di Bonaventura, G., Hebraud, M., Jaglic, Z., Kacaniova, M., Knochel, S., Lourenco, A., Mergulhao, F., Meyer, R.L., Nychas, G., Simoes, M., Tresse, O., Sternberg, C., 2017. Critical review on biofilm methods. Crit Rev Microbiol 43, 313-351.

Babu, J.P., Dean, J.W., Pabst, M.J., 1995. Attachment of Fusobacterium nucleatum to fibronectin immobilized on gingival epithelial cells or glass coverslips. J Periodontol 66, 285-290.

Bahador, A., Pourakbari, B., Bolhari, B., Hashemi, F.B., 2015. In vitro evaluation of the antimicrobial activity of nanosilver-mineral trioxide aggregate against frequent anaerobic oral pathogens by a membrane-enclosed immersion test. Biomed J 38, 77-83.

Baker, P.J., Dixon, M., Evans, R.T., Dufour, L., Johnson, E., Roopenian, D.C., 1999. CD4(+) T cells and the proinflammatory cytokines gamma interferon and interleukin-6 contribute to alveolar bone loss in mice. Infect Immun 67, 2804-2809.

Bartold, P.M., Gully, N.J., Zilm, P.S., Rogers, A.H., 1991. Identification of components in Fusobacterium nucleatum chemostat-culture supernatants that are potent inhibitors of human gingival fibroblast proliferation. J Periodontal Res 26, 314-322.

Becker, M.R., Paster, B.J., Leys, E.J., Moeschberger, M.L., Kenyon, S.G., Galvin, J.L., Boches, S.K., Dewhirst, F.E., Griffen, A.L., 2002. Molecular analysis of bacterial species associated with childhood caries. J Clin Microbiol 40, 1001-1009.

Belibasakis, G.N., Guggenheim, B., Bostanci, N., 2013. Down-regulation of NLRP3 inflammasome in gingival fibroblasts by subgingival biofilms: involvement of Porphyromonas gingivalis. Innate Immun 19, 3-9.

Benn, G., Pyne, A.L.B., Ryadnov, M.G., Hoogenboom, B.W., 2019. Imaging live bacteria at the nanoscale: comparison of immobilisation strategies. Analyst 144, 6944-6952.

Beveridge, T.J., 1999. Structures of gram-negative cell walls and their derived membrane vesicles. J Bacteriol 181, 4725-4733.

Bolstad, A.I., Jensen, H.B., Bakken, V., 1996. Taxonomy, biology, and periodontal aspects of Fusobacterium nucleatum. Clin Microbiol Rev 9, 55-71.

Bowden, G.H., Hamilton, I.R., 1998. Survival of oral bacteria. Crit Rev Oral Biol Med 9, 54-85.

Bradshaw, D.J., Marsh, P.D., Watson, G.K., Allison, C., 1998. Role of Fusobacterium nucleatum and coaggregation in anaerobe survival in planktonic and biofilm oral microbial communities during aeration. Infect Immun 66, 4729-4732.

Brandenburg, K.S., Rodriguez, K.J., McAnulty, J.F., Murphy, C.J., Abbott, N.L., Schurr, M.J., Czuprynski, C.J., 2013. Tryptophan inhibits biofilm formation by Pseudomonas aeruginosa. Antimicrob Agents Chemother 57, 1921-1925.

Brewer, M.L., Dymock, D., Brady, R.L., Singer, B.B., Virji, M., Hill, D.J., 2019. Fusobacterium spp. target human CEACAM1 via the trimeric autotransporter adhesin CbpF. J Oral Microbiol 11, 1565043.

Broz, P., Dixit, V.M., 2016. Inflammasomes: mechanism of assembly, regulation and signalling. Nat Rev Immunol 16, 407-420.

Bruchmann, J., Sachsenheimer, K., Rapp, B.E., Schwartz, T., 2015. Multi-channel microfluidic biosensor platform applied for online monitoring and screening of biofilm formation and activity. PLoS One 10, e0117300.

Bui, F.Q., Johnson, L., Roberts, J., Hung, S.C., Lee, J., Atanasova, K.R., Huang, P.R., Yilmaz, O., Ojcius, D.M., 2016. Fusobacterium nucleatum infection of gingival epithelial cells leads to NLRP3 inflammasome-dependent secretion of IL-1beta and the danger signals ASC and HMGB1. Cell Microbiol 18, 970-981.

Casadevall, A., Pirofski, L.A., 1999. Host-pathogen interactions: redefining the basic concepts of virulence and pathogenicity. Infect Immun 67, 3703-3713.

Castellarin, M., Warren, R.L., Freeman, J.D., Dreolini, L., Krzywinski, M., Strauss, J., Barnes, R., Watson, P., Allen-Vercoe, E., Moore, R.A., Holt, R.A., 2012. Fusobacterium nucleatum infection is prevalent in human colorectal carcinoma. Genome Res 22, 299-306.

Cava, F., de Pedro, M.A., Lam, H., Davis, B.M., Waldor, M.K., 2011. Distinct pathways for modification of the bacterial cell wall by non-canonical D-amino acids. EMBO J 30, 3442-3453.

Champney, W.S., Jensen, R.A., 1969. D-Tyrosine as a metabolic inhibitor of Bacillus subtilis. J Bacteriol 98, 205-214.

Chaushu, S., Wilensky, A., Gur, C., Shapira, L., Elboim, M., Halftek, G., Polak, D., Achdout, H., Bachrach, G., Mandelboim, O., 2012. Direct recognition of Fusobacterium nucleatum by the NK cell natural cytotoxicity receptor NKp46 aggravates periodontal disease. PLoS Pathog 8, e1002601.

Chen, R., Qiao, D., Wang, P., Li, L., Zhang, Y., Yan, F., 2021. Gold Nanoclusters Exert Bactericidal Activity and Enhance Phagocytosis of Macrophage Mediated Killing of Fusobacterium nucleatum. Frontiers in Materials 8.

Choi, J., Borrello, M.A., Smith, E., Cutler, C.W., Sojar, H., Zauderer, M., 2001. Prior exposure of mice to Fusobacterium nucleatum modulates host response to Porphyromonas gingivalis. Oral Microbiol Immunol 16, 338-344.

Citron, D.M., 2002. Update on the taxonomy and clinical aspects of the genus fusobacterium. Clin Infect Dis 35, S22-27.

Clark, W.B., Beem, J.E., Nesbitt, W.E., Cisar, J.O., Tseng, C.C., Levine, M.J., 1989. Pellicle receptors for Actinomyces viscosus type 1 fimbriae in vitro. Infect Immun 57, 3003-3008.

Cochrane, K., Robinson, A.V., Holt, R.A., Allen-Vercoe, E., 2020. A survey of Fusobacterium nucleatum genes modulated by host cell infection. Microb Genom 6.

Conrads, G., Claros, M.C., Citron, D.M., Tyrrell, K.L., Merriam, V., Goldstein, E.J.C., 2002. 16S-23S rDNA internal transcribed spacer sequences for analysis of the phylogenetic relationships among species of the genus Fusobacterium. Int J Syst Evol Microbiol 52, 493-499.

Coppenhagen-Glazer, S., Sol, A., Abed, J., Naor, R., Zhang, X., Han, Y.W., Bachrach, G., 2015. Fap2 of Fusobacterium nucleatum is a galactose-inhibitable adhesin involved in coaggregation, cell adhesion, and preterm birth. Infect Immun 83, 1104-1113.

Cowan, S.E., Liepmann, D., Keasling, J.D., 2001. Development of engineered biofilms on poly- L-lysine patterned surfaces. Biotechnology Letters 23, 1235-1241.

Dakal, T.C., Kumar, A., Majumdar, R.S., Yadav, V., 2016. Mechanistic Basis of Antimicrobial Actions of Silver Nanoparticles. Frontiers in Microbiology 7.

Darveau, R.P., Tanner, A., Page, R.C., 1997. The microbial challenge in periodontitis. Periodontol 2000 14, 12-32.

Davey, M.E., O'Toole G, A., 2000. Microbial biofilms: from ecology to molecular genetics. Microbiol Mol Biol Rev 64, 847-867.

de Beer, D., Stoodley, P., Roe, F., Lewandowski, Z., 1994. Effects of biofilm structures on oxygen distribution and mass transport. Biotechnol Bioeng 43, 1131-1138.

Diaz, P.I., Chalmers, N.I., Rickard, A.H., Kong, C., Milburn, C.L., Palmer, R.J., Jr., Kolenbrander, P.E., 2006. Molecular characterization of subject-specific oral microflora during initial colonization of enamel. Appl Environ Microbiol 72, 2837-2848.

Diaz, P.I., Rogers, A.H., 2004. The effect of oxygen on the growth and physiology of Porphyromonas gingivalis. Oral Microbiol Immunol 19, 88-94.

Diaz, P.I., Zilm, P.S., Rogers, A.H., 2000a. The response to oxidative stress of Fusobacterium nucleatum grown in continuous culture. FEMS Microbiology Letters 187, 31-34.

Diaz, P.I., Zilm, P.S., Rogers, A.H., 2000b. The response to oxidative stress of Fusobacterium nucleatum grown in continuous culture. FEMS Microbiol Lett 187, 31-34.

Diaz, P.I., Zilm, P.S., Rogers, A.H., 2002. Fusobacterium nucleatum supports the growth of Porphyromonas gingivalis in oxygenated and carbon-dioxide-depleted environments. Microbiology 148, 467-472.

Dige, I., Nilsson, H., Kilian, M., Nyvad, B., 2007. In situ identification of streptococci and other bacteria in initial dental biofilm by confocal laser scanning microscopy and fluorescence in situ hybridization. Eur J Oral Sci 115, 459-467.

Dige, I., Raarup, M.K., Nyengaard, J.R., Kilian, M., Nyvad, B., 2009. Actinomyces naeslundii in initial dental biofilm formation. Microbiology 155, 2116-2126.

Ding, Q., Tan, K.S., 2016. The Danger Signal Extracellular ATP Is an Inducer of Fusobacterium nucleatum Biofilm Dispersal. Front Cell Infect Microbiol 6, 155.

Donlan, R.M., Costerton, J.W., 2002. Biofilms: survival mechanisms of clinically relevant microorganisms. Clin Microbiol Rev 15, 167-193.

Dzink, J.L., Sheenan, M.T., Socransky, S.S., 1990. Proposal of three subspecies of Fusobacterium nucleatum Knorr 1922: Fusobacterium nucleatum subsp. nucleatum subsp. nov., comb. nov.; Fusobacterium nucleatum subsp. polymorphum subsp. nov., nom. rev.,

comb. nov.; and Fusobacterium nucleatum subsp. vincentii subsp. nov., nom. rev., comb. nov. Int J Syst Bacteriol 40, 74-78.

Ebbers, M., Lubcke, P.M., Volzke, J., Kriebel, K., Hieke, C., Engelmann, R., Lang, H., Kreikemeyer, B., Muller-Hilke, B., 2018. Interplay between P. gingivalis, F. nucleatum and A. actinomycetemcomitans in murine alveolar bone loss, arthritis onset and progression. Sci Rep 8, 15129.

Eggert, F.M., Drewell, L., Bigelow, J.A., Speck, J.E., Goldner, M., 1991. The pH of gingival crevices and periodontal pockets in children, teenagers and adults. Arch Oral Biol 36, 233-238.

El Tahir, Y., Skurnik, M., 2001. YadA, the multifaceted Yersinia adhesin. Int J Med Microbiol 291, 209-218.

El-Awady, A., de Sousa Rabelo, M., Meghil, M.M., Rajendran, M., Elashiry, M., Stadler, A.F., Foz, A.M., Susin, C., Romito, G.A., Arce, R.M., Cutler, C.W., 2019. Polymicrobial synergy within oral biofilm promotes invasion of dendritic cells and survival of consortia members. NPJ Biofilms Microbiomes 5, 11.

Elliott, A.D., 2020. Confocal Microscopy: Principles and Modern Practices. Curr Protoc Cytom 92, e68.

Espaillat, A., Carrasco-Lopez, C., Bernardo-Garcia, N., Rojas-Altuve, A., Klett, J., Morreale, A., Hermoso, J.A., Cava, F., 2021. Binding of non-canonical peptidoglycan controls Vibrio cholerae broad spectrum racemase activity. Comput Struct Biotechnol J 19, 1119-1126.

Espinoza, J.L., Harkins, D.M., Torralba, M., Gomez, A., Highlander, S.K., Jones, M.B., Leong, P., Saffery, R., Bockmann, M., Kuelbs, C., Inman, J.M., Hughes, T., Craig, J.M., Nelson, K.E., Dupont, C.L., 2018. Supragingival Plaque Microbiome Ecology and Functional Potential in the Context of Health and Disease. mBio 9.

Fardini, Y., Wang, X., Temoin, S., Nithianantham, S., Lee, D., Shoham, M., Han, Y.W., 2011. Fusobacterium nucleatum adhesin FadA binds vascular endothelial cadherin and alters endothelial integrity. Mol Microbiol 82, 1468-1480.

Feuille, F., Ebersole, J.L., Kesavalu, L., Stepfen, M.J., Holt, S.C., 1996. Mixed infection with Porphyromonas gingivalis and Fusobacterium nucleatum in a murine lesion model: potential synergistic effects on virulence. Infect Immun 64, 2094-2100.

Ford, P.J., Gemmell, E., Chan, A., Carter, C.L., Walker, P.J., Bird, P.S., West, M.J., Cullinan, M.P., Seymour, G.J., 2006. Inflammation, heat shock proteins and periodontal pathogens in atherosclerosis: an immunohistologic study. Oral Microbiol Immunol 21, 206-211.

Fuqua, W.C., Winans, S.C., Greenberg, E.P., 1994. Quorum sensing in bacteria: the LuxR-LuxI family of cell density-responsive transcriptional regulators. J Bacteriol 176, 269-275.

Gashti, M.P., Asselin, J., Barbeau, J., Boudreau, D., Greener, J., 2016. A microfluidic platform with pH imaging for chemical and hydrodynamic stimulation of intact oral biofilms. Lab Chip 16, 1412-1419.

Genco, R.J., 1992. Host responses in periodontal diseases: current concepts. J Periodontol 63, 338-355.

George, W.L., Kirby, B.D., Sutter, V.L., Citron, D.M., Finegold, S.M., 1981. Gram-negative anaerobic bacilli: Their role in infection and patterns of susceptibility to antimicrobial agents. II. Little-known Fusobacterium species and miscellaneous genera. Rev Infect Dis 3, 599-626.

Gharbia, S.E., Shah, H.N., 1989. Heterogeneity within Fusobacterium nucleatum, proposal of four subspeces. Lett Appl Microbiol 10, 105-108.

Gharbia, S.E., Shah, H.N., Lawson, P.A., Haapasalo, M., 1990. Distribution and frequency of Fusobacterium nucleatum subspecies in the human oral cavity. Oral Microbiol Immunol 5, 324-327.

Graves, D., 2008. Cytokines that promote periodontal tissue destruction. J Periodontol 79, 1585-1591.

Grimaudo, N.J., Nesbitt, W.E., 1997. Coaggregation of Candida albicans with oral Fusobacterium species. Oral Microbiol Immunol 12, 168-173.

Guggenheim, B., Giertsen, E., Schupbach, P., Shapiro, S., 2001. Validation of an in vitro biofilm model of supragingival plaque. J Dent Res 80, 363-370.

Guo, L., Shokeen, B., He, X., Shi, W., Lux, R., 2017. Streptococcus mutans SpaP binds to RadD of Fusobacterium nucleatum ssp. polymorphum. Mol Oral Microbiol 32, 355-364.

Gur, C., Ibrahim, Y., Isaacson, B., Yamin, R., Abed, J., Gamliel, M., Enk, J., Bar-On, Y., Stanietsky-Kaynan, N., Coppenhagen-Glazer, S., Shussman, N., Almogy, G., Cuapio, A., Hofer, E., Mevorach, D., Tabib, A., Ortenberg, R., Markel, G., Miklic, K., Jonjic, S., Brennan, C.A., Garrett, W.S., Bachrach, G., Mandelboim, O., 2015. Binding of the Fap2 protein of Fusobacterium nucleatum to human inhibitory receptor TIGIT protects tumors from immune cell attack. Immunity 42, 344-355.

Haffajee, A.D., Socransky, S.S., 2005. Microbiology of periodontal diseases: introduction. Periodontol 2000 38, 9-12.

Haffajee, A.D., Socransky, S.S., Gunsolley, J.C., 2003. Systemic anti-infective periodontal therapy. A systematic review. Ann Periodontol 8, 115-181.

Haffajee, A.D., Socransky, S.S., Patel, M.R., Song, X., 2008. Microbial complexes in supragingival plaque. Oral Microbiol Immunol 23, 196-205.

Hajishengallis, G., Liang, S., Payne, M.A., Hashim, A., Jotwani, R., Eskan, M.A., McIntosh, M.L., Alsam, A., Kirkwood, K.L., Lambris, J.D., Darveau, R.P., Curtis, M.A., 2011. Low-abundance biofilm species orchestrates inflammatory periodontal disease through the commensal microbiota and complement. Cell Host Microbe 10, 497-506.

Hall, I.C., 1929. A Review of the Development and Application of Physical and Chemical Principles in the Cultivation of Obligately Anaerobic Bacteria. J Bacteriol 17, 255-301.

Hall-Stoodley, L., Costerton, J.W., Stoodley, P., 2004. Bacterial biofilms: from the natural environment to infectious diseases. Nat Rev Microbiol 2, 95-108.

Ham, H., Sreelatha, A., Orth, K., 2011. Manipulation of host membranes by bacterial effectors. Nat Rev Microbiol 9, 635-646.

Han, Y.W., 2011. Oral health and adverse pregnancy outcomes - what's next? J Dent Res 90, 289-293.

Han, Y.W., 2015. Fusobacterium nucleatum: a commensal-turned pathogen. Curr Opin Microbiol 23, 141-147.

Han, Y.W., Fardini, Y., Chen, C., Iacampo, K.G., Peraino, V.A., Shamonki, J.M., Redline, R.W., 2010. Term stillbirth caused by oral Fusobacterium nucleatum. Obstet Gynecol 115, 442-445.

Han, Y.W., Ikegami, A., Rajanna, C., Kawsar, H.I., Zhou, Y., Li, M., Sojar, H.T., Genco, R.J., Kuramitsu, H.K., Deng, C.X., 2005. Identification and characterization of a novel adhesin unique to oral fusobacteria. J Bacteriol 187, 5330-5340.

Han, Y.W., Redline, R.W., Li, M., Yin, L., Hill, G.B., McCormick, T.S., 2004. Fusobacterium nucleatum induces premature and term stillbirths in pregnant mice: implication of oral bacteria in preterm birth. Infect Immun 72, 2272-2279.

Han, Y.W., Shi, W., Huang, G.T., Kinder Haake, S., Park, N.H., Kuramitsu, H., Genco, R.J., 2000. Interactions between periodontal bacteria and human oral epithelial cells: Fusobacterium nucleatum adheres to and invades epithelial cells. Infect Immun 68, 3140-3146.

Han, Y.W., Wang, X., 2013. Mobile microbiome: oral bacteria in extra-oral infections and inflammation. J Dent Res 92, 485-491.

Hanisakova, N., Vitezova, M., Rittmann, S.K.R., 2022. The Historical Development of Cultivation Techniques for Methanogens and Other Strict Anaerobes and Their Application in Modern Microbiology. Microorganisms 10.

Hannan, S., Ready, D., Jasni, A.S., Rogers, M., Pratten, J., Roberts, A.P., 2010. Transfer of antibiotic resistance by transformation with eDNA within oral biofilms. FEMS Immunol Med Microbiol 59, 345-349.

He, Y., Ketagoda, D.H.K., Bright, R., Britza, S.M., Zechner, J., Musgrave, I., Vasilev, K., Zilm, P., 2023. Synthesis of Cationic Silver Nanoparticles with Highly Potent Properties against Oral Pathogens and Their Biofilms. CHEMNANOMAT 9.

Hernandez-Sierra, J.F., Ruiz, F., Pena, D.C., Martinez-Gutierrez, F., Martinez, A.E., Guillen Ade, J., Tapia-Perez, H., Castanon, G.M., 2008. The antimicrobial sensitivity of Streptococcus mutans to nanoparticles of silver, zinc oxide, and gold. Nanomedicine 4, 237-240.

Huang, G.T., Kim, D., Lee, J.K., Kuramitsu, H.K., Haake, S.K., 2001. Interleukin-8 and intercellular adhesion molecule 1 regulation in oral epithelial cells by selected periodontal bacteria: multiple effects of Porphyromonas gingivalis via antagonistic mechanisms. Infect Immun 69, 1364-1372.

Huang, R., Li, M., Gregory, R.L., 2011. Bacterial interactions in dental biofilm. Virulence 2, 435-444.

Huggan, P.J., Murdoch, D.R., 2008. Fusobacterial infections: clinical spectrum and incidence of invasive disease. J Infect 57, 283-289.

Hung, P.J., Lee, P.J., Sabounchi, P., Lin, R., Lee, L.P., 2005. Continuous perfusion microfluidic cell culture array for high-throughput cell-based assays. Biotechnol Bioeng 89, 1-8.

Ikegami, A., Chung, P., Han, Y.W., 2009. Complementation of the fadA mutation in Fusobacterium nucleatum demonstrates that the surface-exposed adhesin promotes cellular invasion and placental colonization. Infect Immun 77, 3075-3079.

Ivashchenko, R., 2020. Prism 8 for OS X, 8.4.3 ed. Software MacKiev (TM), San Diego, California, USA.

Jacobson, A.P., Thunberg, R.L., Johnson, M.L., Hammack, T.S., Andrews, W.H., 2004. Alternative anaerobic enrichments to the bacteriological analytical manual culture method for isolation of Shigella sonnei from selected types of fresh produce. J AOAC Int 87, 1115-1122.

Jewett, A., Hume, W.R., Le, H., Huynh, T.N., Han, Y.W., Cheng, G., Shi, W., 2000. Induction of apoptotic cell death in peripheral blood mononuclear and polymorphonuclear cells by an oral bacterium, Fusobacterium nucleatum. Infect Immun 68, 1893-1898.

Jia, Z., Xiu, P., Li, M., Xu, X., Shi, Y., Cheng, Y., Wei, S., Zheng, Y., Xi, T., Cai, H., Liu, Z., 2016. Bioinspired anchoring AgNPs onto micro-nanoporous TiO2 orthopedic coatings: Trap-killing of bacteria, surface-regulated osteoblast functions and host responses. Biomaterials 75, 203-222.

Jousimies-Somer, H., 1997. Recently described clinically important anaerobic bacteria: taxonomic aspects and update. Clin Infect Dis 25 Suppl 2, S78-87.

Jun, H.K., Jung, Y.J., Choi, B.K., 2017. Treponema denticola, Porphyromonas gingivalis, and Tannerella forsythia induce cell death and release of endogenous danger signals. Arch Oral Biol 73, 72-78.

Kapatral, V., Anderson, I., Ivanova, N., Reznik, G., Los, T., Lykidis, A., Bhattacharyya, A., Bartman, A., Gardner, W., Grechkin, G., Zhu, L., Vasieva, O., Chu, L., Kogan, Y., Chaga, O., Goltsman, E., Bernal, A., Larsen, N., D'Souza, M., Walunas, T., Pusch, G., Haselkorn, R., Fonstein, M., Kyrpides, N., Overbeek, R., 2002. Genome sequence and analysis of the oral bacterium Fusobacterium nucleatum strain ATCC 25586. J Bacteriol 184, 2005-2018.

Kapatral, V., Ivanova, N., Anderson, I., Reznik, G., Bhattacharyya, A., Gardner, W.L., Mikhailova, N., Lapidus, A., Larsen, N., D'Souza, M., Walunas, T., Haselkorn, R., Overbeek, R., Kyrpides, N., 2003. Genome analysis of F. nucleatum sub spp vincentii and its comparison with the genome of F. nucleatum ATCC 25586. Genome Res 13, 1180-1189.

Kaplan, C.W., Lux, R., Haake, S.K., Shi, W., 2009. The Fusobacterium nucleatum outer membrane protein RadD is an arginine-inhibitable adhesin required for inter-species adherence and the structured architecture of multispecies biofilm. Mol Microbiol 71, 35-47.

Kaplan, C.W., Ma, X., Paranjpe, A., Jewett, A., Lux, R., Kinder-Haake, S., Shi, W., 2010. Fusobacterium nucleatum outer membrane proteins Fap2 and RadD induce cell death in human lymphocytes. Infect Immun 78, 4773-4778.

Karpathy, S.E., Qin, X., Gioia, J., Jiang, H., Liu, Y., Petrosino, J.F., Yerrapragada, S., Fox, G.E., Haake, S.K., Weinstock, G.M., Highlander, S.K., 2007. Genome sequence of Fusobacterium nucleatum subspecies polymorphum - a genetically tractable fusobacterium. PLoS One 2, e659.

Kassebaum, N.J., Bernabe, E., Dahiya, M., Bhandari, B., Murray, C.J., Marcenes, W., 2014. Global burden of severe periodontitis in 1990-2010: a systematic review and meta-regression. J Dent Res 93, 1045-1053.

Keijser, B.J., Zaura, E., Huse, S.M., van der Vossen, J.M., Schuren, F.H., Montijn, R.C., ten Cate, J.M., Crielaard, W., 2008. Pyrosequencing analysis of the oral microflora of healthy adults. J Dent Res 87, 1016-1020.

Khider, D., Rossi-Fedele, G., Fitzsimmons, T., Vasilev, K., Zilm, P.S., 2021. Disruption of Enterococcus Faecalis biofilms using individual and plasma polymer encapsulated D-amino acids. Clin Oral Investig 25, 3305-3313.

Kigure, T., Saito, A., Seida, K., Yamada, S., Ishihara, K., Okuda, K., 1995. Distribution of Porphyromonas gingivalis and Treponema denticola in human subgingival plaque at different periodontal pocket depths examined by immunohistochemical methods. J Periodontal Res 30, 332-341.

Kim, H.S., Lee, D.S., Chang, Y.H., Kim, M.J., Koh, S., Kim, J., Seong, J.H., Song, S.K., Shin, H.S., Son, J.B., Jung, M.Y., Park, S.N., Yoo, S.Y., Cho, K.W., Kim, D.K., Moon, S., Kim, D., Choi, Y., Kim, B.O., Jang, H.S., Kim, C.S., Kim, C., Choe, S.J., Kook, J.K., 2010. Application of rpoB and zinc protease gene for use in molecular discrimination of Fusobacterium nucleatum subspecies. J Clin Microbiol 48, 545-553.

Kim, S.M., Kim, H.C., Lee, S.W., 2011. Characterization of antibiotic resistance determinants in oral biofilms. J Microbiol 49, 595-602.

Kistler, J.O., Pesaro, M., Wade, W.G., 2015. Development and pyrosequencing analysis of an in-vitro oral biofilm model. BMC Microbiol 15, 24.

Kleivdal, H., Benz, R., Jensen, H.B., 1995. The Fusobacterium nucleatum major outer-membrane protein (FomA) forms trimeric, water-filled channels in lipid bilayer membranes. Eur J Biochem 233, 310-316.

Kleivdal, H., Benz, R., Tommassen, J., Jensen, H.B., 1999. Identification of positively charged residues of FomA porin of Fusobacterium nucleatum which are important for pore function. Eur J Biochem 260, 818-824.

Kolenbrander, P.E., 2000. Oral microbial communities: biofilms, interactions, and genetic systems. Annu Rev Microbiol 54, 413-437.

Kolenbrander, P.E., Andersen, R.N., Blehert, D.S., Egland, P.G., Foster, J.S., Palmer, R.J., Jr., 2002. Communication among oral bacteria. Microbiol Mol Biol Rev 66, 486-505, table of contents.

Kolenbrander, P.E., Andersen, R.N., Moore, L.V., 1989. Coaggregation of Fusobacterium nucleatum, Selenomonas flueggei, Selenomonas infelix, Selenomonas noxia, and Selenomonas sputigena with strains from 11 genera of oral bacteria. Infect Immun 57, 3194-3203.

Kolenbrander, P.E., London, J., 1993. Adhere today, here tomorrow: oral bacterial adherence. J Bacteriol 175, 3247-3252.

Kolenbrander, P.E., Palmer, R.J., Jr., Periasamy, S., Jakubovics, N.S., 2010. Oral multispecies biofilm development and the key role of cell-cell distance. Nat Rev Microbiol 8, 471-480.

Kolenbrander, P.E., Palmer, R.J., Jr., Rickard, A.H., Jakubovics, N.S., Chalmers, N.I., Diaz, P.I., 2006. Bacterial interactions and successions during plaque development. Periodontol 2000 42, 47-79.

Koliarakis, I., Messaritakis, I., Nikolouzakis, T.K., Hamilos, G., Souglakos, J., Tsiaoussis, J., 2019. Oral Bacteria and Intestinal Dysbiosis in Colorectal Cancer. Int J Mol Sci 20.

Kolodkin-Gal, I., Romero, D., Cao, S., Clardy, J., Kolter, R., Losick, R., 2010. D-amino acids trigger biofilm disassembly. Science 328, 627-629.

Komiya, Y., Shimomura, Y., Higurashi, T., Sugi, Y., Arimoto, J., Umezawa, S., Uchiyama, S., Matsumoto, M., Nakajima, A., 2019. Patients with colorectal cancer have identical strains of Fusobacterium nucleatum in their colorectal cancer and oral cavity. Gut 68, 1335-1337.

Kook, J.K., Park, S.N., Lim, Y.K., Cho, E., Jo, E., Roh, H., Shin, Y., Paek, J., Kim, H.S., Kim, H., Shin, J.H., Chang, Y.H., 2017. Genome-Based Reclassification of Fusobacterium nucleatum Subspecies at the Species Level. Curr Microbiol 74, 1137-1147.

Kook, J.K., Park, S.N., Lim, Y.K., Choi, M.H., Cho, E., Kong, S.W., Shin, Y., Paek, J., Chang, Y.H., 2013. Fusobacterium nucleatum subsp. fusiforme Gharbia and Shah 1992 is a later synonym of Fusobacterium nucleatum subsp. vincentii Dzink et al. 1990. Curr Microbiol 66, 414-417.

Kostic, A.D., Chun, E., Robertson, L., Glickman, J.N., Gallini, C.A., Michaud, M., Clancy, T.E., Chung, D.C., Lochhead, P., Hold, G.L., El-Omar, E.M., Brenner, D., Fuchs, C.S., Meyerson, M., Garrett, W.S., 2013. Fusobacterium nucleatum potentiates intestinal tumorigenesis and modulates the tumor-immune microenvironment. Cell Host Microbe 14, 207-215.

Kostic, A.D., Gevers, D., Pedamallu, C.S., Michaud, M., Duke, F., Earl, A.M., Ojesina, A.I., Jung, J., Bass, A.J., Tabernero, J., Baselga, J., Liu, C., Shivdasani, R.A., Ogino, S., Birren, B.W., Huttenhower, C., Garrett, W.S., Meyerson, M., 2012. Genomic analysis identifies association of Fusobacterium with colorectal carcinoma. Genome Res 22, 292-298.

Kunzmann, A.T., Proenca, M.A., Jordao, H.W., Jiraskova, K., Schneiderova, M., Levy, M., Liska, V., Buchler, T., Vodickova, L., Vymetalkova, V., Silva, A.E., Vodicka, P., Hughes, D.J., 2019. Fusobacterium nucleatum tumor DNA levels are associated with survival in colorectal cancer patients. Eur J Clin Microbiol Infect Dis 38, 1891-1899.

Kurgan, S., Kansal, S., Nguyen, D., Stephens, D., Koroneos, Y., Hasturk, H., Van Dyke, T.E., Kantarci, A., 2017. Strain-Specific Impact of Fusobacterium nucleatum on Neutrophil Function. J Periodontol 88, 380-389.

Kwon, T., Lamster, I.B., Levin, L., 2021. Current Concepts in the Management of Periodontitis. Int Dent J 71, 462-476.

Lam, H., Oh, D.C., Cava, F., Takacs, C.N., Clardy, J., de Pedro, M.A., Waldor, M.K., 2009. D-amino acids govern stationary phase cell wall remodeling in bacteria. Science 325, 1552-1555.

Lam, K.L., Lin, S., Liu, C., Wu, X., Tang, S., Kwan, H.S., Cheung, P.C., 2018. Low-Cost Method Generating In Situ Anaerobic Conditions on a 96-Well Plate for Microbial Fermentation in Food Research. J Agric Food Chem 66, 11839-11845.

Lam, R.H., Cui, X., Guo, W., Thorsen, T., 2016a. High-throughput dental biofilm growth analysis for multiparametric microenvironmental biochemical conditions using microfluidics. Lab Chip 16, 1652-1662.

Lam, S.J., O'Brien-Simpson, N.M., Pantarat, N., Sulistio, A., Wong, E.H., Chen, Y.Y., Lenzo, J.C., Holden, J.A., Blencowe, A., Reynolds, E.C., Qiao, G.G., 2016b. Combating multidrug-resistant Gram-negative bacteria with structurally nanoengineered antimicrobial peptide polymers. Nat Microbiol 1, 16162.

Lancy, P., Jr., Dirienzo, J.M., Appelbaum, B., Rosan, B., Holt, S.C., 1983. Corncob formation between Fusobacterium nucleatum and Streptococcus sanguis. Infect Immun 40, 303-309.

Leiman, S.A., May, J.M., Lebar, M.D., Kahne, D., Kolter, R., Losick, R., 2013. D-amino acids indirectly inhibit biofilm formation in Bacillus subtilis by interfering with protein synthesis. J Bacteriol 195, 5391-5395.

Lemos, J.A., Abranches, J., Koo, H., Marquis, R.E., Burne, R.A., 2010. Protocols to study the physiology of oral biofilms. Methods Mol Biol 666, 87-102.

Lertpimonchai, A., Rattanasiri, S., Arj-Ong Vallibhakara, S., Attia, J., Thakkinstian, A., 2017. The association between oral hygiene and periodontitis: a systematic review and meta-analysis. Int Dent J 67, 332-343.

Li, J., Helmerhorst, E.J., Leone, C.W., Troxler, R.F., Yaskell, T., Haffajee, A.D., Socransky, S.S., Oppenheim, F.G., 2004. Identification of early microbial colonizers in human dental biofilm. J Appl Microbiol 97, 1311-1318.

Li, J., Rong, K., Zhao, H., Li, F., Lu, Z., Chen, R., 2013. Highly selective antibacterial activities of silver nanoparticles against Bacillus subtilis. J Nanosci Nanotechnol 13, 6806-6813.

Li, Z., Nair, S.K., 2012. Quorum sensing: how bacteria can coordinate activity and synchronize their response to external signals? Protein Sci 21, 1403-1417.

Lima, B.P., Shi, W., Lux, R., 2017. Identification and characterization of a novel Fusobacterium nucleatum adhesin involved in physical interaction and biofilm formation with Streptococcus gordonii. Microbiologyopen 6.

Liu, H., Redline, R.W., Han, Y.W., 2007. Fusobacterium nucleatum induces fetal death in mice via stimulation of TLR4-mediated placental inflammatory response. J Immunol 179, 2501-2508.

Liu, J., Hsieh, C.L., Gelincik, O., Devolder, B., Sei, S., Zhang, S., Lipkin, S.M., Chang, Y.F., 2019. Proteomic characterization of outer membrane vesicles from gut mucosa-derived fusobacterium nucleatum. J Proteomics 195, 125-137.

Liu, P.F., Shi, W., Zhu, W., Smith, J.W., Hsieh, S.L., Gallo, R.L., Huang, C.M., 2010. Vaccination targeting surface FomA of Fusobacterium nucleatum against bacterial co-aggregation: Implication for treatment of periodontal infection and halitosis. Vaccine 28, 3496-3505.

Loe, H., Theilade, E., Jensen, S.B., 1965. Experimental Gingivitis in Man. J Periodontol 36, 177-187.

Loesche, W.J., 1996. Microbiology of Dental Decay and Periodontal Disease, in: th, Baron, S. (Eds.), Medical Microbiology, Galveston (TX).

Lu, Z., Rong, K., Li, J., Yang, H., Chen, R., 2013. Size-dependent antibacterial activities of silver nanoparticles against oral anaerobic pathogenic bacteria. J Mater Sci Mater Med 24, 1465-1471.

Manson McGuire, A., Cochrane, K., Griggs, A.D., Haas, B.J., Abeel, T., Zeng, Q., Nice, J.B., MacDonald, H., Birren, B.W., Berger, B.W., Allen-Vercoe, E., Earl, A.M., 2014. Evolution of invasion in a diverse set of Fusobacterium species. mBio 5, e01864.

Marambio-Jones, C., Hoek, E.M.V., 2010. A review of the antibacterial effects of silver nanomaterials and potential implications for human health and the environment. Journal of Nanoparticle Research 12, 1531-1551.

Mark Welch, J.L., Rossetti, B.J., Rieken, C.W., Dewhirst, F.E., Borisy, G.G., 2016. Biogeography of a human oral microbiome at the micron scale. Proc Natl Acad Sci U S A 113, E791-800.

Marquis, R.E., 1995. Oxygen metabolism, oxidative stress and acid-base physiology of dental plaque biofilms. J Ind Microbiol 15, 198-207.

Marsh, P.D., 1994. Microbial ecology of dental plaque and its significance in health and disease. Adv Dent Res 8, 263-271.

Marsh, P.D., 2003. Are dental diseases examples of ecological catastrophes? Microbiology 149, 279-294.

Marsh, P.D., 2004. Dental plaque as a microbial biofilm. Caries Res 38, 204-211.

Marsh, P.D., 2005. Dental plaque: biological significance of a biofilm and community life-style. J Clin Periodontol 32 Suppl 6, 7-15.

Marsh, P.D., Moter, A., Devine, D.A., 2011. Dental plaque biofilms: communities, conflict and control. Periodontol 2000 55, 16-35.

Martinez, S., Garcia, J.G., Williams, R., Elmassry, M., West, A., Hamood, A., Hurtado, D., Gudenkauf, B., Ventolini, G., Schlabritz-Loutsevitch, N., 2020. Lactobacilli spp.: real-time evaluation of biofilm growth. BMC Microbiol 20, 64.

Matsumoto, M., Kunisawa, A., Hattori, T., Kawana, S., Kitada, Y., Tamada, H., Kawano, S., Hayakawa, Y., Iida, J., Fukusaki, E., 2018. Free D-amino acids produced by commensal bacteria in the colonic lumen. Sci Rep 8, 17915.

McDermid, A.S., McKee, A.S., Marsh, P.D., 1988. Effect of environmental pH on enzyme activity and growth of Bacteroides gingivalis W50. Infect Immun 56, 1096-1100.

McNab, R., Ford, S.K., El-Sabaeny, A., Barbieri, B., Cook, G.S., Lamont, R.J., 2003. LuxS-based signaling in Streptococcus gordonii: autoinducer 2 controls carbohydrate metabolism and biofilm formation with Porphyromonas gingivalis. J Bacteriol 185, 274-284.

Mima, K., Nishihara, R., Qian, Z.R., Cao, Y., Sukawa, Y., Nowak, J.A., Yang, J., Dou, R., Masugi, Y., Song, M., Kostic, A.D., Giannakis, M., Bullman, S., Milner, D.A., Baba, H., Giovannucci, E.L., Garraway, L.A., Freeman, G.J., Dranoff, G., Garrett, W.S., Huttenhower, C., Meyerson, M., Meyerhardt, J.A., Chan, A.T., Fuchs, C.S., Ogino, S., 2016. Fusobacterium nucleatum in colorectal carcinoma tissue and patient prognosis. Gut 65, 1973-1980.

Mira, A., Buetas, E., Rosier, B., Mazurel, D., Villanueva-Castellote, A., Llena, C., Ferrer, M.D., 2019. Development of an in vitro system to study oral biofilms in real time through impedance technology: validation and potential applications. J Oral Microbiol 11, 1609838.

Mira, A., Pushker, R., Legault, B.A., Moreira, D., Rodriguez-Valera, F., 2004. Evolutionary relationships of Fusobacterium nucleatum based on phylogenetic analysis and comparative genomics. BMC Evol Biol 4, 50.

Moore, W.E., Holdeman, L.V., Smibert, R.M., Hash, D.E., Burmeister, J.A., Ranney, R.R., 1982. Bacteriology of severe periodontitis in young adult humans. Infect Immun 38, 1137-1148.

Moore, W.E., Moore, L.V., 1994. The bacteria of periodontal diseases. Periodontol 2000 5, 66-77.

Muchova, M., Balacco, D.L., Grant, M.M., Chapple, I.L.C., Kuehne, S.A., Hirschfeld, J., 2022. Fusobacterium nucleatum Subspecies Differ in Biofilm Forming Ability in vitro. Front Oral Health 3, 853618.

Muras, A., Mayer, C., Romero, M., Camino, T., Ferrer, M.D., Mira, A., Otero, A., 2018. Inhibition of Steptococcus mutans biofilm formation by extracts of Tenacibaculum sp. 20J, a bacterium with wide-spectrum quorum quenching activity. J Oral Microbiol 10, 1429788.

Murray, C.J., Vos, T., Lozano, R., Naghavi, M., Flaxman, A.D., Michaud, C., Ezzati, M., Shibuya, K., Salomon, J.A., Abdalla, S., Aboyans, V., Abraham, J., Ackerman, I., Aggarwal, R., Ahn, S.Y., Ali, M.K., Alvarado, M., Anderson, H.R., Anderson, L.M., Andrews, K.G., Atkinson, C., Baddour, L.M., Bahalim, A.N., Barker-Collo, S., Barrero, L.H., Bartels, D.H.,

Basanez, M.G., Baxter, A., Bell, M.L., Benjamin, E.J., Bennett, D., Bernabe, E., Bhalla, K., Bhandari, B., Bikbov, B., Bin Abdulhak, A., Birbeck, G., Black, J.A., Blencowe, H., Blore, J.D., Blyth, F., Bolliger, I., Bonaventure, A., Boufous, S., Bourne, R., Boussinesq, M., Braithwaite, T., Brayne, C., Bridgett, L., Brooker, S., Brooks, P., Brugha, T.S., Bryan-Hancock, C., Bucello, C., Buchbinder, R., Buckle, G., Budke, C.M., Burch, M., Burney, P., Burstein, R., Calabria, B., Campbell, B., Canter, C.E., Carabin, H., Carapetis, J., Carmona, L., Cella, C., Charlson, F., Chen, H., Cheng, A.T., Chou, D., Chugh, S.S., Coffeng, L.E., Colan, S.D., Colquhoun, S., Colson, K.E., Condon, J., Connor, M.D., Cooper, L.T., Corriere, M., Cortinovis, M., de Vaccaro, K.C., Couser, W., Cowie, B.C., Criqui, M.H., Cross, M., Dabhadkar, K.C., Dahiya, M., Dahodwala, N., Damsere-Derry, J., Danaei, G., Davis, A., De Leo, D., Degenhardt, L., Dellavalle, R., Delossantos, A., Denenberg, J., Derrett, S., Des Jarlais, D.C., Dharmaratne, S.D., Dherani, M., Diaz-Torne, C., Dolk, H., Dorsey, E.R., Driscoll, T., Duber, H., Ebel, B., Edmond, K., Elbaz, A., Ali, S.E., Erskine, H., Erwin, P.J., Espindola, P., Ewoigbokhan, S.E., Farzadfar, F., Feigin, V., Felson, D.T., Ferrari, A., Ferri, C.P., Fevre, E.M., Finucane, M.M., Flaxman, S., Flood, L., Foreman, K., Forouzanfar, M.H., Fowkes, F.G., Fransen, M., Freeman, M.K., Gabbe, B.J., Gabriel, S.E., Gakidou, E., Ganatra, H.A., Garcia, B., Gaspari, F., Gillum, R.F., Gmel, G., Gonzalez-Medina, D., Gosselin, R., Grainger, R., Grant, B., Groeger, J., Guillemin, F., Gunnell, D., Gupta, R., Haagsma, J., Hagan, H., Halasa, Y.A., Hall, W., Haring, D., Haro, J.M., Harrison, J.E., Havmoeller, R., Hay, R.J., Higashi, H., Hill, C., Hoen, B., Hoffman, H., Hotez, P.J., Hoy, D., Huang, J.J., Ibeanusi, S.E., Jacobsen, K.H., James, S.L., Jarvis, D., Jasrasaria, R., Jayaraman, S., Johns, N., Jonas, J.B., Karthikeyan, G., Kassebaum, N., Kawakami, N., Keren, A., Khoo, J.P., King, C.H., Knowlton, L.M., Kobusingye, O., Koranteng, A., Krishnamurthi, R., Laden, F., Lalloo, R., Laslett, L.L., Lathlean, T., Leasher, J.L., Lee, Y.Y., Leigh, J., Levinson, D., Lim, S.S., Limb, E., Lin, J.K., Lipnick, M., Lipshultz, S.E., Liu, W., Loane, M., Ohno, S.L., Lyons, R., Mabweijano, J., MacIntyre, M.F., Malekzadeh, R., Mallinger, L., Manivannan, S., Marcenes, W., March, L., Margolis, D.J., Marks, G.B., Marks, R., Matsumori, A., Matzopoulos, R., Mayosi, B.M., McAnulty, J.H., McDermott, M.M., McGill, N., McGrath, J., Medina-Mora, M.E., Meltzer, M., Mensah, G.A., Merriman, T.R., Meyer, A.C., Miglioli, V., Miller, M., Miller, T.R., Mitchell, P.B., Mock, C., Mocumbi, A.O., Moffitt, T.E., Mokdad, A.A., Monasta, L., Montico, M., Moradi-Lakeh, M., Moran, A., Morawska, L., Mori, R., Murdoch, M.E., Mwaniki, M.K., Naidoo, K., Nair, M.N., Naldi, L., Narayan, K.M., Nelson, P.K., Nelson, R.G., Nevitt, M.C., Newton, C.R., Nolte, S., Norman, P., Norman, R., O'Donnell, M., O'Hanlon, S., Olives, C., Omer, S.B., Ortblad, K., Osborne, R., Ozgediz, D., Page, A., Pahari, B., Pandian, J.D., Rivero, A.P., Patten, S.B., Pearce, N., Padilla, R.P., Perez-Ruiz, F., Perico, N., Pesudovs, K., Phillips, D., Phillips, M.R., Pierce, K., Pion, S., Polanczyk, G.V., Polinder, S., Pope, C.A., 3rd, Popova, S., Porrini, E., Pourmalek, F., Prince, M., Pullan, R.L., Ramaiah, K.D., Ranganathan, D., Razavi, H., Regan, M., Rehm, J.T., Rein, D.B., Remuzzi, G., Richardson, K., Rivara, F.P., Roberts, T., Robinson, C., De Leon, F.R., Ronfani, L., Room, R., Rosenfeld, L.C., Rushton, L., Sacco, R.L., Saha, S., Sampson, U., Sanchez-Riera, L., Sanman, E., Schwebel, D.C., Scott, J.G., Segui-Gomez, M., Shahraz, S., Shepard, D.S., Shin, H., Shivakoti, R., Singh, D., Singh, G.M., Singh, J.A., Singleton, J., Sleet, D.A., Sliwa, K., Smith, E., Smith, J.L., Stapelberg, N.J., Steer, A., Steiner, T., Stolk, W.A., Stovner, L.J., Sudfeld, C., Syed, S., Tamburlini, G., Tavakkoli, M., Taylor, H.R., Taylor, J.A., Taylor, W.J., Thomas, B., Thomson, W.M., Thurston, G.D., Tleyjeh, I.M., Tonelli, M., Towbin, J.A., Truelsen, T., Tsilimbaris, M.K., Ubeda, C., Undurraga, E.A., van der Werf, M.J., van Os, J., Vavilala, M.S., Venketasubramanian, N., Wang, M., Wang, W., Watt, K., Weatherall, D.J., Weinstock, M.A., Weintraub, R., Weisskopf, M.G., Weissman, M.M., White, R.A., Whiteford, H., Wiebe, N., Wiersma, S.T., Wilkinson, J.D., Williams, H.C., Williams, S.R., Witt, E., Wolfe, F., Woolf, A.D., Wulf, S., Yeh, P.H., Zaidi, A.K., Zheng, Z.J., Zonies, D.,

Lopez, A.D., AlMazroa, M.A., Memish, Z.A., 2012. Disability-adjusted life years (DALYs) for 291 diseases and injuries in 21 regions, 1990-2010: a systematic analysis for the Global Burden of Disease Study 2010. Lancet 380, 2197-2223.

Nance, W.C., Dowd, S.E., Samarian, D., Chludzinski, J., Delli, J., Battista, J., Rickard, A.H., 2013. A high-throughput microfluidic dental plaque biofilm system to visualize and quantify the effect of antimicrobials. J Antimicrob Chemother 68, 2550-2560.

Nie, S., Tian, B., Wang, X., Pincus, D.H., Welker, M., Gilhuley, K., Lu, X., Han, Y.W., Tang, Y.W., 2015. Fusobacterium nucleatum subspecies identification by matrix-assisted laser desorption ionization-time of flight mass spectrometry. J Clin Microbiol 53, 1399-1402.

Nunez-Anita, R.E., Acosta-Torres, L.S., Vilar-Pineda, J., Martinez-Espinosa, J.C., de la Fuente-Hernandez, J., Castano, V.M., 2014. Toxicology of antimicrobial nanoparticles for prosthetic devices. Int J Nanomedicine 9, 3999-4006.

Nyvad, B., Kilian, M., 1987. Microbiology of the early colonization of human enamel and root surfaces in vivo. Scand J Dent Res 95, 369-380.

Ozaki, M., Miyake, Y., Shirakawa, M., Takemoto, T., Okamoto, H., Suginaka, H., 1990. Binding specificity of Fusobacterium nucleatum to human erythrocytes, polymorphonuclear leukocytes, fibroblasts, and HeLa cells. J Periodontal Res 25, 129-134.

Page, R.C., 1986. Gingivitis. J Clin Periodontol 13, 345-359.

Palmer, R.J., Jr., Gordon, S.M., Cisar, J.O., Kolenbrander, P.E., 2003. Coaggregation-mediated interactions of streptococci and actinomyces detected in initial human dental plaque. J Bacteriol 185, 3400-3409.

Park, J., Shokeen, B., Haake, S.K., Lux, R., 2016. Characterization of Fusobacterium nucleatum ATCC 23726 adhesins involved in strain-specific attachment to Porphyromonas gingivalis. International Journal of Oral Science 8, 138-144.

Park, S.N., Kong, S.W., Park, M.S., Lee, J.W., Cho, E., Lim, Y.K., Choi, M.H., Kim, H.S., Chang, Y.H., Shin, J.H., Park, H.S., Choi, S.H., Kook, J.K., 2012. Draft genome sequence of Fusobacterium nucleatum subsp. fusiforme ATCC 51190T. J Bacteriol 194, 5445-5446.

Park, S.R., Kim, D.J., Han, S.H., Kang, M.J., Lee, J.Y., Jeong, Y.J., Lee, S.J., Kim, T.H., Ahn, S.G., Yoon, J.H., Park, J.H., 2014. Diverse Toll-like receptors mediate cytokine production by Fusobacterium nucleatum and Aggregatibacter actinomycetemcomitans in macrophages. Infect Immun 82, 1914-1920.

Paster, B.J., Olsen, I., Aas, J.A., Dewhirst, F.E., 2006. The breadth of bacterial diversity in the human periodontal pocket and other oral sites. Periodontol 2000 42, 80-87.

Petersen, P.E., Ogawa, H., 2012. The global burden of periodontal disease: towards integration with chronic disease prevention and control. Periodontol 2000 60, 15-39.

Polak, D., Wilensky, A., Shapira, L., Halabi, A., Goldstein, D., Weiss, E.I., Houri-Haddad, Y., 2009. Mouse model of experimental periodontitis induced by Porphyromonas gingivalis/Fusobacterium nucleatum infection: bone loss and host response. J Clin Periodontol 36, 406-410.

Potempa, J., Sroka, A., Imamura, T., Travis, J., 2003. Gingipains, the major cysteine proteinases and virulence factors of Porphyromonas gingivalis: structure, function and assembly of multidomain protein complexes. Curr Protein Pept Sci 4, 397-407.

Qing, Y., Cheng, L., Li, R., Liu, G., Zhang, Y., Tang, X., Wang, J., Liu, H., Qin, Y., 2018. Potential antibacterial mechanism of silver nanoparticles and the optimization of orthopedic implants by advanced modification technologies. Int J Nanomedicine 13, 3311-3327.

Radkov, A.D., Moe, L.A., 2018. A Broad Spectrum Racemase in Pseudomonas putida KT2440 Plays a Key Role in Amino Acid Catabolism. Front Microbiol 9, 1343.

Radzig, M.A., Nadtochenko, V.A., Koksharova, O.A., Kiwi, J., Lipasova, V.A., Khmel, I.A., 2013. Antibacterial effects of silver nanoparticles on gram-negative bacteria: influence on the growth and biofilms formation, mechanisms of action. Colloids Surf B Biointerfaces 102, 300-306.

Raghunathan, D., Wells, T.J., Morris, F.C., Shaw, R.K., Bobat, S., Peters, S.E., Paterson, G.K., Jensen, K.T., Leyton, D.L., Blair, J.M., Browning, D.F., Pravin, J., Flores-Langarica, A., Hitchcock, J.R., Moraes, C.T., Piazza, R.M., Maskell, D.J., Webber, M.A., May, R.C., MacLennan, C.A., Piddock, L.J., Cunningham, A.F., Henderson, I.R., 2011. SadA, a trimeric autotransporter from Salmonella enterica serovar Typhimurium, can promote biofilm formation and provides limited protection against infection. Infect Immun 79, 4342-4352.

Rickard, A.H., Gilbert, P., High, N.J., Kolenbrander, P.E., Handley, P.S., 2003. Bacterial coaggregation: an integral process in the development of multi-species biofilms. Trends Microbiol 11, 94-100.

Roberts, A.P., Pratten, J., Wilson, M., Mullany, P., 1999. Transfer of a conjugative transposon, Tn5397 in a model oral biofilm. FEMS Microbiol Lett 177, 63-66.

Rogers, A.H., Chen, J., Zilm, P.S., Gully, N.J., 1998. The behaviour of Fusobacterium nucleatum chemostat-grown in glucose- and amino acid-based chemically defined media. Anaerobe 4, 111-116.

Romero, D., Aguilar, C., Losick, R., Kolter, R., 2010. Amyloid fibers provide structural integrity to Bacillus subtilis biofilms. Proc Natl Acad Sci U S A 107, 2230-2234.

Rosen, E., Tsesis, I., Elbahary, S., Storzi, N., Kolodkin-Gal, I., 2016. Eradication of Enterococcus faecalis Biofilms on Human Dentin. Front Microbiol 7, 2055.

Rubinstein, M.R., Baik, J.E., Lagana, S.M., Han, R.P., Raab, W.J., Sahoo, D., Dalerba, P., Wang, T.C., Han, Y.W., 2019. Fusobacterium nucleatum promotes colorectal cancer by inducing Wnt/beta-catenin modulator Annexin A1. EMBO Rep 20.

Rubinstein, M.R., Wang, X., Liu, W., Hao, Y., Cai, G., Han, Y.W., 2013. Fusobacterium nucleatum promotes colorectal carcinogenesis by modulating E-cadherin/beta-catenin signaling via its FadA adhesin. Cell Host Microbe 14, 195-206.

Saito, A., Inagaki, S., Kimizuka, R., Okuda, K., Hosaka, Y., Nakagawa, T., Ishihara, K., 2008a. Fusobacterium nucleatum enhances invasion of human gingival epithelial and aortic endothelial cells by Porphyromonas gingivalis. FEMS Immunol Med Microbiol 54, 349-355.

Saito, A., Kokubu, E., Inagaki, S., Imamura, K., Kita, D., Lamont, R.J., Ishihara, K., 2012. Porphyromonas gingivalis entry into gingival epithelial cells modulated by Fusobacterium nucleatum is dependent on lipid rafts. Microb Pathog 53, 234-242.

Saito, Y., Fujii, R., Nakagawa, K.I., Kuramitsu, H.K., Okuda, K., Ishihara, K., 2008b. Stimulation of Fusobacterium nucleatum biofilm formation by Porphyromonas gingivalis. Oral Microbiol Immunol 23, 1-6.

Samarian, D.S., Jakubovics, N.S., Luo, T.L., Rickard, A.H., 2014. Use of a high-throughput in vitro microfluidic system to develop oral multi-species biofilms. J Vis Exp.

Sanders, B.E., Umana, A., Lemkul, J.A., Slade, D.J., 2018. FusoPortal: an Interactive Repository of Hybrid MinION-Sequenced Fusobacterium Genomes Improves Gene Identification and Characterization. mSphere 3.

Schauder, S., Shokat, K., Surette, M.G., Bassler, B.L., 2001. The LuxS family of bacterial autoinducers: biosynthesis of a novel quorum-sensing signal molecule. Mol Microbiol 41, 463-476.

Seil, J.T., Webster, T.J., 2012. Antimicrobial applications of nanotechnology: methods and literature. Int J Nanomedicine 7, 2767-2781.

Shahverdi, A.R., Fakhimi, A., Shahverdi, H.R., Minaian, S., 2007. Synthesis and effect of silver nanoparticles on the antibacterial activity of different antibiotics against Staphylococcus aureus and Escherichia coli. Nanomedicine 3, 168-171.

Shu, M., Wong, L., Miller, J.H., Sissons, C.H., 2000. Development of multi-species consortia biofilms of oral bacteria as an enamel and root caries model system. Arch Oral Biol 45, 27-40.

Shumi, W., Kim, S.H., Lim, J., Cho, K.S., Han, H., Park, S., 2013. Shear stress tolerance of Streptococcus mutans aggregates determined by microfluidic funnel device (muFFD). J Microbiol Methods 93, 85-89.

Silva, V.L., Diniz, C.G., Cara, D.C., Santos, S.G., Nicoli, J.R., Carvalho, M.A., Farias, L.M., 2005. Enhanced pathogenicity of Fusobacterium nucleatum adapted to oxidative stress. Microb Pathog 39, 131-138.

Slots, J., 1999. Update on Actinobacillus Actinomycetemcomitans and Porphyromonas gingivalis in human periodontal disease. J Int Acad Periodontol 1, 121-126.

Socransky, S.S., Haffajee, A.D., Cugini, M.A., Smith, C., Kent, R.L., Jr., 1998. Microbial complexes in subgingival plaque. J Clin Periodontol 25, 134-144.

Socransky, S.S., Haffajee, A.D., Smith, C., Duff, G.W., 2000. Microbiological parameters associated with IL-1 gene polymorphisms in periodontitis patients. J Clin Periodontol 27, 810-818.

Socransky, S.S., Haffajee, A.D., Smith, C., Martin, L., Haffajee, J.A., Uzel, N.G., Goodson, J.M., 2004. Use of checkerboard DNA-DNA hybridization to study complex microbial ecosystems. Oral Microbiol Immunol 19, 352-362.

Socransky, S.S., Smith, C., Haffajee, A.D., 2002. Subgingival microbial profiles in refractory periodontal disease. J Clin Periodontol 29, 260-268.

Spaulding, E.H., Rettger, L.F., 1937. The Fusobacterium Genus: II. Some Observations on Growth Requirements and Variation. J Bacteriol 34, 549-563.

Stegink, L.D., Zike, W.L., Andersen, D.W., Killion, D., 1987. Oligosaccharides as an intravenous energy source in postsurgical patients: utilization when infused with glucose, amino acids, and lipid emulsion. Am J Clin Nutr 46, 461-466.

Strauss, J., Kaplan, G.G., Beck, P.L., Rioux, K., Panaccione, R., Devinney, R., Lynch, T., Allen-Vercoe, E., 2011. Invasive potential of gut mucosa-derived Fusobacterium nucleatum positively correlates with IBD status of the host. Inflamm Bowel Dis 17, 1971-1978.

Strauss, J., White, A., Ambrose, C., McDonald, J., Allen-Vercoe, E., 2008. Phenotypic and genotypic analyses of clinical Fusobacterium nucleatum and Fusobacterium periodonticum isolates from the human gut. Anaerobe 14, 301-309.

Subramanian, S., Huiszoon, R.C., Chu, S., Bentley, W.E., Ghodssi, R., 2020. Microsystems for biofilm characterization and sensing – A review. Biofilm 2.

Sukumar, S., Martin, F., Huges, T., Alder, C., 2020. Think before you prescribe: how dentistry contributes to antibiotic resistance. Australian Dental Journal 65, 21-29.

Swidsinski, A., Dorffel, Y., Loening-Baucke, V., Theissig, F., Ruckert, J.C., Ismail, M., Rau, W.A., Gaschler, D., Weizenegger, M., Kuhn, S., Schilling, J., Dorffel, W.V., 2011. Acute appendicitis is characterised by local invasion with Fusobacterium nucleatum/necrophorum. Gut 60, 34-40.

Tadepalli, S., Narayanan, S.K., Stewart, G.C., Chengappa, M.M., Nagaraja, T.G., 2009. Fusobacterium necrophorum: a ruminal bacterium that invades liver to cause abscesses in cattle. Anaerobe 15, 36-43.

Takahashi, N., Saito, K., Schachtele, C.F., Yamada, T., 1997. Acid tolerance and acid-neutralizing activity of Porphyromonas gingivalis, Prevotella intermedia and Fusobacterium nucleatum. Oral Microbiol Immunol 12, 323-328.

Takahashi, N., Schachtele, C.F., 1990. Effect of pH on the growth and proteolytic activity of Porphyromonas gingivalis and Bacteroides intermedius. J Dent Res 69, 1266-1269.

Taxman, D.J., Swanson, K.V., Broglie, P.M., Wen, H., Holley-Guthrie, E., Huang, M.T., Callaway, J.B., Eitas, T.K., Duncan, J.A., Ting, J.P., 2012. Porphyromonas gingivalis mediates inflammasome repression in polymicrobial cultures through a novel mechanism involving reduced endocytosis. J Biol Chem 287, 32791-32799.

Temoin, S., Chakaki, A., Askari, A., El-Halaby, A., Fitzgerald, S., Marcus, R.E., Han, Y.W., Bissada, N.F., 2012. Identification of oral bacterial DNA in synovial fluid of patients with arthritis with native and failed prosthetic joints. J Clin Rheumatol 18, 117-121.

Teoh, L., Stewart, K., Marino, R., McCullough, M., 2018. Antibiotic resistance and relevance to general dental practice in Australia. Aust Dent J 63, 414-421.

ter Steeg, P.F., Van der Hoeven, J.S., de Jong, M.H., van Munster, P.J., Jansen, M.J., 1987. Enrichment of subgingival microflora on human serum leading to accumulation of Bacteroides species, Peptostreptococci and Fusobacteria. Antonie Van Leeuwenhoek 53, 261-272.

Thurnheer, T., Karygianni, L., Flury, M., Belibasakis, G.N., 2019. Fusobacterium Species and Subspecies Differentially Affect the Composition and Architecture of Supra- and Subgingival Biofilms Models. Front Microbiol 10, 1716.

Tjalsma, H., Boleij, A., Marchesi, J.R., Dutilh, B.E., 2012. A bacterial driver-passenger model for colorectal cancer: beyond the usual suspects. Nat Rev Microbiol 10, 575-582.

Todd, S.M., Settlage, R.E., Lahmers, K.K., Slade, D.J., 2018. Fusobacterium Genomics Using MinION and Illumina Sequencing Enables Genome Completion and Correction. mSphere 3.

Truant, A.L., Menge, S., Milliorn, K., Lairscey, R., Kelly, M.T., 1983. Fusobacterium nucleatum pericarditis. J Clin Microbiol 17, 349-351.

Umana, A., Sanders, B.E., Yoo, C.C., Casasanta, M.A., Udayasuryan, B., Verbridge, S.S., Slade, D.J., 2019. Utilizing Whole Fusobacterium Genomes To Identify, Correct, and Characterize Potential Virulence Protein Families. J Bacteriol 201.

Vahdati, S.N., Behboudi, H., Navasatli, S.A., Tavakoli, S., Safavi, M., 2022. New insights into the inhibitory roles and mechanisms of D-amino acids in bacterial biofilms in medicine, industry, and agriculture. Microbiol Res 263, 127107.

Van Acker, H., Van Dijck, P., Coenye, T., 2014. Molecular mechanisms of antimicrobial tolerance and resistance in bacterial and fungal biofilms. Trends Microbiol 22, 326-333.

Van Dyke, T.E., Bartold, P.M., Reynolds, E.C., 2020. The Nexus Between Periodontal Inflammation and Dysbiosis. Front Immunol 11, 511.

Vollmer, W., Blanot, D., de Pedro, M.A., 2008. Peptidoglycan structure and architecture. FEMS Microbiol Rev 32, 149-167.

Vyas, H.K.N., Xia, B., Mai-Prochnow, A., 2022. Clinically relevant in vitro biofilm models: A need to mimic and recapitulate the host environment. Biofilm 4, 100069.

Wang, B.Y., Chi, B., Kuramitsu, H.K., 2002. Genetic exchange between Treponema denticola and Streptococcus gordonii in biofilms. Oral Microbiol Immunol 17, 108-112.

Wang, X., Buhimschi, C.S., Temoin, S., Bhandari, V., Han, Y.W., Buhimschi, I.A., 2013. Comparative microbial analysis of paired amniotic fluid and cord blood from pregnancies complicated by preterm birth and early-onset neonatal sepsis. PLoS One 8, e56131.

Wang, Y., Malkmes, M.J., Jiang, C., Wang, P., Zhu, L., Zhang, H., Zhang, Y., Huang, H., Jiang, L., 2021. Antibacterial mechanism and transcriptome analysis of ultra-small gold nanoclusters as an alternative of harmful antibiotics against Gram-negative bacteria. J Hazard Mater 416, 126236.

Wecke, J., Kersten, T., Madela, K., Moter, A., Gobel, U.B., Friedmann, A., Bernimoulin, J., 2000. A novel technique for monitoring the development of bacterial biofilms in human periodontal pockets. FEMS Microbiol Lett 191, 95-101.

Weiss, E.I., Shaniztki, B., Dotan, M., Ganeshkumar, N., Kolenbrander, P.E., Metzger, Z., 2000. Attachment of Fusobacterium nucleatum PK1594 to mammalian cells and its coaggregation with periodontopathogenic bacteria are mediated by the same galactose-binding adhesin. Oral Microbiol Immunol 15, 371-377.

White, B.D., Chien, A.J., Dawson, D.W., 2012. Dysregulation of Wnt/beta-catenin signaling in gastrointestinal cancers. Gastroenterology 142, 219-232.

Wick, R.R., Judd, L.M., Gorrie, C.L., Holt, K.E., 2017a. Completing bacterial genome assemblies with multiplex MinION sequencing. Microb Genom 3, e000132.

Wick, R.R., Judd, L.M., Gorrie, C.L., Holt, K.E., 2017b. Unicycler: Resolving bacterial genome assemblies from short and long sequencing reads. PLoS Comput Biol 13, e1005595.

Winkel, E.G., Van Winkelhoff, A.J., Timmerman, M.F., Van der Velden, U., Van der Weijden, G.A., 2001. Amoxicillin plus metronidazole in the treatment of adult periodontitis patients. A double-blind placebo-controlled study. J Clin Periodontol 28, 296-305.

Wu, T., Cen, L., Kaplan, C., Zhou, X., Lux, R., Shi, W., He, X., 2015. Cellular Components Mediating Coadherence of Candida albicans and Fusobacterium nucleatum. J Dent Res 94, 1432-1438.

Xiao, J., Klein, M.I., Falsetta, M.L., Lu, B., Delahunty, C.M., Yates, J.R., 3rd, Heydorn, A., Koo, H., 2012. The exopolysaccharide matrix modulates the interaction between 3D architecture and virulence of a mixed-species oral biofilm. PLoS Pathog 8, e1002623.

Xie, H., Gibbons, R.J., Hay, D.I., 1991. Adhesive properties of strains of Fusobacterium nucleatum of the subspecies nucleatum, vincentii and polymorphum. Oral Microbiol Immunol 6, 257-263.

Ximenez-Fyvie, L.A., Haffajee, A.D., Socransky, S.S., 2000. Comparison of the microbiota of supra- and subgingival plaque in health and periodontitis. J Clin Periodontol 27, 648-657.

Xu, H., Liu, Y., 2011a. d-Amino acid mitigated membrane biofouling and promoted biofilm detachment. Journal of Membrane Science 376, 266-274.

Xu, H., Liu, Y., 2011b. Reduced microbial attachment by D-amino acid-inhibited AI-2 and EPS production. Water Res 45, 5796-5804.

Xu, M., Yamada, M., Li, M., Liu, H., Chen, S.G., Han, Y.W., 2007. FadA from Fusobacterium nucleatum utilizes both secreted and nonsecreted forms for functional oligomerization for attachment and invasion of host cells. J Biol Chem 282, 25000-25009.

Yamaguchi, Y., Kurita-Ochiai, T., Kobayashi, R., Suzuki, T., Ando, T., 2017. Regulation of the NLRP3 inflammasome in Porphyromonas gingivalis-accelerated periodontal disease. Inflamm Res 66, 59-65.

Yamaguchi-Kuroda, Y., Kikuchi, Y., Kokubu, E., Ishihara, K., 2023. Porphyromonas gingivalis diffusible signaling molecules enhance Fusobacterium nucleatum biofilm formation via gene expression modulation. J Oral Microbiol 15, 2165001.

Ye, X., Wang, R., Bhattacharya, R., Boulbes, D.R., Fan, F., Xia, L., Adoni, H., Ajami, N.J., Wong, M.C., Smith, D.P., Petrosino, J.F., Venable, S., Qiao, W., Baladandayuthapani, V., Maru, D., Ellis, L.M., 2017. Fusobacterium Nucleatum Subspecies Animalis Influences Proinflammatory Cytokine Expression and Monocyte Activation in Human Colorectal Tumors. Cancer Prev Res (Phila) 10, 398-409.

Yoshida, Y., Palmer, R.J., Yang, J., Kolenbrander, P.E., Cisar, J.O., 2006. Streptococcal receptor polysaccharides: recognition molecules for oral biofilm formation. BMC Oral Health 6 Suppl 1, S12.

Yu, C., Li, X., Zhang, N., Wen, D., Liu, C., Li, Q., 2016. Inhibition of biofilm formation by D-tyrosine: Effect of bacterial type and D-tyrosine concentration. Water Res 92, 173-179.

Yu, O.Y., Zhao, I.S., Mei, M.L., Lo, E.C., Chu, C.H., 2017a. Dental Biofilm and Laboratory Microbial Culture Models for Cariology Research. Dent J (Basel) 5.

Yu, T., Guo, F., Yu, Y., Sun, T., Ma, D., Han, J., Qian, Y., Kryczek, I., Sun, D., Nagarsheth, N., Chen, Y., Chen, H., Hong, J., Zou, W., Fang, J.Y., 2017b. Fusobacterium nucleatum Promotes Chemoresistance to Colorectal Cancer by Modulating Autophagy. Cell 170, 548-563 e516.

Zepeda-Rivera, M., Minot, S.S., Bouzek, H., Wu, H., Blanco-Miguez, A., Manghi, P., Jones, D.S., LaCourse, K.D., Wu, Y., McMahon, E.F., Park, S.N., Lim, Y.K., Kempchinsky, A.G., Willis, A.D., Cotton, S.L., Yost, S.C., Sicinska, E., Kook, J.K., Dewhirst, F.E., Segata, N., Bullman, S., Johnston, C.D., 2024. A distinct Fusobacterium nucleatum clade dominates the colorectal cancer niche. Nature 628, 424-432.

Zhang, Y., Chen, R., Wang, Y., Wang, P., Pu, J., Xu, X., Chen, F., Jiang, L., Jiang, Q., Yan, F., 2022a. Antibiofilm activity of ultra-small gold nanoclusters against Fusobacterium nucleatum in dental plaque biofilms. J Nanobiotechnology 20, 470.

Zhang, Y., Zhang, L., Zheng, S., Li, M., Xu, C., Jia, D., Qi, Y., Hou, T., Wang, L., Wang, B., Li, A., Chen, S., Si, J., Zhuo, W., 2022b. Fusobacterium nucleatum promotes colorectal cancer cells adhesion to endothelial cells and facilitates extravasation and metastasis by inducing ALPK1/NF-kappaB/ICAM1 axis. Gut Microbes 14, 2038852.

Zhang, Y.B., Jiang, J., Chen, Y.D., Zhu, R., Shi, Y., Zhang, Q.Y., Gui, J.F., 2007. The innate immune response to grass carp hemorrhagic virus (GCHV) in cultured Carassius auratus blastulae (CAB) cells. Dev Comp Immunol 31, 232-243.

Zheng, K., Xie, J., 2020. Composition-Dependent Antimicrobial Ability of Full-Spectrum Au(x)Ag(25-x) Alloy Nanoclusters. ACS Nano 14, 11533-11541.

Zhu, Y., Dashper, S.G., Chen, Y.Y., Crawford, S., Slakeski, N., Reynolds, E.C., 2013. Porphyromonas gingivalis and Treponema denticola synergistic polymicrobial biofilm development. PLoS One 8, e71727.

Zilm, P.S., Butnejski, V., Rossi-Fedele, G., Kidd, S.P., Edwards, S., Vasilev, K., 2017. D-amino acids reduce Enterococcus faecalis biofilms in vitro and in the presence of antimicrobials used for root canal treatment. PLoS One 12, e0170670.